NTNU

Norwegian University of
Science and Technology

Modelling and control of a pneumatic starting system for medium-speed gas engines

Trond Inge Eide

Master of Science in Marine Technology
Submission date: June 2011
Supervisor: Roger Skjetne
Co-supervisor: Rune Nordrik, Rolls-Royce Marine

Norwegian University of Science and Technology
Department of Marine Technology

Abstract

This thesis investigates starting systems for marine gas engines. Large combustion engines are usually started by means of pneumatic starting arrangements. The most common ways of starting a combustion engine with compressed air, are to use a pneumatic engine coupled to the engine flywheel, or to inject the air directly into the engine cylinders through a valve in the cylinder air. Pneumatic starting engines are prefered for gas engines with a prechamber.

The main challenge related to starting of gas fueled engines, is to avoid ignitable consentrations of gas outside the engine cylinders. Gas engines have an increased emission of unburned gas during starting and stoping. If the consentration of unburnes gases in the exhaust system of the combustion engine gets to large, the gas can be ignited by hot spots or sparks. In addition, we are conserned with the air consume of the starting system. The capacity of the starting system is regulated by class rules. To reduce the cost of the system, we want to reduce the air consume per start.

In this thesis, mathematical models of the combustion engine and the starting system are developed and validated against experimental results from starting tests of the real system. The objective is to give means for investigating, by using computer simulations, if the existing starting system can be improved. The validation showed that the model captures the main dynamics of the system.

To avoid large concentrations of unburned fuel mixtures in the exhaust system, the starting system is used to purge the engine before allowing fuel to the engine cylinders. In practice, the combustion engine is operated as an air pump which pumps air from the charge air system, via the engine cylinders, and to the exhaust system. A way of improving the safety of the starting sequence by purging the engine for a fixed number of rotations, is proposed. This method gives stricter control of the purged volume, but increases air consume.

To reduce air consume, it is advantegous to keep the engine speed low during purging. Three concept for reducing the engine speed are explored. The simulations indicate that the best performance is obtained by using an electrically controlled pressure control valve, in combination with a Proportional-Integral-Derivative feedback controller, to regulate the engine speed. This concept is extensively tested by means of simulations, to evaluate its robustness with regards to system uncertainties and different plant dimensions.

Acknowledgements

This master thesis is the result of the work carried out during the last semester of the master degree in marine technology, at Norwegian University of Technology and Science (NTNU). The thesis is a continuation of my work from the specialization project in marine control systems, autumn 2010. The subject of the thesis was proposed by Rolls-Royce Marine Engines Bergen, and was formulated in cooperation with people in the Technology and Development department of this company

First, I would like to thank my main supervisor Professor Roger Skjetne for valuable guidance on formulating and solving control problems and for sharing his experience on writing technical papers. Also, thanks to co-supervisor Dr. Ing Rune Nordrik at Rolls-Royce Marine: first for suggesting the topic of the thesis, then for valuable feedback with regards to the project formulation, and for being helpful on solving practical challenges related to the thesis work. Thanks to Erlend Vaktskjold at Rolls-Royce Marine for being a valuable discussion partner on the modelling on combustion engine, and for helping me carrying out the starting test. I would also like to thanks the rest of Rolls-Royce Marine Engines Bergen, the only manufacturer of combustion engines in Norway.

Last but not least, thanks to Kristine for making many nice figures and illustrations, for proofreading the manuscript, and for always being supportive.

NTNU Trondheim
Norwegian University of Science and Technology
Department of Marine Technology

PROJECT DESCRIPTION SHEET

Name of the candidate: Trond Inge Eide

Field of study: Marine control engineering

Thesis title (Norwegian): Modellering av startesystem for forbrenningsmotor

Thesis title (English): Modeling of combustion engine starting system

Background
Traditionally, large 4-stroke combustion engines are started by the aid of compressed air, either injected directly into the engine cylinders, or through a pneumatic starting engine coupled to the flywheel.

Modelling of the starting system requires considerations of the fluid dynamics and control of the starting engines air circuit. On the combustion engine side the inertial components of the shaft system, the mass of the reciprocating parts, friction in bearings and cylinders, and compression forces must be taken into account.

Work description
1. Give a brief description of the existing starting system of the Rolls-Royce Bergen engines, and its control.
2. Look at different concepts and control strategies for starting engines. Discuss advantages/disadvantages for the different concepts. Evaluation of alternative methods for starting large combustion engines. Consider class rules for starting systems.
3. Modeling of the engine shaft system and the air circuit and its control in relevant simulation software (Simulink/Matlab, GT-Suite). Discussion of the complexity and realism of the different parts of the model.
4. Define key parameters for the performance of the starting engine through evaluation of simulation results.

Tentative:
5. Define goals for optimum starting sequence.
6. Optimization of the starting sequence. Strategies for different plants (gas/diesel, genset/propulsion)

Guidelines
The scope of work may prove to be larger than initially anticipated. By the approval from the supervisor, described topics may be deleted or reduced in extent without consequences with regard to grading.

The candidate shall present his personal contribution to the resolution of problems within the scope of work. Theories and conclusions should be based on mathematical derivations and logic reasoning identifying the various steps in the deduction.

The report shall be organized in a rational manner to give a clear exposition of results, assessments, and conclusions. The text should be brief and to the point, with a clear language. The report shall be written in English (preferably US) and contain the following elements: Abstract, acknowledgements, table of contents, main body, conclusions with recommendations for further work, list of symbols and acronyms, references and (optional) appendices. All figures, tables, and equations shall be numerated. The original contribution of the candidate and material taken from other sources shall be clearly identified. Work from

other sources shall be properly acknowledged using a Harvard citation style (e.g. DCU). Any plagiarism is taken very seriously by the university, and any such practice will have consequences.

The thesis shall be submitted in 2 printed copies, each signed by the candidate. The final revised version of this project description must be included. The report must appear in a bound volume or a binder according to the NTNU standard template. Computer code and a PDF version of the report should be included electronically.

A 15 min. presentation (conference style) on your main results is expected to be delivered at a scheduled time around deadline.

Start date:	September 1, 2010	**Due date:**	As specified by the administration.
Supervisor:	Roger Skjetne		
Co-advisor(s):	None		

Trondheim, 24.08.2010

_____

Roger Skjetne
Supervisor

Contents

Nomenclature

α	[-]	PID filter coefficient
$\bar{u}$	[-]	Pressure set point
δ	[-]	Stribeck coefficient 2
Δ_ϕ	[rad]	Duration of combustion
ϵ	[m]	Absolute roughness
η_c	[-]	Combustion efficiency
κ	[-]	Heat capacity ratio
λ	[-]	Connecting-rod ratio
μ	[kg/(ms)]	Dynamic viscosity
μ_c	[-]	Coulomb friction coefficient
ω	[rad/s]	Rotational velocity
ω_d	[rad/s]	Disengagement speed
ω_s	[rad/s]	Stribeck coefficient
ω_{fo}	[rad/s]	Fuel-on speed
ω_{ref}	[rad/s]	Reference speed
ϕ	[rad]	Crank angle
ϕ_0	[rad]	Initial crank angle
ϕ_1	[rad]	Crank angle of first cylinder
ϕ_a	[rad]	Angle for closing of air valve
ϕ_e	[rad]	Angle for opening of exhaust valve
ϕ_p	[rad]	Purging crank angle
ϕ_s	[rad]	Crank angle for start of combustion
ϕ_{fc}	[rad]	Angle for closing of fuel valve
ϕ_{fo}	[rad]	Angle for opening of fuel valve
Ψ	[-]	Sliding mode function

ρ	$[kg/m^3]$	Density
ρ_f	$[kg/m^3]$	Fuel density
ρ_{atm}	[kg/m^3]	Atmosheric density of air
τ	[Nm]	Torque
τ_c	[Nm]	Coulomb friction
τ_e	[Nm]	Starting engine torque lowspeed side
τ_f	[Nm]	Friction torque
τ_p	[Nm]	Piston torque
τ_s	[Nm]	Static friction
τ_v	[Nm]	Viscous friction
τ_w	[Pa]	Wall shear
τ_{aux}	[Nm]	Load torque from auxiliary equipment
$\tau_{c,a}$	[Nm]	Combustion torque bound
$\tau_{p,a}$	[Nm]	Piston torque bound
τ_{wb}	[Nm]	Waterbreak torque
ε_1	[-]	Hyperbolic tangent function coefficient 1
ε_2	[-]	Hyperbolic tangent function coefficient 2
ζ_d	[-]	Notch filter damping 2
ζ_n	[-]	Notch filter damping 1
A	$[m^2]$	Area
a	[-]	Wiebe coefficient 1
A_d	$[m^2]$	Diaphragm area
A_n	$[m^2]$	Fuel nozzle flow area
A_p	$[m^2]$	Piston area
a_p	$[m/s^2]$	Piston acceleration
$A_{\omega,max}$	[rad/s]	Max amplitude of speed oscillations
B	[m]	Engine Bore
C_d	[-]	Discharge coefficient
c_v	[-]	Specific heat capacity
cr	[-]	Compression ratio
D	[m]	Diameter
e	[-]	Control error
f	[-]	Darcy friction factor

F_I	[N]	Inertia force
F_N	[N]	Normal force
F_p	[N]	Piston force
f_v	[-]	Viscous friction coefficient
G_g	[N]	Gas force
h_0	[-]	System transfer function
h_d	[-]	Delay transfer function
h_r	[-]	Controller transfer function
h_u	[-]	Plant transfer function
HV	[J/kg]	Heating value
I	[kgm^2]	Inertia
i	[-]	Gear ratio
K	[-]	Sliding mode gain 1
k	[-]	Fuel rack constant
K_d	[-]	Derivative gain
K_I	[-]	Integral gain
K_p	[-]	Proportional gain
L	[-]	Sliding mode gain 2
L_e	[m]	Equivalent length
m	[-]	Wiebe coefficient 2
m_f	[kg]	Fuel mass
m_p	[kg]	Piston mass
n	[-]	Number of engine cylinders
n_B	[-]	Number of cylinder banks
P	[Pa]	Pressure
P_d	[Pa]	Desired pressure
Q	[K]	Heat
Q_{in}	[K]	Heat released from combustion
R	[J/kgK]	Specific gas constant
r	[m]	Crank radius
Re	[-]	Reynolds number
S	[m]	Engine Stroke
s	[-]	Complex Laplace argument

T	[K]	Temperature
t	[s]	Time
T_0	[K]	Initial tank temperature
t_p	[s]	Purging time
$t_{d,f}$	[s]	Time delay fuel rack
$t_{d,v}$	[s]	Time delay starting valve
t_{fo}	[s]	Fuel on time
u	[-]	Control input
V	$[m^3]$	Volume
v_p	$[m/s]$	Piston velocity
v_s	$[m/s]$	Speed of sound
V_c	$[m^3]$	Combustion chamber volume
V_d	$[m^3]$	Displaced cylinder volume
V_{ex}	$[m^3]$	Exhaust manifold volume
V_{tot}	$[m^3]$	Total cylinder volume
V_t	$[m^3]$	Tank volume
w	$[m/s]$	Flow velocity
x_b	[-]	Mass fraction burned
x_p	[m]	Piston position
z	[-]	Gear teeth number

Chapter 1

Introduction

1.1 Background

All combustion engines rely on some sort of external power system to crank the engine and produce sufficient cylinder pressure for ignition of the fuel. In small automotive engines, electric starter motors are normally used. For larger engines, like the ones used in ships, the power demand is so vast that an electrical starting system powerful enough to accelerate the system would be unpractical large. Instead alternative starting systems with better power-to-size ratio is used.

This thesis deals with modelling and control of starting systems for large combustion engines. Particularly pneumatic starting systems, used for starting medium speed marine gas engines. Marine gas engines have been used since the early eightees, but the use of gas engines in ships and offshore structures are only starting to gain momentum these days. Increased focus on emissions from the ship industry, improvements in the engine technology, and improved availability of the fuel, are factors which contribute to the increased interest in gas and dual-fuel engines.

Seeing that the gas engine combustion technology differ from diesel engines on some points, the use of gas fueled engines in ships introduces some new challenges in the marine industry. Liquefied Natural Gas (LNG) is in general considered to be a safe fuel. However, if vaporized gas consentrations escape outside the engine cylinders, there is a risk that the gas can be ignited by hot surfaces, or sparks. Gas engines have an increased emission of unburned fuel during starting and stoping. Therefore, it is of great importance that precautions are taken during starting, to avoid igniteable concentrations of unburned fuel mixtures in the exhaust system of the engine.

1.2 System overview

The main task of the starting system is to accelerate the engine to the speed required for ignition. The engine should then fire and run up to self-sustaining speed and the starting system can be shut-off. In addition, the starting system can be used to purge the exhaust system prior to allowing fuel to the cylinders, to eject any unburned fuels.

For safety reasons the starting systems used in ships are subject to class rules. Obviously, the loss of power resulting from inability to start the engine, has safety implications. The class rules regulate the capacity of the energy storage component of the starting system. For pneumatic systems this means that the air tanks, used to store compressed air, should have enough capacity for a minimum number of starts before reloading. This leads to a concern with energy efficiency. Reduced energy consumption per start means that smaller tanks can be used, resulting in reduced installation cost and space requirements. Since the space in the engine room of a ship usually are limited, this is an important factor.

When cranking the engine with the starting system, air is pumped from the charge air system of the engine, through the engine cylinder, and to the exhaust system. To eject any renemnants of unburned fuel in the exhaust system priot to starting, we can add a delay before starting the fuel supply to assure that the volum pumped through the system is large enough. This is termed purging. In practice, the combustion engine operate as an air pump driven by the starting engine.

Increased purging time might increase the safety of operation, however, this also increases the air consume per start. To design a starting system which is considered safe, while reducing the air consume of the system, it is advantageous to be able to accurately control the engine speed during the periode when the starting system is active.

To accelerate the engine the starting system needs to overcome the resistant forces of the combustion engine. These include friction in bearings and cylinders, the inertial effects of the shafting and the load from compression/expansion of the air in the cylinders. The magnitude of the resistance depend on properties specific to the each plant and engine type, like compression ratio, mass moment of inertia of the rotating masses, number of cylinders etc. These are properties that are difficult to alter. Instead optimization of the starting sequence needs to focus on the components of the starting system itself, and their efficiency. However, the changing properties of the combustion engine must be taken into considerations if one wants to design a redundant starting system.

1.3 Objectives

To summarize the previous section, the starting sequence of a gas fueled engine is a critical part of the engine operation. This is due to the risk of igniteable concentraton of unburned fuel in the exhaust system. To reduce the risk of ignitiable fuel mixtures outside the engine cylinders, air can be pumped through

the system by rotating the engine with the starting system before allowing fuel to the cylinders. However, there is a contradictory relationship between increasing the safety by using a long purging period, and reducing the air consume per start.

The main motivation for this study is to design a starting sequence which is considered safe, while keeping the air consume at a minimum. To obtain this, the potential of using speed control of the engine during starting is investigated. Different methods for controlling the engine speed with the starting system are considered and evaluated, by using computer simulations. To give means for evaluating the performance of the different starting sequence designs, simulation models of both the starting system and the combustion engine are developed.

1.4 Structure of the report

The thesis starts with a more in detail system description of the starting system and the combustion engine, in Chapter 2. The components which constitute the starting system and their properties are described, to increase system understanding. Some background is given on gas fueled engines, and differences from convential diesel engines are discussed. Focus is put on the properities which is important during starting. In addition, different control valves and their characteristics are investigated, to give means for controlling the torque from the starting system.

Chapter 3 gives a theoretical investigation of the forces acting on the combustion engine. A simulation model of the engine is developed, for the purpose of simulating engine starting. Several simplifications are made, however, the model is assumed to capture the main dynamics of the engine.

In Chapter 4 the theoretical nature of the starting system is investigated. A brief study of the fluid- and thermodynamic theory which describes the properties of the system are given, and a mathematical model of the system is developed.

The performance of the models developed in chapters 3 and 4, are investigated in Chapter 5, where simulation result are validated against data from experiments. Also, test setups for starting tests and friction measurements are described in this chapter.

Chapter 6 deals with control design and ways of improving the existing starting sequence. The control objectives are stated, and a problem statement is given. On the basis of the problem statement, three different control designs are developed, and simulated against the system model to evaluate their performance.

In Chapter 7 extensive simulation tests are presented, to evaluate the robustness of the starting sequence and the best performing controller from Chapter 6. The empasize is put on the robustness of the system with regards to system uncertainties and varying engine dimensions

Finally, in Chapter 8 a conclusion from the work done in the thesis is presented, and recommendations for further work is given.

Chapter 2

System Description

The total engine installation consists of a liquefied natural gas (LNG) fueled internal combustion engine, started by a pneumatic starting system. The starting system acts on the engine flywheel, to accelerate the engine to ignition speed.

In general starting systems for combustion engines can operate on different energy sources. The most common types are electric, hydraulic and pneumatic starting systems. However, all types of starting systems operate on the same basic principle. Energy has to be stored, and then released. The type of starting system used in a specific installation is decided by a range of factors, like the amount of energy needed, the operation conditions, etc.

2.1 Starting system

The vast majority of starting systems for large combustion engines are powered by air. The dominance of pneumatic systems can be partially explained by their high power-to- size and power-to-weight ratio. Another reason is the fact that compressed air has many other uses on board ships and at power plants, e.g. for operating valves, for pneumatic tools, and for control and automation of various machinery. In other words the infrastructure, like compressors, piping, receivers etc., are already in place.

Air is also chosen for safety reasons. Air systems do not produce sparks and have low heat build-up. In contrast to electric starters air is also unaffected by temperature.

Mainly two types of pneumatic starting systems are used;

1. Systems with pneumatic starter engines geared to the main engine flywheel,
2. Systems with timed injection of air directly into the engine cylinders, through a valve in the cylinder head.

Type (1) tend to be used in smaller medium speed engines (<5000 kW), while type (2) is often preferred for larger engines. Type one is also prefered for engines

with a prechamber, due to limited space for a starting valve in the cylinder head. This thesis focus solely on starting systems with a starting engine.

2.1.1 System overview

A circuit diagram of the pneumatic starting system is given in Figure 2.1. The air bottles, at the bottom left corner, are loaded to the maximum operation pressure of 30 [bar] by the compressors. Air pipes runs from the receivers to a pneumatic starting engine, where the pressure is converted to torque. A particle filter is fitted in the piping to prevent particles from entering the starting engine.

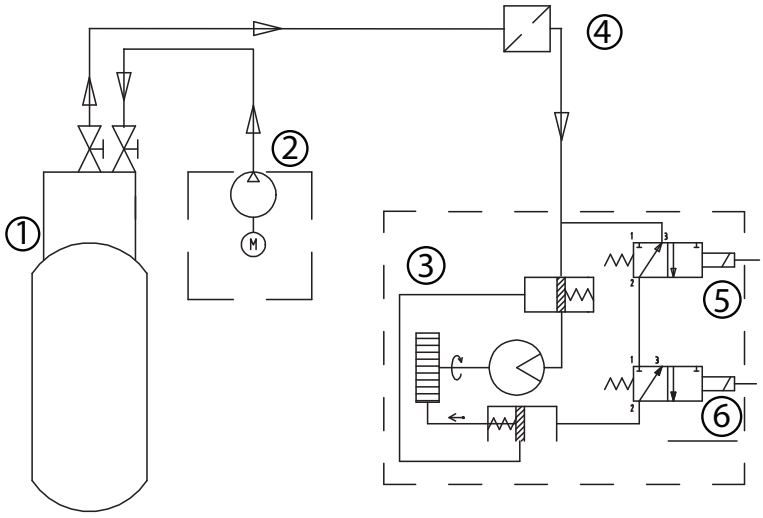

Figure 2.1: Circuit diagram of the starting system.(1)Air bottle, (2)Compressor, (3)Starting engine, (4)Particle filter, (5) and (6)Release valves, [Courtesy: Rolls-Royce, 2010].

The main release valve is a 3/2-way solenoid valve, which can be remotely controlled from the engine control room. When the release valve is opened, the air pressure acts on a piston which pushes the pinion forward in axial direction, to engage with the flywheel of the combustion engine. Once the starting engine is engaged, air flows back to equalize the pressure on the back side of the second piston, which opens the main flow to the starting engine. The engine rotates as the pressure exerted on the internal element of the engine, creates rotational motion.

The classification societies specify requirements to the number of starts which the starting system should have capacity for before reloading the air bottles. In addition, for redundancy, all major classification companies require that the starting air capacity shall be divided between at least two air receivers, and two compressors.

2.1.2 Starting Engine

Pneumatic engines are usually categorized by the type of internal element used to produce torque. The most commonly used pneumatic engines for starting purposes, are gear, vane, and turbine type engines.

The pneumatic starting engine considered in this thesis, is a gear type pneumatic engine. A cross-section of the engine is shown in Figure 2.2. The engine consists of two matched gears enclosed in a case. Compressed air flows from the top of the housing and exits at the bottom, and produces torque from direct action of the pressurized air on the gears. Both gears rotate. One of the gears is mounted on a driveshaft with a pinion in one end. When the engine is engaged, the pinion is geared to the flywheel of the combustion engine.

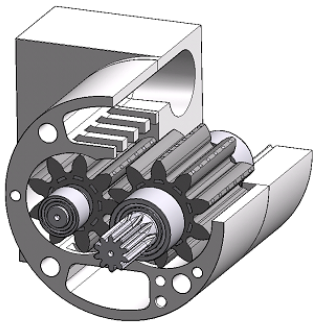

Figure 2.2: Cross section of the starting engine.

The ideal torque-speed characteristic of the engine is given by the solid line of Figure 2.3. The torque decreases linearly with speed for a fixed working pressure, giving maximum torque at zero speed. In practice, however, the torque curve tends to fall for speeds close to zero because of break-away friction. The ideal power-speed relationship, given by the dash-dotted line, follows a curved path with zero power at zero and free speed, and max power halfway between these.

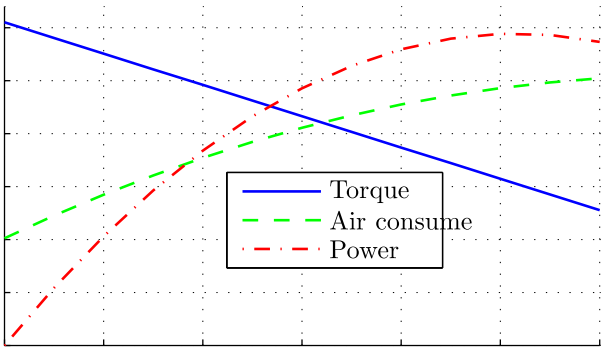

Figure 2.3: Starting engine characteristics vs. speed.

The steepness of the torque curve and the width of the power curve can be altered by adequate gearing. Higher gear-ratio gives steeper torque curve and vice-versa. The principal torque and power characteristics shown in Figure 2.3, are shared by all types of pneumatic engines.

The air consume as a function of speed is given by the dashed line. Obviously the air consume increases with speed for a fixed pressure. The starting engine is speed limited by a governor, to prevent damage to the engine from excessive friction when over speeding.

2.1.3 Current starting sequence

Since the release valve of the existing starting system is a two-position valve, that is, it can only be completely open or completely shut, there is no means of actively controlling the torque from the starting engine. However, feedback from the engine speed measurements are used to take logic-based descisions on whether to start/stop the starting system and the fuel gas supply to the combustion engine.

Reference is made to Figure 2.4, which show experimental results for the combustion engine speed, during a typical starting sequence of the Rolls-Royce Bergen C26:33L9 Gas engine. The fuel-supply logic are defined by two fixed parameters programmed into the *Programmable Logic Controller (PLC)* of the engine. The *fuel-on speed* ω_{fo}, is used as a lower limit for starting the fuel supply. It should be defined such that the pressure and temperture in the engine cylinders at this speed, is sufficient for the combustion to take place. However, the fuel supply to the engine is not started when the engine crosses the fuel-on speed. Instead a delay, defined by the *purging time* t_p, is applied to the fuel-supply. The fuel supply logic becomes,

$$\text{fuel supply} := \begin{cases} \text{off} & \textbf{if } \omega < \omega_{fo} \vee (t - t_{fo} < t_p, \\ \text{on} & \textbf{if } \omega \geq \omega_{fo} \wedge (t - t_{fo}) \geq t_p \end{cases} \tag{2.1}$$

where t_{fo} is the time when the fuel-on speed is reached, and $\vee$ and $\wedge$ is the logic symbols for *or* and *and*.

The delay introduced by the purging time is a safety precaution. If the combustion in LNG engines is incomplete, e.g. if there is insufficient oxygen in the cylinders for the fuel to react completely, some of the fuel mixture will escape to the exhaust system of the engine. In case of misfire, all the fuel gas is ejected into the exhaust system. Liquefied natural gas vapors at lower temperatures than diesel. If the consentration of unburned fuel in the exhaust system gets to high, it may form ignitable vapor consentrations. The consequences of contact between these highly explosive gases, and sparks, or hot spots in the exhaust system, can be severe.

LNG engines have an increased emission of unburned fuels during starting and stoping (Kviste Jensen [2007]). Especially after a failed starting attempt, the concentration on unburned fuel mixtures in the exhaust system can be high. Therefore, it is necessary to purge any renemnants of unburned fuel out of the

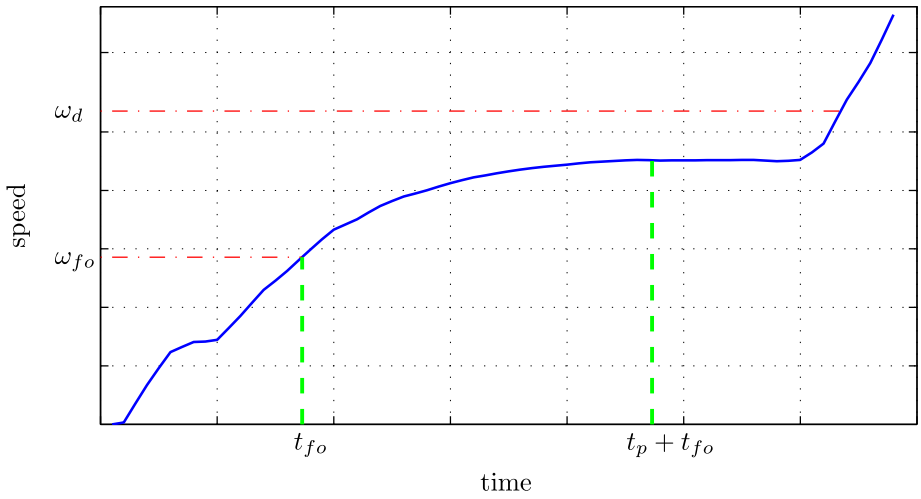

Figure 2.4: Experimental result for the engine speed during starting.

exhaust system, prior to starting the fuel supply. During starting, the combustion engine is used as an air pump to purge the exhaust system before allowing fuel to the cylinders. When the engine is rotated by the starting engine, air is pumped from the air intake of the engine, through the air receivers, cylinders and the exhaust system, to the exhaust pipe. The delay caused by the purging time, is introduced to make sure that a large enough volume is purged.

From Figure 2.4, we see that there is also a time delay between starting the fuel supply at $t_p + t_{fo}$, and the increase in speed due to combustion. This is obviously due to the fact that it takes some time before ignition is obtain in all engine cylinders.

The logic for starting and stoping the starting system, is given by

$$\text{starting system} := \begin{cases} \text{on} & \textbf{if } \omega < \omega_d, \\ \text{off} & \textbf{if } \omega \geq \omega_d, \end{cases} \tag{2.2}$$

where ω_d is the disenagement speed of the starting system. The value for the disengagement speed is taken as the speed where we assume that the torque from the combustion forces is large enough to accelerate the engine, without the aid of the starting system.

2.2 Combustion engine

The combustion engine is a multi-cylinder 4-stroke, gas-fueled engine. The basic architecture of a multi-cylinder in-line engine is shown in figure 2.4. The pressure in the engine cylinders, resulting from the combustion process, exerts a force

on the pistons. This force is converted to a torque through the connecting-rod mechanism.

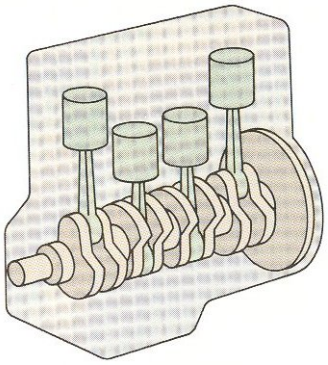

Figure 2.5: Basic architecture on an inline reciprocating engine.

The total torque output from the engine are not smooth, but oscillate with an amplitude dependent on the cylinder geometry and the number of engine cylinders. For a 4-stroke engine the frequency of the oscillations are given by,

$$\frac{n\omega}{2}[rad/s], \tag{2.3}$$

where n is the number of cylinders for the engine, and ω is the rotational velocity in [rad/s]. To get a smooth rotational velocity, flywheels with relative large inertias are used. However, at the low speeds encountered during starting, the influence of the torque fluctuations will be significant.

Reciprocating gas-fueled engines have been extensively used for land based power generation for many years. The first ships using LNG as bunker, were built in the early 1980s (Eidang and Haavik [2000]). However, the use of gas engines in the marine marked have been limited, and almost exclusively for passenger ferries transiting between fixed destinations. Due to increased focus on emissions from ships and advances in the technology, the interest in gas engines is increasing, and the marked for marine gas engines is growing. Recently, marine gas engines have been sold for use in many different ship types. E.g. supply vessels, fishing vessels, cruise vessels and container ships.

Gas engines gives reduced carbon dioxide, nitrogen oxides and particles emssions compared to diesel engines, and almost completely eliminates sulfur and particle emissions (Woodyard [2009]). The emission of unburned methane is somewhat increased compared to diesel, but new technology is being developed for reducing this emission.

2.2.1 Combustion technology

The combustion technology used in gas engines differ from conventional diesel engines on a number of points. In contrast to diesel engines, which ignites solely

on the the heat and pressure created by the compression in the cylinders, gas fueled engines need some sort of ignition system to provide sparks for ignition. The air/fuel ratio window where the gas is able to ignite, is relativly narrow compared to other fuels. Therefore it is important to be able to accurately control the air/fuel ratio in the cylinders. A non-optimal air/fuel ratio, e.g. a to rich mixture, increases the chance of misfire, which can results in emission of unburned fuels.

In diesel engines, the fuel is injected directly into the combustion chamber when the piston is close to the top positon. In contrast to this, most gas engines operate with a premixed air−gas mixture in the combustion chamber. That is, the gas fuel is injected into the air intake and mixed with air, prior to being drawn into the cylinders when the intake valve is open.

The principal of operation of the Rolls-Royce Bergen gas engines is shown in 2.7. In addition to the fuel supply control system, the air supply is controlled by using *Variable Turbocharger Geometry (VTG)* and throtteling of the flow to the air receiver.

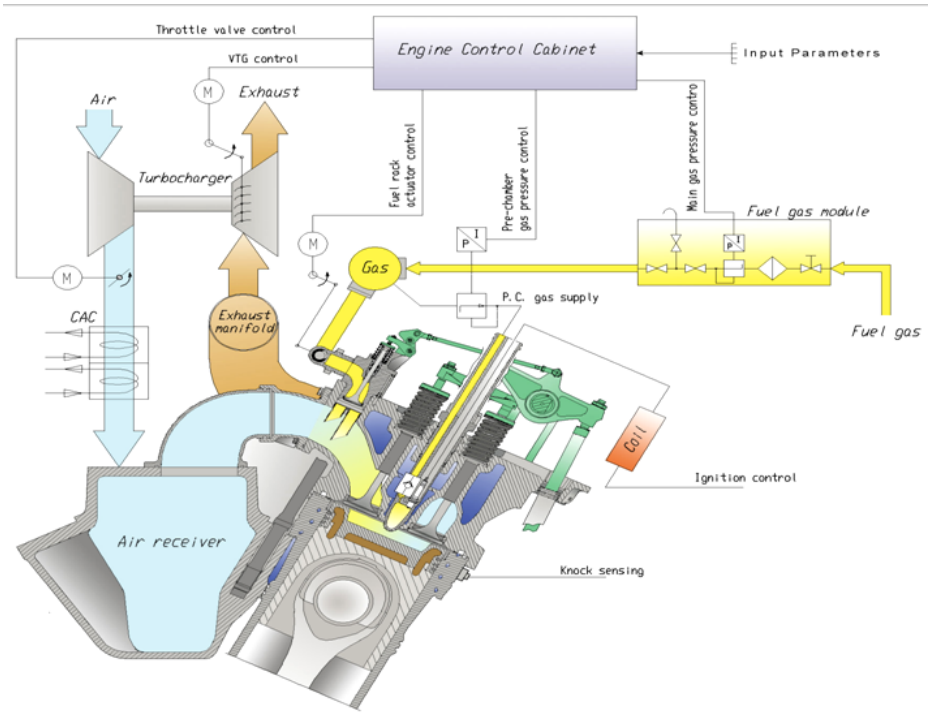

Figure 2.6: Principal of operation of the Rolls-Royce Bergen Gas engines.

The engine operates on the lean-burn principle. That is, the air/fuel ratio is kept higher than the stochiometric ratio needed to obtain complete combustion. Pure gas is injected into a prechamber, which is a small chamber equipped with a spark plug, connected to the main combustion chamber. When the lean air/fuel mixture in the main combustion chamber are compressed, some of it is pushed

into the prechamber and a richer, igniteable mixture is formed. The spark plug ignites the rich mixture in the prechamber, and the ignition discharge from the prechamber, ignites the leaner mixture in the combustion chamber.

The pre-chamber technology enables the use of leaner mixture, since the main mixture don't have to be igniteable. Lean operation gives increases efficiency and specific power, and reduced emission (Woodyard [2009]).

2.2.2 Charge air and exhaust system

As stated in Section 2.1.3, incomplete combustion of the fuel gas, or misfire, results in emission of unburned fuel-mixtures into the exhaust system. Since the exhaust system often contains renemnants of unburned fuel before start, it is necessary to flush the system prior to start. A Rolls-Royce Bergen Gas engine with the complete exhaust system is shown in 2.7.

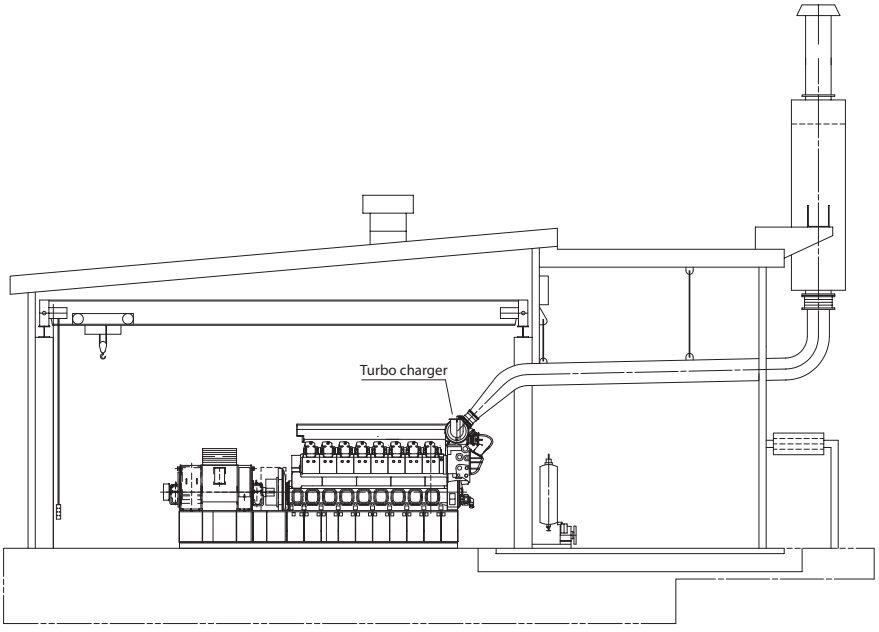

Figure 2.7: Exhaust system of Rolls-Royce Bergen Gas engines, [Courtesy: Rolls-Royce, 2010]].

The part of the exhaust system on the downstream side of the turbocharger, are usually equipped with some sort of fan or pump which flushes this part of the system. However, the exhaust manifold, between the engine cylinders and the turbocharger, needs to be purged by the starting system. A principle drawing of the charge air and exhaust system on the engine side of the turbocharger is shown in 2.8. By rotating the engine with the starting system, air is pumped from the charge air receiver through the cylinders and into the exhaust manifold. A four-stroke engine needs two rotations to pump a volume equal to its total

cylinder volume, into the exhaust system. To pump a volume equivalent to the exhaust manifold volume through the system, the engine must be rotated

$$n = \frac{2V_{ex}}{V_{tot}}, \tag{2.4}$$

rotations, where V_{ex} is the exhaust manifold volume and V_{tot} is the total cylinder volume.

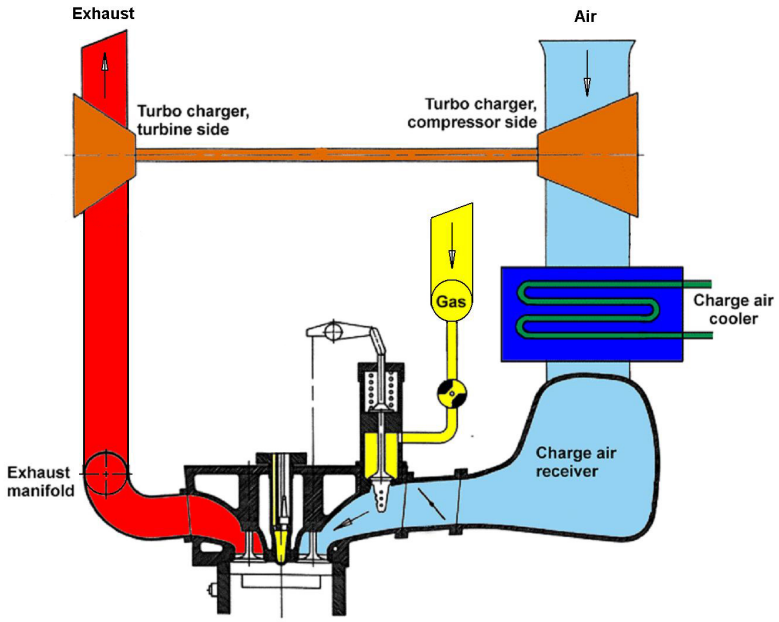

Figure 2.8: Principal sketch of cylinder, charge air system, and exhaust system.

2.3 Control valves

This thesis investigates the potential for improving safety of the starting sequence and reducing the starting system cost, by using automatic control. The torque input from the starting engine, is a function of its rotational velocity and supply pressure. To enable active control of the torque from the starting engine, we need a control valve to control the supply pressure.

Pneumatic control valves are described e.g. in Beater [2007] and Pinches and Callear [1996]. Seeing that we want to control the supply pressure to the starting engine, we want to use a pressure control valve. Pressure control valves are defined as valves "whose function is to control pressure" (Beater [2007]). This usually means reduction of the supply pressure by throtteling. By reducing the flow area the downstream flow rate increases, which leads to a reduction of the downstream pressure.

2.3.1 Characteristics of pressure control valves

For ideal pressure control valves, the downstream pressure is independent of the upstream flow rate and pressure, for ratios of downstream/upstream pressures lower than one. For real valves supplied with a constant pressure, the downstream pressure tends to fall when the upstream flow rate increases. An example is shown in the left graph in Figure 2.9. For constant upstream flow rate, the downstream pressure tends to fall when the pressure ratio gets to close one, as shown in the right graph in the figure.

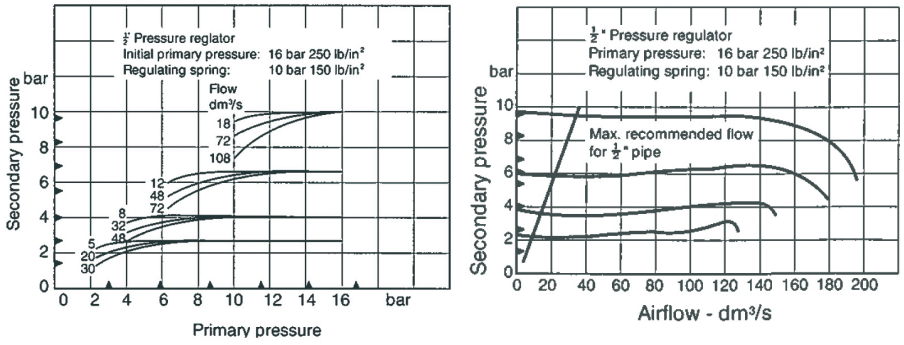

Figure 2.9: Examples of pressure/flow and pressure-ratio characteristics of a pressure control valve [Courtesy: Pinches and Callear, 1996]].

The characteristics of the pressure/flow curve and pressure ratio curve is heavily dependent on the internal design and the size of the valve. High pressision pressure control valves are available for applications were the pressure must be controlled within tight tolerances. In general the cost of the valve and the complexity of the design, increases with the requirements for precission.

2.3.2 Types of pressure control valves

Pressure control valves are categorized by the type of actuator used to control the flow area, whether they can be remotely controlled or not, and whether they are of relieving or non-relieving type. Relieving type valves releases some of the compressed air to the atmosphere if the downstream pressure is above the set point. Since we are conserned with the air consume of the system, we want a non-relieving valve.

A simple form of pressure control valve, is a springe controlled valve. This is a self-regulating valve which uses downstream pressure to control the valve opening. In steady state, there is a balance between the spring force and the downstream pressure. Usually the pressure setpoint of the valve can be controlled manually, by adjusting the spring force. However, there is no means of actively changing the setpoint with an electric controller.

For automatic control of the starting engine torque, we need an electrically operated pressure control valve. Electrically operated valves uses a proportional solenoid, which generates a force proportional to the electric signal. Similarly to spring controlled valves, the solenoid force balances the the downstream pressure in steady state operation. High precission is achived for valves with a pressure sensor, and an internal feedback from the upstream pressure.

Chapter 3

Combustion engine model

To crank the engine, the starting system need to overcome the resisting forces of the combustion engine. Thus, to simulate engine starting, it is necessary to study the components that constitute the forces acting on the engine. In this chapter, a simplified mathematical model of these forces are developed. Although several simplification are made, the model captures the main dynamics related to starting of the engine. As such, it should facilitate a study of the parameters effecting the performance of the starting system.

The main torques acting on the engine crankshaft during start-up, can be split into the following components:

1. The external torque from the starting-system, e.g. the starting engine. This will be denoted τ_e.
2. The torque from the engine piston τ_p, acting on the crankshaft through the connecting-rod mechanism.
3. The friction forces from the rotating and reciprocating parts of the engine, and the friction from the driven equipment (generators, gears etc.) τ_f. This includes both friction and load from auxiliary equipment driven from the crankshaft, like fuel and lubricatio pumps, and the valve-train.

The forces acting on a 4-cylinder generator set, is illustrated in Figure 3.1, where the friction surfaces are marked red. The piston forces, F_p, are coverted to torque through the crank mechanism of the connecting-rod.

The load and the friction from the auxiliary equipment, denoted by τ_a in Figure 3.1, usually act on the crankshaft through a gearwheel or some sort of belt or chain drive. If the load from the auxiliary equipment is added to the total friction forces τ_f the total torque acting on the shaft system can be found from

$$\tau = \tau_e - \tau_f + \tau_p. \tag{3.1}$$

If the flexibility of the rotating masses are neglected, the inertia of the shaft system can be modelled as one lumped mass I. The dynamics of the rigid shaft

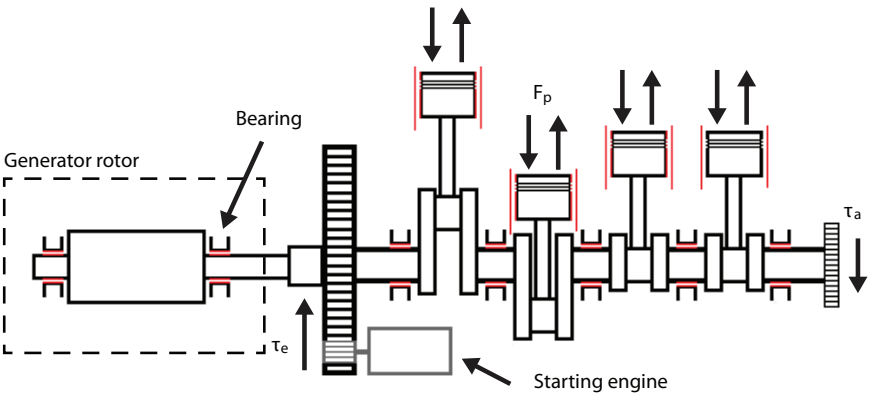

Figure 3.1: Illustration of the forces acting on a 4-cylinder engine during start-up.

system is governed by Newtons second law of motion for rotation, which states that the inertia force is equal to the sum of the torques acting on the system

$$\tau = \dot{\omega} I. \tag{3.2}$$

Inserting the expression for the total torque from Eq. 3.1 and rearranging, we arrive at a 2nd Order state-space model of combustion engine

$$\begin{aligned} \dot{\phi} &= \omega, \\ \dot{\omega} &= -\frac{1}{I}\tau_f + \frac{1}{I}\tau_p + \frac{1}{I}\tau_e, \end{aligned} \tag{3.3}$$

where the state variables are the angular position of the crankshaft ϕ relative to top dead centre of cylinder one, and the angular speed of the crankshaft ω. In the following sections the different load components in Eq. 3.3 are discussed, and an expression for each of these is deduced.

3.1 Piston torque

The torque component resulting from the forces acting on the engine pistons, is in this thesis denoted *piston torque*. The total force F_p acting on the piston,

stems from different sources. During an engine cycle the pressure rise in the cylinders result in gas forces F_g, acting on the pistons. In addition, when the pistons are accelerated, the piston motion results in an inertia force F_I. The total piston force from one piston is found by superposition of these contributions

$$F_p = F_g + F_I. \tag{3.4}$$

The forces are converted to a torque component τ_p acting on the crankshaft through the connecting-rod mechanism. The nature of the connecting-rod mechanism is investigated next.

3.1.1 Connecting-rod mechanism

The connecting-rod mechanism of the engine translates the linear motion of the piston to rotational motion in the crankshaft. To study how the piston forces are converted to crankshaft torque, we need to study this mechanism. A detailed derivation of the equations in this section are found in Appendix A. Here only the results that are of direct relevance to our model are repeated.

The relationship between the position of the piston x_p and the crank angel ϕ is, as can be seen from Figure 3.2, a purely geometric relationship, and can be determined through the law of cosine.

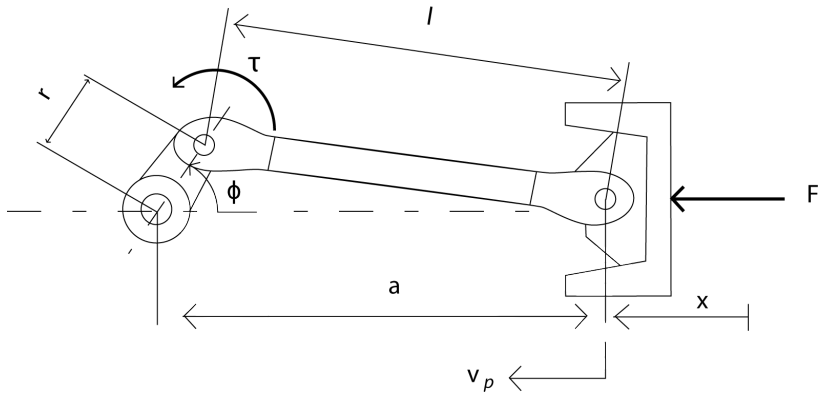

Figure 3.2: Illustration of the forces acting on a 4-cylinder engine during start-up.

The position is often expressed in terms of the connecting rod ratio λ, defined as the crank radius r divided by the connecting rod length l. The piston position relative to its uppermost position as a function of crank angle, is given by

$$x_p(\phi) = f_1(\phi) = r\left[1 - cos(\phi) + \frac{1}{\lambda}\left(1 - \sqrt{1 - \lambda^2 sin^2(\phi)}\right)\right]. \tag{3.5}$$

The velocity v_p of the piston as a function of the crankshaft velocity ω can be found by taking the derivative of 3.5 with respect to time, which gives

$$v_p(\phi,\omega) = f_2(\phi)\omega = r\left[sin(\phi) + \frac{1}{2}\frac{\lambda sin(2\phi)}{\sqrt{1-\lambda^2 sin^2(\phi)}}\right]\omega. \tag{3.6}$$

Similarly, the piston acceleration can be found by taking the second derivative of 3.5 with respect to time:

$$a_p(\phi) = f_3(\phi)\omega^2 = r\left[cos(\phi) + \frac{\lambda cos(2\phi)}{\sqrt{1-\lambda^2 sin^2(\phi)}} + \frac{\lambda^3 sin^2(2\phi)}{4\sqrt{1-\lambda^2 sin^2(\phi)}^3}\right]\omega^2. \tag{3.7}$$

The relationship between force on the piston and torque on the crankshaft, can be developed through conservation of power, or by decomposition of the piston force. The torque is given by

$$\tau_p(\phi) = f_2(\phi)F_p = r\left[sin(\phi) + \frac{1}{2}\frac{\lambda sin(2\phi)}{\sqrt{1-\lambda^2 sin^2(\phi)}}\right]F_p. \tag{3.8}$$

It can be observed that the trigonometric function $f_2(\phi)$ defining the transfer function between torque and the piston force, is equal to the transfer function between piston velocity and the rotational speed.

3.2 The Four-stroke cycle

As the pistons reciprocate in the engine cylinders, the cylinder pressure fluctuate. This give rise to varying gas forces acting on the pistons. The course of the cylinder pressure is defined by the engine cycle. The four-stroke cycle, corresponding to two rotations of the crankshaft, is illustrated in figure 3.3. If we assume that the exhaust and intake valve close exactly at top-dead and bottom-dead-center, the 4-stroke cycle can be split into the following four steps,

1. Expansion stroke: $0\,^\circ < 180\,^\circ$. Both valves are closed, as the piston travels down. The pressure in the cylinder at the top dead center is positive, which gives a positive force on the piston, and a corresponding positive torque on the crankshaft.
2. Exhaust stroke: $180\,^\circ < 360\,^\circ$. The exhaust valve opens at bottom dead centre and air flows out of the cylinders as the piston travels up. This gives a slight excess pressure in the cylinders, giving a negative contribution to the engine torque.

3. Intake stroke: $360\,^\circ < 540\,^\circ$. The intake valve opens and air flows into the cylinders as the piston travels down. This gives a slight under pressure in the cylinders, contribution negatively to the torque.

4. Compression stroke: $540\,^\circ < 720\,^\circ$. The intake valve closes at bottom dead centre and the air in the cylinders are compressed. Also here the contribution to the torque is negative.

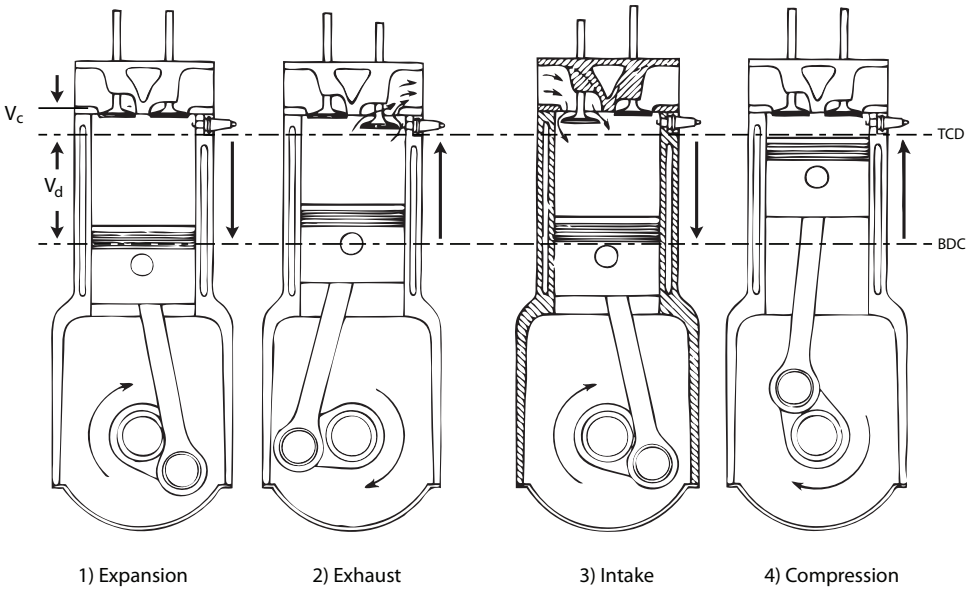

Figure 3.3: The steps of the four-stroke cycle, [Courtesy: Heywood, 1988]].

In case of combustion, the engine fires close to top-dead center during the expansion stroke. In this case the positive torque contribution during the expansion torque will exceed the negative torque from the compression stroke. In case of no combustion, the magnitude of the positive torque during the expansion stroke is equal to the magnitude of the negative torque during the compression stroke. If we neglect thermal losses and the pumping losses from the exhaust and intake stroke, the mean work over an engine cycle is zero in case of no combustion, and positive in case of combustion.

However, during the first revolution of the engine after starting, the engine has not built up a positive cylinder pressure from the compression stroke when the expansion stroke starts. This means that during the first revolutions of the engine, the mean work from the gas forces will be negative.

The work done in the cylinder over an engine cycle is often illustrated by means of pressure-volume diagrams. By plotting the pressure as a function of volume, the total work over the cycle can be found by taking the integral of the enclosed area. Pressure-volume diagrams are shown in Figure 3.4. The left diagram show the pressure volume diagram in the case of combustion. The combustion leads to a constant volume pressure increase. The middle and right plot show the diagram for no combustion, where the right plot is for the first engine

rotation. The expansion stroke for the first rotation leads to a pressure decrease which gives a negative work over the cycle, whereas the following rotations, as illustrated by the middle figure, gives zero mean work.

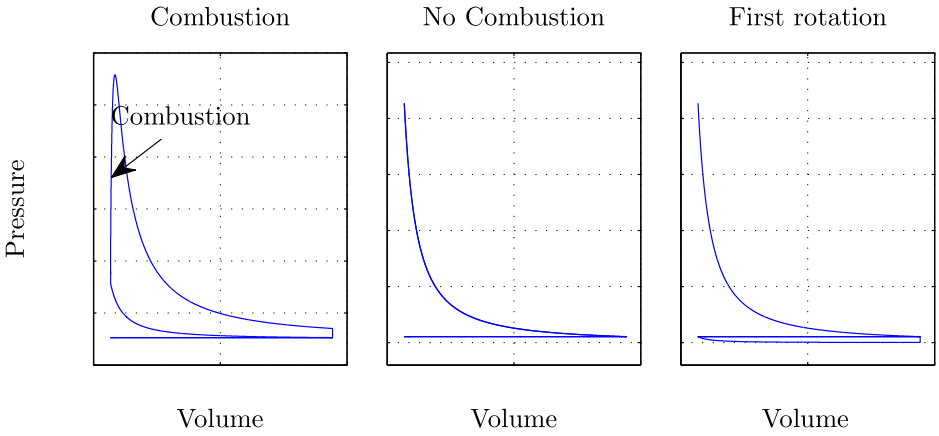

Figure 3.4: Pressure volume diagrams for combustion (left plot), no combustion (middle plot), and first engine rotation (right plot).

The valves of modern engines usually do not close exactly at top and bottom dead centre. Often the intake valve is closed some degrees before or after bottom dead centre to improve thermal efficiency or reduce emission. The loss of air charge is compensated with supercharging. In addition, the exhaust valves will often open before bottom dead centre to avoid pump work against high cylinder pressure during the first part of the exhaust stroke.

3.2.1 Gas forces

The forces that the cylinder pressure exerts on the piston are called gas forces. The contributions to the total gas force can be divided into

1. The restoring gas force due to the pressure build-up from compression/expansion of the charge air in the cylinders.
2. The gas force from the pressure build up due to heat released during combustion.

Before ignition of the fuel-gas, only component (1) is present. We assume that the cylinder pressure for the period where the valves are open is equal to atmospheric pressure. In reality it will be slightly lower during the intake stroke, and slightly higher during the exhaust stroke. However, at relatively low engine speeds this deviation is neglectable.

An expression for the total cylinder pressure for the period with closed valves can be developed from the first law of thermodynamics (conservation of energy), which states that the internal energy U in the cylinder, is equal to heat supplied

minus work done

$$dU = \delta Q - \delta W, \tag{3.9}$$

where Q is heat and W is work. The work done is equal to the integral of the pressure with respect to volume, PdV. The internal energy is equal to the integral of the specific heat capacity c_v times mass, with respect to temperature ([Ferguson and Kirkpatrick, 2001]). This yields

$$mc_v dT = \delta Q - PdV. \tag{3.10}$$

If we assume ideal gas behaviour, we can use the ideal gas law. The ideal gas law in differential form is

$$mdT = \frac{1}{R}(PdV + VdP), \tag{3.11}$$

where R is the specific gas constant. Inserting this in 3.10, and solving for pressure yields

$$dP = \frac{R}{c_v}\frac{1}{V}\delta Q - \frac{P}{V}dV(1 + \frac{R}{c_v}). \tag{3.12}$$

The heat capacity ratio κ is equal to $\frac{R}{c_v} + 1$. Per time unit the differential equation then becomes

$$\dot{P} = \frac{\kappa - 1}{V}\dot{Q} - \kappa\frac{P}{V}\dot{V}. \tag{3.13}$$

The first term in the equation corresponds to the combustion forces, whereas the second term corresponds to the restoring force. By solving the differential equation, we can find the gas force by multiplying the pressure by the piston area A_p

$$F_{gas} = A_p P. \tag{3.14}$$

However, to solve the differential equation we need expressions for the change in volume $\dot{V}$ and the heat release rate $\dot{Q}$. The variable cylinder volume is given by the sum of the combustion chamber volume V_c, which is equal to the cylinder volume when the cylinder is at top dead centre, and the variable volume V_d

defined by the position of the piston (ref. Figure 3.3). The total volume can be calculated as a function of the crank angle from

$$V(\phi) = V_c + \frac{x(\phi)}{2r} V_d. \tag{3.15}$$

Inserting the expression for the piston position $x(\phi)$ from Eq. 3.15 we get

$$V(\phi) = V_c + \frac{f_1(\phi)}{2r} V_d. \tag{3.16}$$

The change in volume can be found by differantiating the equation with respect to time. This yields

$$\dot{V} = \omega \frac{dV}{d\phi} = \omega \frac{f_2(\phi)}{2r} V_d, \tag{3.17}$$

where the function $f_2[\phi]$ is given by Eq. 3.6.

The heat supplied to the cylinders, depends on the amount of fuel injected into the cylinders. An expression for the heat release in terms of the amount of fuel injected, is derived in the next section.

3.2.2 Combustion heat release

The heat release rate in an engine, is defined as the "rate at which the the chemical energy of the fuel is released by the combustion process" ([Heywood, 1988]). The heat release curve in an internal combustion engine as a function of crank angle, typically have a characteristic S-shape, similar to the one showed in Figure 3.5. An often used functional form of the curve, which has shown good agreement with experimental data, is the so-called Wiebe function

$$x_b(\phi) = 1 - exp\left[-a\left(\frac{\phi - \phi_s}{\Delta_\phi}\right)^m\right], \tag{3.18}$$

where ϕ_s is the crank angle at the start of the combustion process, Δ_ϕ is the total combustion duration, and a and m are adjustable coefficients. The Wiebe function goes from a value of zero at $\phi = \phi_s$, to one at $\phi = \phi_s + \Delta_\phi$. A model of the heat release ratio $\dot{Q}$ are found by differentiating the Wiebe function with respect to time and multiplying with the total heat released from the combustion process, Q_{in} ([Ferguson and Kirkpatrick, 2001]). This yields

$$\dot{Q} = \omega \frac{dx_b(\phi)}{d\phi} Q_{in} = \omega \left[a\left(\frac{\phi - \phi_0}{\Delta\phi}\right)^m \frac{m+1}{\Delta\phi e^{a\left(\frac{\phi-\phi_0}{\delta\phi}\right)^{m+1}}}\right] Q_{in} \tag{3.19}$$

If we assume complete combustion of all the fuel supplied to the cylinders Q_{in}, can be found by multiplying the mass of the injected fuel with the heating value of the fuel

$$Q_{in} = HVm_f. \tag{3.20}$$

The heating value HV is a measure of the energy density of the fuel, and is a characteristic value for each fuel. In reality, not all the energy of the fuel will be converted to heat during the combustion process. If there is insufficient amount of air in the cylinder for a complete reaction, the energy released in the combustion process can be significantly less than the total energy of the fuel. The air/fuel ratio in the cylinders will vary with the operation conditions, and not always be high enough for complete combustion.

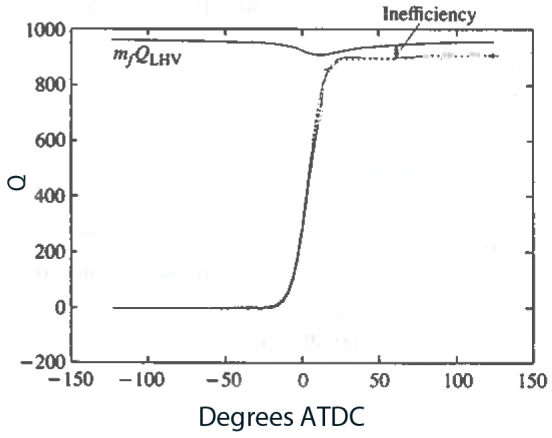

Figure 3.5: Heat release as a function of crank angle, [Courtesy: Heywood, 1988]].

To find the actual air/fuel ratio in the cylinders we need a model of the air supply to the engine, including the effects of the tubocharger. A simple empirical based model for a turbocharged diesel engine with a *Fixed Geometry Turbocharger*, are developed in [Stronach and Smith, 1988]. For a gas engine with VTG and throttling of the air supply the problem gets significantly more complicated, since we have to take into account the air supply control system. Here, we will simplify the problem by multiplying the ideal value with a constant combustion efficiency factor η_c. The total heat released from the combustion process becomes

$$Q_{in} = \eta_c HVm_f. \tag{3.21}$$

The mass of fuel supplied to the cylinders can be found from ([Heywood, 1988])

$$\dot{m}_f = C_D A_n \sqrt{2\rho_f \Delta P} \tag{3.22}$$

where C_D is the discharge coefficient of the fuel nozzle, A_n is the minimum flow area of the nozzle, ρ_f is the fuel density, and ΔP is the pressure drop over the nozzle. C_D and A_n are constant parameters for a specific engine. The fuel density ρ_f are dependent on the fuel supply pressure. The pressure drop ΔP is the difference between the fuel supply pressure, which is controlled by the fuel rack position z, and the charge air supply pressure, which is controlled by the charge air control system.

For simplicity, we will neglect the dependency on the charge air pressure. The fuel supply can then be modelled by using a linear model, only dependent on the fuel rack position

$$\dot{m}_f = kz \tag{3.23}$$

where k is a constant parameter. A simple PID based speed controller will be implemented in the model and tuned against experimental data, to implement the variable fuel rack z.

The assumption of constant combustion efficiency, and neglection of the fuel mass flow dependency on the charge air pressure, are rough simplications. These simplifications makes the model unfit for use in engine simulations with large variations in load and speed, if the requirements to accuracy is high. However, for the purpose of engine starting simulations, the model is assumed to be good enough. The combustion model only affects the piston torque at the last part of the starting sequence.

The model also assume no misfireing in the engine cylinders. This is a more vulnarable assumption, since there is always a chance that the spark plugs could fail to ignite the fuel gas. E.g. if the air/fuel ratio is outside the window where the mix can ignite. Misfireing in one or more cylinders leads to a reduction in the combustion torque, and thus reduces the acceleration of the engine.

3.2.3 Inertia force

As the pistons reciprocate in the cylinder, they produce an inertia force. The magnitude of the force depends on the mass of the reciprocating parts. From Newtons second law we have

$$F_I = m_p a_p, \tag{3.24}$$

where m_p is the piston mass, and the piston acceleration a_p as a function of crank angle and speed is given by Eq. 3.7. Inserting this in Eq. 3.24, yields

$$F_I(\phi) = m_p f_3(\phi)\omega^2. \tag{3.25}$$

The inertia force is translated to a crankshaft torque through the relationship defined by Eq 3.8. The inertia forces are important if the internal dynamics of

the rotating masses are considered. However, if the flexibility of the shafting is neglected the contributions from the different cylinders in a multi cylinder engine tends to counteract each other, such that the net torque on the crankshaft will be small. However, the effect of the inertia force will be included in the model for completeness.

3.2.4 Total Piston Torque

The total piston force from one cylinder is found by superposition of the contributions from inertia and gas forces, given by Eq. 3.14 and Eq. 3.25

$$F_p = F_{gas} + F_{mass} = A_p P + m_p f_3(\phi)\omega^2 \tag{3.26}$$

The corresponding *piston torque* from one cylinder is found by using the relationship defined by Eq. 3.8

$$\tau_{p,1} = F_p f_2(\phi) = \left[A_p P + m_p f_3(\phi)\omega^2\right] f_2(\phi). \tag{3.27}$$

The variables P, ϕ, and ω in the equation, are found from Equations 3.3, 3.13, 3.17, 3.19, 3.20, and 3.23. This yields the engine cylinder model given in the box below

$$\dot{\phi} = \omega \tag{3.28}$$

$$\dot{\omega} = -\frac{1}{I}\left[A_p P + m_p f_3(\phi)\omega^2\right] f_2(\phi) - \frac{1}{I}\tau_f + -\frac{1}{I}\tau_e \tag{3.29}$$

$$\dot{P} = \frac{\kappa - 1}{V}\dot{Q} - \kappa\frac{P}{V}\dot{V} \tag{3.30}$$

$$\dot{V} = \omega\frac{f_2(\phi)}{2r}V_d \tag{3.31}$$

$$\dot{Q} = \omega\left[a\left(\frac{\phi - \phi_0}{\Delta\phi}\right)^m \frac{m+1}{\Delta\phi e^{a\left(\frac{\phi-\phi_0}{\delta\phi}\right)^{m+1}}}\right]\eta_c H_{LV} m_f \tag{3.32}$$

$$\dot{m}_f = kz \tag{3.33}$$

For a multicylinder engine with n cylinders, the total piston torque will have contributions from n cranks. Usually the cranks are evenly distributed on the crankshaft, as shown in Figure 3.5. The angle between consecutive cranks can be found by dividing the two rotations of the four-stroke cycle by the number of cylinders of the engine.

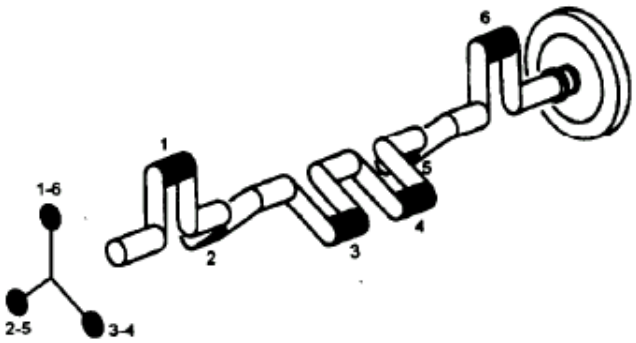

Figure 3.6: Illustration of the crank arangement of a six-cylinder in-line engine.

The crank angle of cylinder i relative to the the crank angle ϕ_1 of cylinder one, can thus be found from

$$\phi_i = \phi_1 + i\frac{4\pi}{n}. \tag{3.34}$$

From this we can find the total piston torque from n cylinders as

$$\tau_p(\phi, \omega, P) = \sum_{i=1}^{n} F_p f_2(\phi_i) = \sum_{i=1}^{n} \left[A_p P(\phi_i) + m_p f_3(\phi_i)\omega^2\right] f_2(\phi_i). \tag{3.35}$$

3.3 Friction torque

The work needed to overcome the resistance to relative motion of the moving parts of the engine, is termed friction work. Modern combustion engines usually have a mechanical efficiency of over 90 percent at rated speed and load, meaning that under 10 percent of the piston work is used to overcome the friction forces and losses from the auxiliary equipment. During transient operation the amount of friction work is harder to quantify.

The friction of the complete engine is made up of contributions from the individual components,

- Crankshaft main bearing and crank bearing,
- Piston, piston rings and crosshead bearing,
- Valve train,
- Auxiliary equipment like cooling, fuel and lubrication pumps.

In addition comes the load friction, e.g. resistance from bearings in generators and gears. Friction data often come from measurements. In complicated machinery like a combustion engine where there are many rubbing surfaces it is

hard to sort out the contribution from the individual components. Therefore an aggregate friction model for the whole plant will be employed.

3.3.1 Friction as a function of velocity

The friction force as a function of steady velocity is called the Stribeck-curve. Stribeck [1902] studied friction in roller and journal bearings, and presented his result as a function of the non-dimensional parameter $\mu\omega/\bar{P}$, where μ is the dynamic viscosity of the lubricant, ω is the rotational speed of the shaft, and $\bar{P}$ is the loading force per area. The generalized Stribeck-curve is shown in Figure 3.8.

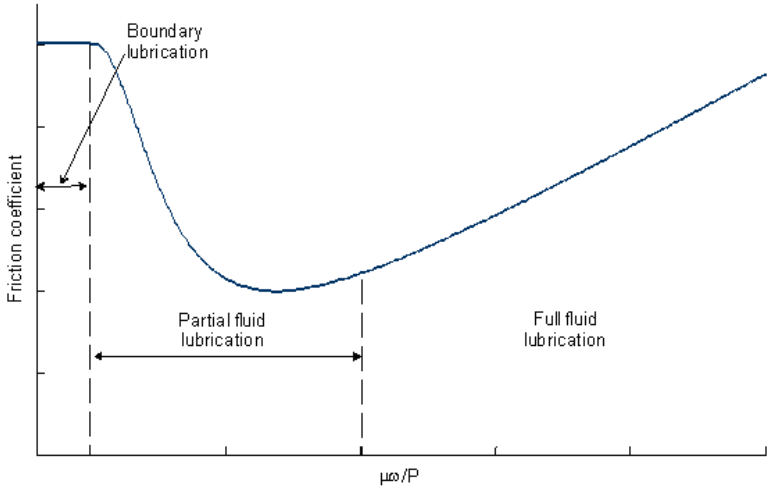

Figure 3.7: The generalized Stribeck curve.

On the basis of the Stribeck-curve the friction for sliding lubricated surfaces has been categorized into four regimes (Armstrong-Helouvry [1991]).

1. Static friction,
2. Boundary lubrication,
3. Partial fluid lubrication,
4. Full fluid lubrication.

The *static friction* is traditionally considered to be the torque necessary to initiate motion from rest. This is often greater than the kinetic friction, giving rise to the expression *break-away torque*, which is the torque required to overcome static friction.

An important aspect of the static friction is that the break-away torque is dependent on the dwell-time. As the sliding forces spend much time at zero velocity, the junction asperities between the surfaces deforms plastically, giving increased contact area and increased friction.

In the *boundary lubrication* regime the velocity is not sufficient to build a fluid film. However, additives to the bulk oil will react with the material to form a solid boundary layer between the material surfaces. Shearing will occur in the boundary layer, giving rise to a friction force dependant on the shear strength of the layer.

The *partial fluid lubrication* regime describes the transition from fully dry-friction to full fluid friction. Lubricants are drawn into the contact area through motion, forming a fluid film between the surfaces. The thickness of the fluid film will depend on the velocity. As long as the fluid film is thinner than the height of the asperities of the material, some solid-to-solid contact will occur. The behaviour in this regime is often termed the *Stribeck-effect*. The friction decreases with velocity as the fluid film grows thicker.

In the full fluid lubrication regime solid-to-solid contact is totally eliminated and the friction is a function of the viscosity of the lubricant and the velocity.

3.3.2 Steady velocity friction models

The classical model of friction consists of different components, each depicting the different friction phenomena. Dry friction is described by the so-called Coulomb friction model, where the friction is independent of velocity, and proportional to the normal force F_N, i.e

$$\tau_c = \mu_c F_N sgn(\omega). \tag{3.36}$$

The Coulomb friction coefficient μ_c is dependent on the shear strength of the material, or for boundary lubrication, the boundary layer shear strenght, in addition to the true contact area between the surfaces.

The viscous friction τ_v is normally described by a model proportional to the velocity

$$\tau_v = f_v \omega. \tag{3.37}$$

The viscous friction coefficient f_v in Eq. 3.37 is dependent on the viscosity of the lubricant, the loading, and the contact area. Alternatively a nonlinear model can be used, where the velocity is raised to some potential, dependent on the contact geometry.

Various continuous models depicting the Stribeck-curve by combing the contributions from coulomb, viscous and static friction, exists. As a theoreticaly derived model of the curve is not yet available, all of these are based on experimental data. A model proposed by Hess & Soom, and repeated in many books and papers, e.g. Egeland and Gravdal [2002] and Armstrong-Helouvry [1991],

is given by,

$$\tau_f(\omega) = \tau_c + \frac{\tau_s - \tau_c}{1 + \left(\frac{\omega}{\omega_s}\right)^2} + f_v\omega, \tag{3.38}$$

where τ_s is static friction and ω_s is an empirical parameter defining the curve in the partial fluid lubrication regime. Another model is given by Bo and Pavelescu and presented in Armstrong-Helouvry [1991],

$$\tau_f(\omega) = \tau_c + (\tau_s - \tau_c)exp\left[-\left(\frac{\omega}{\omega_s}\right)^\delta\right] + f_v\omega, \tag{3.39}$$

The difference from the Hess & Soom model, is that the Bo & Pavelescu model incorporates an extra empirical parameter δ, which give one more degree of freedom to alter the shape of the curve in the partial fluid lubrication regime. Different values for δ are proposed in the literature depending on the boundary lubricant.

Here, the Bo and Pavelescu model will be used, with $\delta = 2$, which gives good agreement with experimental results.

3.3.3 Dynamic friction effects

Not all friction phenomena are captured by steady velocity friction models. The main effects not taken into account by these models are,

1. The Dahl-effect which arises from elastic deformation of the surfaces before sliding occurs. Experiments have shown that the sliding junctions of the surfaces behave like a spring for small displacements. This gives maximum break-away torque at a small displacement from the starting point. Experiments have also shown that the break-away force depends on the rate of increase of the external force (Olsson et al. [1998]).
2. The effect on the break-away torque from the dwell-time, as described in Section 4.2.1.
3. Friction-lag, which is understood as the time from an increase in velocity to a corresponding increase in the friction. Experiments show that the friction will lag the velocity (Armstrong-Helouvry [1991]).

Different models taking these effects into account have been developed. Examples are the LuGree and the Dahl model. Such models are described in e.g. Egeland and Gravdal [2002] and Olsson et al. [1998]. These models will not be further investigated, or utilised here. Instead the simpler steady velocity models are assumed to be sufficient to describe the main friction effects of the engine.

3.4 Combustion engine simulation model

From Equations 3.3, 3.35 and 3.39, the combustion engine model becomes

$$\dot{\phi} = \omega, \tag{3.40}$$

$$\dot{\omega} = -\frac{1}{I}\tau_f + \frac{1}{I}\tau_p + \frac{1}{I}\tau_e, \tag{3.41}$$

$$\tau_f(\omega) = \tau_c + (\tau_s - \tau_c)exp\left[-\left(\frac{\omega}{\omega_s}\right)^2\right] + f_v\omega, \tag{3.42}$$

$$\tau_p(\phi, \omega, P) = \sum_{i=1}^{n}\left[A_p P(\phi_i) + m_p f_3(\phi_i)\omega^2\right] f_2(\phi_i). \tag{3.43}$$

The equations for the variable cylinder pressure P in Eq. 3.43, are given in Section 3.2.4 and the trigonometric functions $f_2(\phi_i)$ and $f_3(\phi_i)$ are defined in Section 3.1.1.

In general the piston torque can be decribed as a function of crank angle, rotational velocity and time $\tau_p(\phi, \omega, t)$, where the time dependency is due to the variable fuel rack position. The friction torque can be expressed as a function of the engine velocity $\tau_f(\omega)$. A block diagram of the combustion engine simulation model is shown in Figure 3.8.

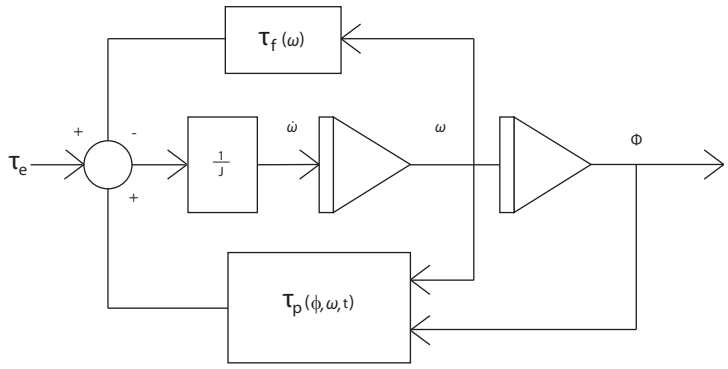

Figure 3.8: Block diagram of the combustion engine simulation model.

The different contributions to the engine friction is modelled by using an aggregate model. Furthermore, dynamic friction effects are neglected, and the total engine friction are found from an approximation of the Stribeck curve. It is assumed that this model are able to represent the real engine friction during starting with sufficient accuracy.

The influence of the air/fuel ratio on the combustion effeciency, is simplified by using a fixed combustion efficiency in the model. A linear model is used for the fuel mass flow, which neglect the effect of the charge air supply pressure. These simplifications makes the model unsuitable for use in combustion engine simulations with large variations in load and speed. However, it is argued that

the model is accurate enough to model the increase in the piston torque during the last part of the starting sequence.

Chapter 4

Starting system model

In the following, fluid dynamic and thermo dynamic theory are applied to develop a simplified model of the air starting system described in Section 2.1.

The system consists of air bottles, piping with valves and filters, and the pneumatic starting engine. When the release valve is opened, air flows from the air bottle to the starting engine, where torque is produced. Due to the discharge from the bottle, the bottle pressure is reduced. The piping gives frictional losses such that the pressure of the air flow when reaching the starting engine, is lower than the tank pressure. The objective of this chapter is to study the characteristics of these physical effects to derive a model of the system. In the following, each of the system components are discussed in more detail and equations for the physical effects are deduced.

4.1 Air tank model

The properties of the air tank closely resemble those of the classical problem of discharge of gas from a tank. This problem is treated in several books e.g. Egeland and Gravdal [2002]. The system is sketched in Figure 4.1. The main assumptions and methods for modelling of the dynamics of the tank are given below.

Air is normally assumed to be an approximation of an ideal gas for values of temperature and pressure far from its critical point. Hence, the tank pressure P_1 at any time can be found from the ideal gas law

$$P_1 = \frac{mRT}{V}. \tag{4.1}$$

The tank volume V is constant, and the change in the specific gas constant R is negliable for small changes in temperature. However, the discharge of gas will give a decreasing mass and temperature. To use Eq. 5.1 we need expressions

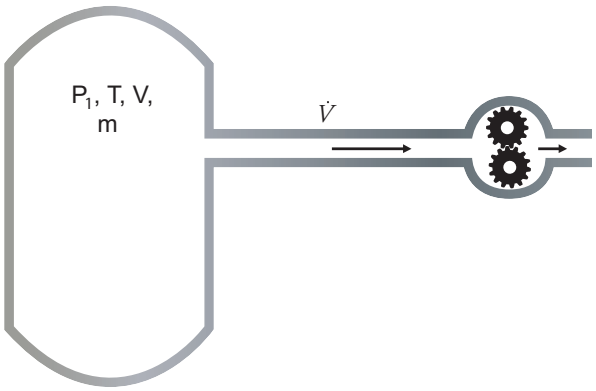

Figure 4.1: Discharge of air, from the air tank.

for these variables. The change of mass can be found from the mass continuity equation

$$\dot{m} = -\rho \dot{V}, \tag{4.2}$$

where $\dot{V}$ is the volumetric flow out of the starting engine. The decrease in temperature can be derived from energy balance for the system. By following along the lines of Egeland and Gravdal [2002], we arrive at

$$\dot{T} = -(\kappa - 1)\frac{\rho \dot{V}}{m} T, \tag{4.3}$$

where the heat capacity ratio κ is the ratio of the heat capacity of air at constant pressure, to the heat capacity at constant volume. The heat capacity ratio can be assumed constant for small changes in temperature.

Hence, we have derived expressions for all the variables in the ideal gas law, and the tank pressure at any time can be calculated from Eq. 4.1.

4.2 Pipe model

The frictional losses in piping, valves, and filters will give a pressure drop between the air receiver and the starting engine. Detailed fluid dynamic equations for pipe bends, filters, and valves are not within the scope of this project. Instead, equations for a straight pipe segment will be utilized, and equivalent lengths will be used to account for the frictional losses of non-uniform and non-straight segments. The assumptions and the fluid dynamic theory used in the model is summarized below.

4.2.1 Flow characteristics

The pressure losses for fluid flow through pipes are strongly dependent on the flow characteristics. The main defining parameter is Reynolds number, which for flow in circular pipes is defined as

$$Re = \frac{\rho w D}{\mu}, \tag{4.4}$$

where w is the flow velocity, D the pipe diameter, and μ is the dynamic viscosity of the fluid. The three regimes of fluid flow are laminar, transition, and turbulent flow. Low Reynolds numbers gives laminar flow. For flow in circular pipes the accepted value for transition is Re = 2300 (White [1998]). Fully turbulent flow is obtained for values of Reynolds number in the order of $10^3 - 10^4$ and higher.

The piping of the starting system usually has diameters lower than 100 [mm]. For the flow velocities encountered in the piping, this gives Reynolds numbers above 10^5. That is, in the turbulent range.

Another important characteristic of the flow is its compressibility. When a fluid flows at velocities comparable to its speed of sound, the effects of density changes become significant, and the flow is termed compressible. The speed of sound for a fluid is given by,

$$v_s = \sqrt{\kappa R T}. \tag{4.5}$$

The condition for treating a gas as incompressible is that the Mach number, defined as the ratio between the fluid velocity, and the speed of sound of the gas is much lower than one (White [1998]). The speed of sound for gases is low, giving strong compressible effects. The flow velocities in the pipe of the starting system will exceed the speed of sound of air. Hence, the theory of compressible flow must be utilized.

4.2.2 Pressure drop equations

For calculation of pressure drop in straight pipes, usually no heat loss (adiabatic) or constant entropy (isentropic) conditions is assumed. For long pipes the flow conditions more closely approximates an isentropic flow (Liu [2003]).

An equation for the pressure drop for isentropic compressible flow in pipes of constant area, can be developed from,

1. Conservation of mass.
2. Conservation of momentum (Navier-Stokes equation).
3. Conservation of energy for the flow (first law of thermodynamics).
4. The ideal gas law.

In addition it is assumed that the wall shear is correlated by the dimensionless Darcy friction factor f such that the wall shear can found from,

$$\tau_w = \frac{1}{8} f \rho w^2. \tag{4.6}$$

Using these five quations, we can derivative the isentropic flow equation. This is done in many books, e.g. Liu [2003] and White [1998], to arrive at

$$P_2 = \sqrt{P_1^2 - P_1 \rho_1 w_1^2 \left[2ln\left(\frac{w_2}{w_1}\right) + \frac{f L_e}{D} \right]}, \tag{4.7}$$

where L_e is the length of the pipe, and the indices 1 and 2 relates to the start and the end of the pipe, respectively. Eq. 4.7 requires knowledge of the flow velocity at both ends of the pipe. Typically the change in velocity over the pipe is small (Beater [2007]). If no change of velocity over the pipe is assumed, then the logarithmic term disappear and the pressure at the end of the pipe can be found from

$$P_2 = \sqrt{P_1^2 - \frac{P_1 \rho w^2 f L_e}{D}}. \tag{4.8}$$

The flow velocity w, is found by dividing the mass flow by the cross-sectional area of the pipe and the density. The density ρ is given by the tank mass divided by the tank volume. We get

$$P_2 = \sqrt{P_1^2 - \frac{16 P_1 V \dot{m}^2 f L_e}{\pi^2 m D^5}}. \tag{4.9}$$

4.2.3 Friction factor

The Darcy-friction factor f is strongly dependent on the Reynolds number. Many different equations for this factor, based on empirical data or theory, exists for the different flow regimes. A schematic representation of the friction factor as a function of Reynolds number and relative pipe roughness, ϵ/D is given in the so-called Moody diagram, presented in a simplified version in Figure 4.2.

As the figure shows, the dependence on pipe roughness disappears in the laminar flow regime. In this regime the diagram is based on the Poiseulle equation

$$f = \frac{64}{Re}. \tag{4.10}$$

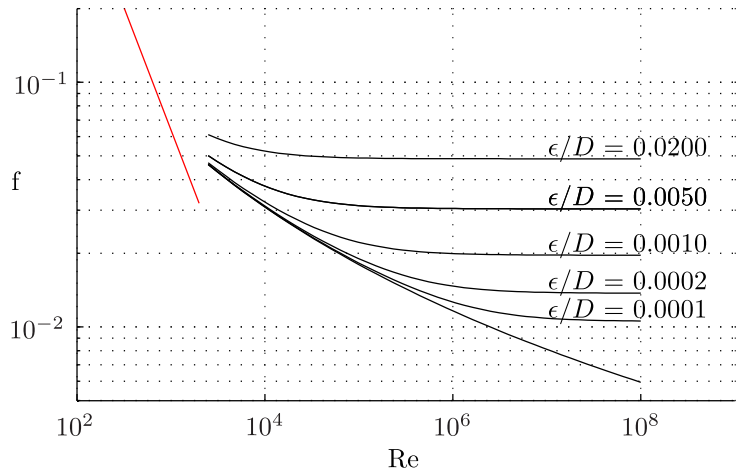

Figure 4.2: Simplified Moody diagram. The Darcy friction factor as a function of Reynolds number and the relative pipe roughness.

In the transition and turbulent flow regiments the diagram is based on an iteration equation developed by Colebrook

$$\frac{1}{\sqrt{f}} = -2log_10\left[\frac{\frac{\epsilon}{D}}{3.7} + \frac{2.51}{Re\sqrt{f}}\right]. \tag{4.11}$$

An approximation to the Colebrook equation which does not require iteration, was proposed by Haaland, and has been repeated in many books and papers

$$\frac{1}{\sqrt{f}} = -1.8log_10\left[\left(\frac{\frac{\epsilon}{D}}{3.7}\right)^{1.1} + \frac{2.51}{Re}\right]. \tag{4.12}$$

According to White [1998], the Haaland equation varies with less than two percent from the Colebrook equation.

Many other alternative formulas for friction factors for different flow conditions have been proposed. The choice of method for finding the friction factor depends on the required accuracy and the flow characteristics. We assume that the Haaland equation gives a sufficiently accurate estimate of the friction factor. Alternatively we could use interpolation in the Moody diagram.

4.3 Valve model

Two valves models will be used. One model for the on/off release valve of the existing starting system, and one model of a proportional pressure control valve, where the flow area of the valve is controlled by an electrical signal.

The valves are modelled as lossless components, meaning that any frictional losses in the valve are accounted for by the pipe model. The delay in the valve dynamics, will be model by adding a time delay to the control signals for the valves. A reasonable value for the time delay are found by studying experimental results from starting tests. In addtition, the valve uses some time before it starts closing, till its completely closed. This effect are modelled by a applying a rate limiter to the control signal.

4.3.1 On/off release valve

The on/off valve is modelled by the simple equation

$$P_3 = uP_2, \tag{4.13}$$

where u is one when the valve is open, and zero when closed. I.e. a lossless valve which can be completely open or completely closed.

4.3.2 Pressure control valve

Pressure control valves uses a piston or diaphragm, to balance the pressure on the downstream side of the valve with the solenoid generated force. The solenoid generates a force which is proportional to the electric signal. If we let u_e be the magnitude of the electrical signal, the solenoid force is given by $F_s = ku_c$, where k is some constant. The force balance becomes

$$P_3 A_d = ku_e, \tag{4.14}$$

where A_d is the area of the piston or diaphragm. Since k and A_d are constants, we can express the downstream pressure as

$$P_3 = \frac{k}{A_d} u_e = \bar{u}, \tag{4.15}$$

where $\bar{u}$ is a modified signal which will be used as control input. We assume ideal performance of the pressure control valve. The relationship between P_2 and P_3 becomes

$$P_3 = \begin{cases} \bar{u} & \textbf{if } \bar{u} < P_2, \\ P_2 & \textbf{if } \bar{u} \geq P_2. \end{cases} \tag{4.16}$$

The assumtion of ideal performance of the valve, is a rough assumtion. For real valves, the downstream pressure tends to fall when the pressure ratio P_2/P_3 is

close to one (ref. Section 2.3). However, if the output from the control law is the torque from the starting system, we need a control allocation algorithm with a mapping from the torque to a pressure set point. This means that as long as the valve characteristics are well known, such that the mapping corresponds to the valve characteristics, the control performance is unaffected by the actual valve characteristics. A control allocation algorithm is defined in Chapter 7

4.4 Starting engine model

A detailed model of the starting engine could be developed from theoretical derivations. Examples of this are given in Zhou and Wen for gear engines and Beater [2007] for vane type engines. This would require detailed knowledge of the geometry of the starting engine. Such a derivation is not within the scope of this project. Instead catalogue values for torque and air consume as a function of pressure and engine speed will be used.

An example of an interpolation graph for a pneumatic gear engine is given in Figure 4.3. As the torque is linearly dependent on speed, few interpolation points are needed. The air consumption needs more interpolation points.

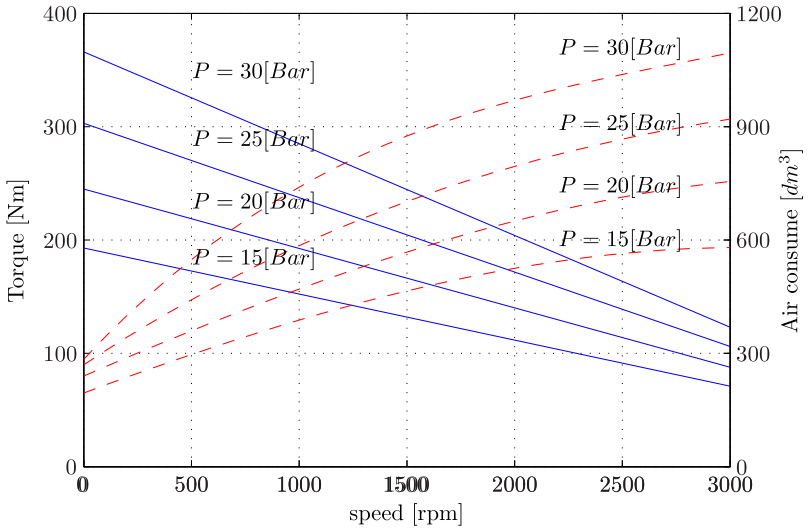

Figure 4.3: Air consumption and torque as a function of rotational velocity and pressure, for a pneumatic starting engine.

The starting engine torque on the low speed (combustion engine) side, can be found from

$$\tau_e = h_1(\omega, P_3), \tag{4.17}$$

where $h_1(\omega, P_3)$ is an interpolation function and ω is the combustion engine

speed. The mass flow out of the engine is given by

$$\dot{m}_{out} = \rho \dot{V} = h_2(\omega, P_3), \tag{4.18}$$

where $h_2(\omega, P_3)$ is a second interpolation function.

4.5 Starting system simulation model

From Eq. 4.17, the output torque from the starting system to the combustion engine, is given by

$$\tau_e = h_1(\omega, P_3), \tag{4.19}$$

where the variables ω and P_3 is the combustion engine speed, and the supply pressure to the starting engine, respectively. The function $h_1(\omega, P_3)$ is an interpolation function which calculates the torque on the combustion engine side of the gear connection.

The speed ω, is input from the combustion engine model developed in the previous chapter. The supply pressure P_3 are found from Eqs. 4.1, 4.2, 4.2, 4.9, 4.13 or 4.16, and 4.18. This yields the compressed air system model, given in the box below

$$P_3 = uP_2 \textbf{ or } \begin{cases} \bar{u} \textbf{ if } \bar{u} < P_2, \\ P_2 \textbf{ if } \bar{u} \geq P_2. \end{cases} \tag{4.20}$$

$$P_2 = \sqrt{\left(\frac{mRT}{V}\right)^2 - \frac{16RT\dot{m}fL_e}{\pi^2 D^5}} \tag{4.21}$$

$$\dot{T} = -(\kappa - 1)\frac{\rho \dot{V}}{m}T, \tag{4.22}$$

$$\dot{m} = -h_2(\omega, P_3) \tag{4.23}$$

where the friction factor f in Eq. 4.21 is found from the Haaland equation, Eq. 4.12. u and $\bar{u}$ are the control input in case of a on/off valve or a pressure control valve, respectively.

A block diagram of the starting system simulation model is shown below.

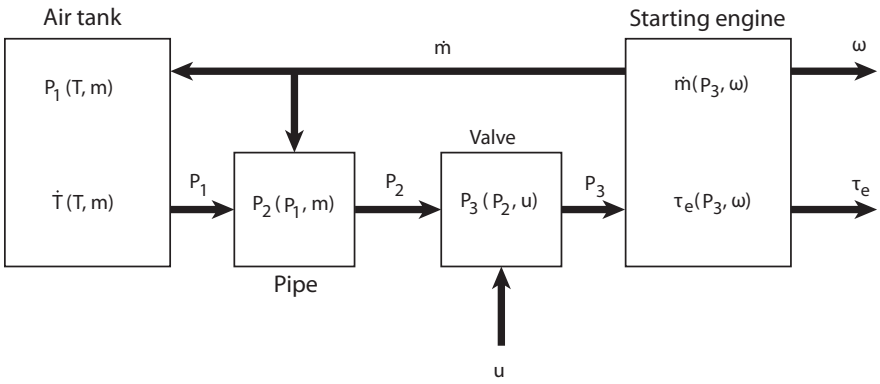

Figure 4.4: Block diagram of the starting system simulation model.

Chapter 5

System Identification and validation

This chapter deals with identification of model parameters and validation of the model against experimental results. To validate the model, starting test were performed on a Rolls-Royce Bergen C26:33L9 gas engine. The model parameters were adapted to the test setup, and the model was validated against the experimental result. In addition, tests were performed to measure the break-away torque of the engine.

As stated in the previous chapters, the model is not developed with the intent that it should give an exact depiction of the behaviour of the real system. The model should cover the main physical aspects, to give means for studying the relative effect of changes to the system. This will also be emphasized when validating the model.

5.1 Measurements

5.1.1 Friction measurements

To identify the static friction torque of the engine, the force needed to rotate the engine was measured by using a load-cell. The test setup is shown in Figure 5.1. A lifting eye bolt was fitted to the engine flywheel. To rotate the engine, a fall block with chain was attached to the eye bolt. Between the eye bolt and the fall block, a load cell was fitted to measure the applied load.

The break-away torque can be calculated directly from the test result by multiplying the peak of the applied torque, by the radius of the flywheel r_{fw}. Several measurements were done, giving a variance of less than 5 percent.

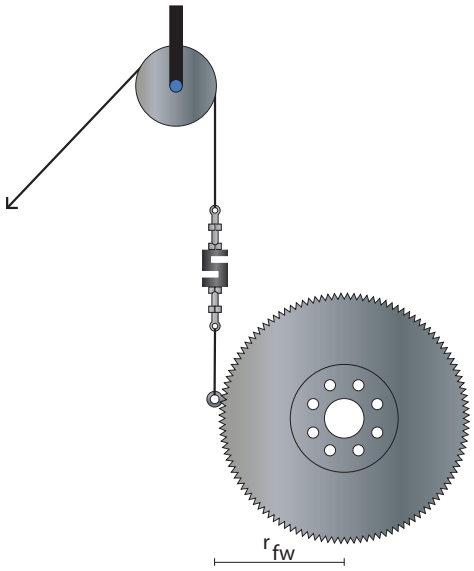

Figure 5.1: Test setup for measuring the break-away torque.

5.1.2 Starting tests

Starting tests were performed on the test engine for cold and hot engine. The engine was fitted to a water break, which regulated the load. Engine speed, load torque, air pressure at the bottle and the starting engine, and fuel rack position were measured.

The 0.5 $[m^2]$ air bottle used in the tests, gave a maximum of two starts, before having to reload the bottles.

5.2 Comparision and validation

To validate the mathematical model developed in the previous chapters, the model was implemented in Matlab Simulink, and results from computer simulations were compared to experimental results. The load from the water break was implemented as an additional load in the model. This was done by altering Eq. 3.3 to

$$\begin{aligned} \dot{\phi} &= \omega, \\ \dot{\omega} &= -\frac{1}{I}\tau_f + \frac{1}{I}\tau_p - \frac{1}{I}\tau_{wb} + \frac{1}{I}\tau_e, \end{aligned} \tag{5.1}$$

where τ_{wb} is the measured load from the water break. The experimental data show a large variance in the time delay between the fuel-on signal, and the acceleration due to combustion. In the simulations a value of 1.6 [s] was applied

to the fuel-on signal to account for the ignition delay. This was the mean of the experimental results.

5.2.1 Validation Results

The first plot in Figure 5.2, show time-series of measured and simulated engine speed during starting. The second figure show the pressure in the starting air bottles for the same run. The pressure in the starting air bottles is initially 24.9 [Bar], and the bottle volume is 0.5 [$m2$]. The full parameter list is found in Appendix B.

As can be observed from the first plot, the simulation results show fairly good accordance with the measurements. The speed is slighly lower and more fluctating in the simualtions for the first two second of the run, and slightly higher in the rest of the run. We see that the fast acceleration due to start of combustion, at approximately 6.5 [s], comes somewhat earlier for the simulated series. This is due to the high variance of the ignition delay for the experimental data.

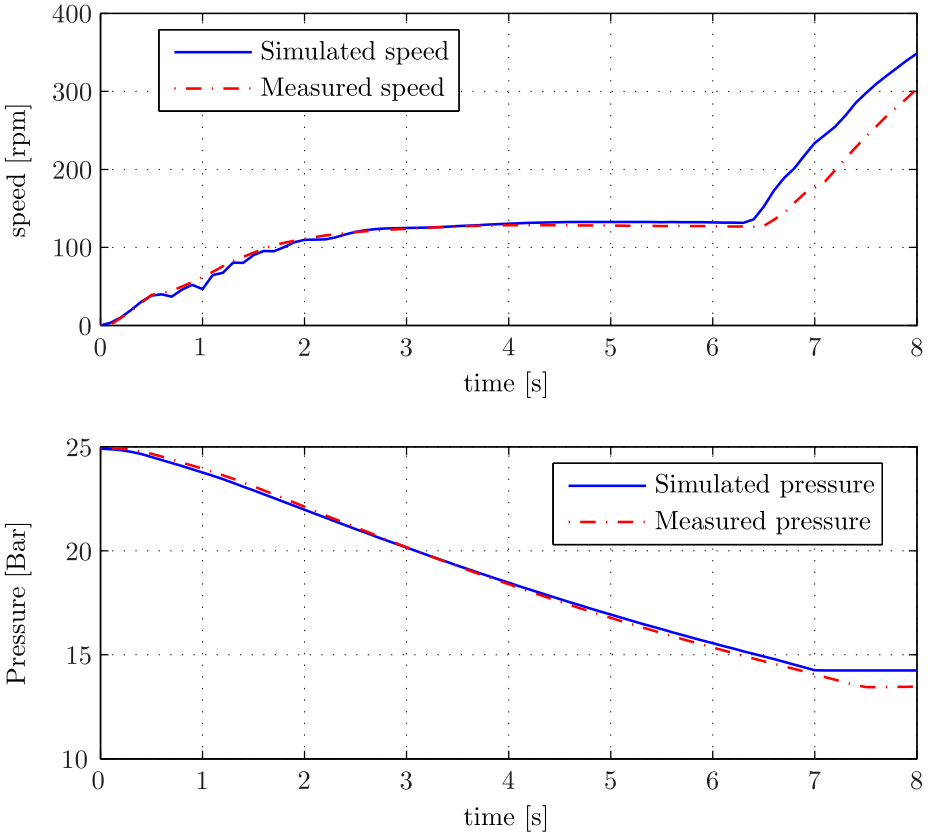

Figure 5.2: Measured and simulated speed and bottle pressure during starting, for an initial bottle pressure of 24.9 [Bar]

Good agreement between measured and simulated results can also be seen in the pressure plot. The deviation at the end of the starting sequence is approximately 0.5 [Bar]. However, this is because the starting system disengages sooner in the simulations, due to earlier acceleration.

In Figure 5.3 the initial bottle pressure is reduced to 14.9 [Bar]. The results show a deviation in the engine speed of 10-15 [rpm] after approximately 2.5 [s]. The speed curve from the simulation is also somewhat more fluctuating. This might be due to high sampling periode in the measurements. Also the bottle pressure show a deviation. However, this is expected since the air consume increases with speed. In spite of this, the deviation at the end of the run is less then 0.8 [Bar]

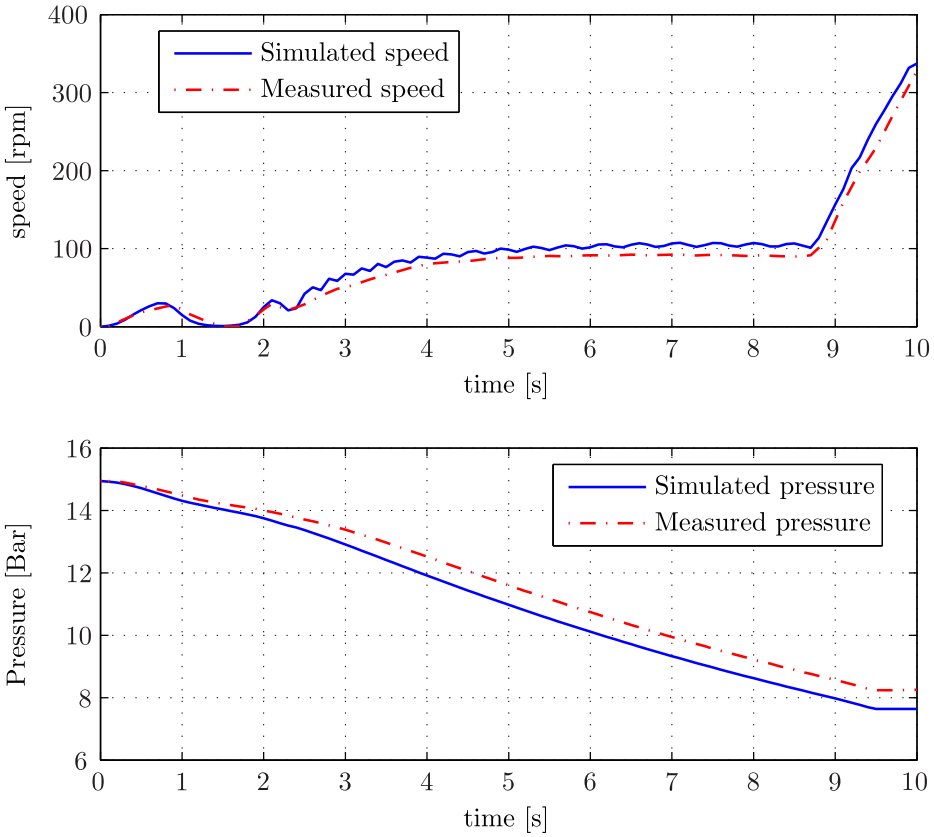

Figure 5.3: Measured and simulated speed and bottle pressure during starting, for an initial bottle pressure of 14.9 [Bar]

5.2.2 Conclusions from the validation

From the results presented above, it can be concluded that the model covers the main physics of the starting system. However, the validation also shows some

deviations between the model and the real system. These deviatons probably stem from the simplifications made when developing the model, and uncertainties in the model parameters.

Since the piston torque and the torque from water brake are fairly well defined, the largest uncertainties are probably connected to the friction and starting engine torque. The break-away torque is measured, and should have fairly good accurancy. However, the effect of the dwell time and the applied load on the magnitude of the friction, might give variations. In additon, there is uncertainty connected to the other friction parameters, like the ω_s coefficient for modelling the Stribeck effect.

The piping and starting bottle model, show relatively good agreement with the experimental results. Therefore, the largest uncertainty connected to the starting engine torque is probably the catalogue data for the starting engine. These data are based on experimental tests done at the test bed of the starting engine manufacturer. However, the real torque and air consume of the engine will probably vary for each starting engine, due to internal leakage, wear of the internal engine elements etc. There is also considerable uncertainty connected to the assumption of a constant time delay between the fuel-on signal and ignition, but this delay is caused by dynamics which is hard to model.

Chapter 6

Control design

As stated in the introduction, the main challenges related to starting of gas engines is to provide a safe start with minimum cost. That is, to avoid ignitable consentrations of unburned fuels in the exhaust system, while reducing the air consume. This chapter considers ways of improving the existing starting system with regards to these objectives, through automatic control of the engine speed and modifications to the fuel-supply logic. Three different concepts for control of the starting system will be developed and evaluated.

The main controlled parameter is the engine speed, however, also the crank angle will be used to make logic-based descitions in the control systems. The control problem for the starting system, will be stated in terms of these two variables.

6.1 Control objective

The ultimate goal of the starting system, is to accelerate the engine to the speed required for ignition. For gas engines, however, care must be taken to avoid misfireing of non-fireing during starting, which may result in unburned fuel-mixtures in the exhaust system. Therefore, the fuel supply can not be opened before the engine has reached a speed that ensures that the fuel gas will ignite.

The starting system is also used for purging the exhaust system prior to ignition, to eject ignitable gas concentrations. The class societies specify requirements to the size of the volume which should be purged before allowing fuel to the cylinders. Often, the requirement is specified in terms of a multiplicative of the volume of the exhaust system (DNV [1999]). This means that the combustion engine is used as an air pump, driven by the starting engine, during the start-up. We can state the following control objectives.

1. Accelerate the engine to the fuel-on speed.
2. Pump a volume equal to the purging volume out of the exhaust system.

In addition, the starting system is used to help accelerate the engine to a self sustained speed after ignition, such that we can define a third control objective.

3. Accelerate the engine to the self sustained speed after ignition.

6.1.1 Performance indexes

Optimization of the starting system, implies that we want to change the system to optimize some performance criteria. The most important performance criteria which will be considered in this work, are

1. Safety - We want to ensure a safe starting sequence. The primary safety concern is the explosion danger related to unburned fuels.
2. Cost - We want to minimize the installation cost of the staring system. The primary focus is to reduce the required size of the starting air bottles, by increasing the number of starts which can be achived before reloading the bottles. However, it is also important not to increase the cost of the other parts of the system.
3. Robustness - We want a starting system which is robust with regards to changes and uncertainties in the system parameters.

In general, the air consume increases with the time the starting system is active. It will therefore not be put any requirements on minimizing the starting time. Instead it will be assumed that by minimzing the air consume we achive a starting sequence which is fast enough.

6.1.2 Purging

In the existing starting sequence, described in Section 2.1.3, the first contol objective is obtained by purging the exhaust system for a fixed number of seconds, the purging time. A four-stroke engine needs two rotations to purge a volume equivalent to its total cylinder volume. Hence, the time it takes to purge the exhaust system once, can be found from

$$t_p = \frac{4\pi V_{ex}}{nV_d\omega} \tag{6.1}$$

where V_{ex} and V_d is the volume of the exhaust manifold and the swept volume for one cylinder, respectively. From Eq. 6.1, it obvious that the time it takes to purge the exhaust system will vary with the speed of the combustion engine. By using a fixed purging time, the purged volume will vary, e.g. for different starting bottle pressures, due to its effect on the course of the engine velocity durting starting. If we specify a low purging time, we risk not being able to purge the required volume, whereas for a long purging time we get unnecessary high air consume and reduced number of starts.

By instead require that the engine shall be purged for a fixed number of *rotations*, the purging volume will not vary with the average speed. The number of

rotations needed to purge a volume equivalent to the complete exhaust system, can be calculated from the volume of the exhaust manifold and the total swept cylinder volume, as shown in Eq. 2.4. The crank angle ϕ_p when the necessary volume is purged is given by

$$\phi_p = \phi_0 + 2\pi \frac{aV_{ex}}{V_d n 0.5} \tag{6.2}$$

Where ϕ_0 is the initial crank angle, and a is a safety constant. We will here require that a volume equivalent to six times the exhaust manifold volume to be purged. That is, $a = 6$. The logic for starting the fuel supply to the cylinders become

$$\text{fuel supply} := \begin{cases} \text{off} & \textbf{if } \omega < \omega_{fo} \vee \phi < \phi_p, \\ \text{on} & \textbf{if } \omega \geq \omega_{fo} \wedge \phi \geq \phi_p \end{cases}$$

where ω_{fo} is the required engine velocity for starting the fuel supply.

6.2 Control plant model

As stated in the previous sections, the main purpose of the starting system is to accelerate the engine to the speed required for ignition. To do this, the torque of the starting engine τ_e needs to overcome the torques τ_f and τ_p in the system model, given by Eq. 3.3 and repeated here for convenience

$$\begin{aligned} \dot{\phi} &= \omega \\ \dot{\omega} &= -\frac{1}{I}\tau_f + \frac{1}{I}\tau_p + \frac{1}{I}\tau_e, \end{aligned} \tag{6.3}$$

where τ_f is a nonlinear function of the rotational velocity, given by an empirical approximation of the Stribeck curve and τ_p is a non-linear function of rotational velocity, crank angle, and time. In the controller development, we will use the general form

$$\begin{aligned} \dot{\phi} &= \omega \\ \dot{\omega} &= f(\phi, \omega, t) + \frac{1}{I}\tau_e, \end{aligned} \tag{6.4}$$

where the function $f(\phi, \omega, t)$ is given by,

$$f(\phi, \omega, t) = -\frac{1}{I}\tau_f(\omega) + \frac{1}{I}\tau_p(\phi, \omega, t), \tag{6.5}$$

Equation 6.4, describe a nonlinear, second-order, control plant model, where the controlled variables is the rotational velocity ω and the crank angle ϕ,and τ_e is the actuator torque. The system is underactuated, in the sense that the starting engine can only produce a positive torque.

6.3 Control allocation

The torque τ_e from the starting engine, is allocated to the combustion engine in term of control inputs $\bar{u}$. Or, in the case of an on/off valve, by the input u. In this chapter we only consider pressure control valves. Therefore, we will use $\bar{u}$ for the control input .

To calculate a pressure set point from the desired torque resulting from the control law, we need a mapping between these variables. By using the valve and starting engine characteristics, the mapping from the control inputs to the torque can be found from Eqs. 4.16 and 4.17. This yields

$$\tau_e\left(\omega, P_3\right) = h_1\left(\omega, P_3\right), \tag{6.6}$$

$$P_3(\bar{u}, P_2) = \begin{cases} \bar{u} & \textbf{if } \bar{u} < P_2, \\ P_2 & \textbf{if } \bar{u} \geq P_2 \end{cases} \tag{6.7}$$

where $h_1(\omega, P_3)$ is an interpolation function. To map the necessary control input to obtain a given torque, we need the inverse relationship. That is, the control input $\bar{u}$ in terms of the torque τ_e. By inversing the relationship in Eqs. 6.6 and 6.7, we get

$$\bar{u} = P_d(\tau_e, \omega). \tag{6.8}$$

where the function $P_d(\tau_e, \omega)$ is the inverse of the function $h_1(\omega, P_2)$.

Normally, there are no sensors available for measuring the actual torque developed, so the mapping can be viewed as an open-loop system. There is no guarantee for fulfilling the thrust command from the controller. Situations where the commanded torque may not be fullfilled, includes if we have bad quality signals for the measurements of the shaft speed ω, or if the valve saturates such that $\bar{u} \geq P_2$. This have to be taken into consideration in the controller development.

6.4 System properties and boundedness

Simulations results for rotational velocity, friction torque, and piston torque as a function of time over a typical starting sequence of a nine-cylinder engine, are shown in Figure 6.1. The figure show results with the existing starting sequence. After the initial acceleration, the speed curve tends to flatten out during purging,

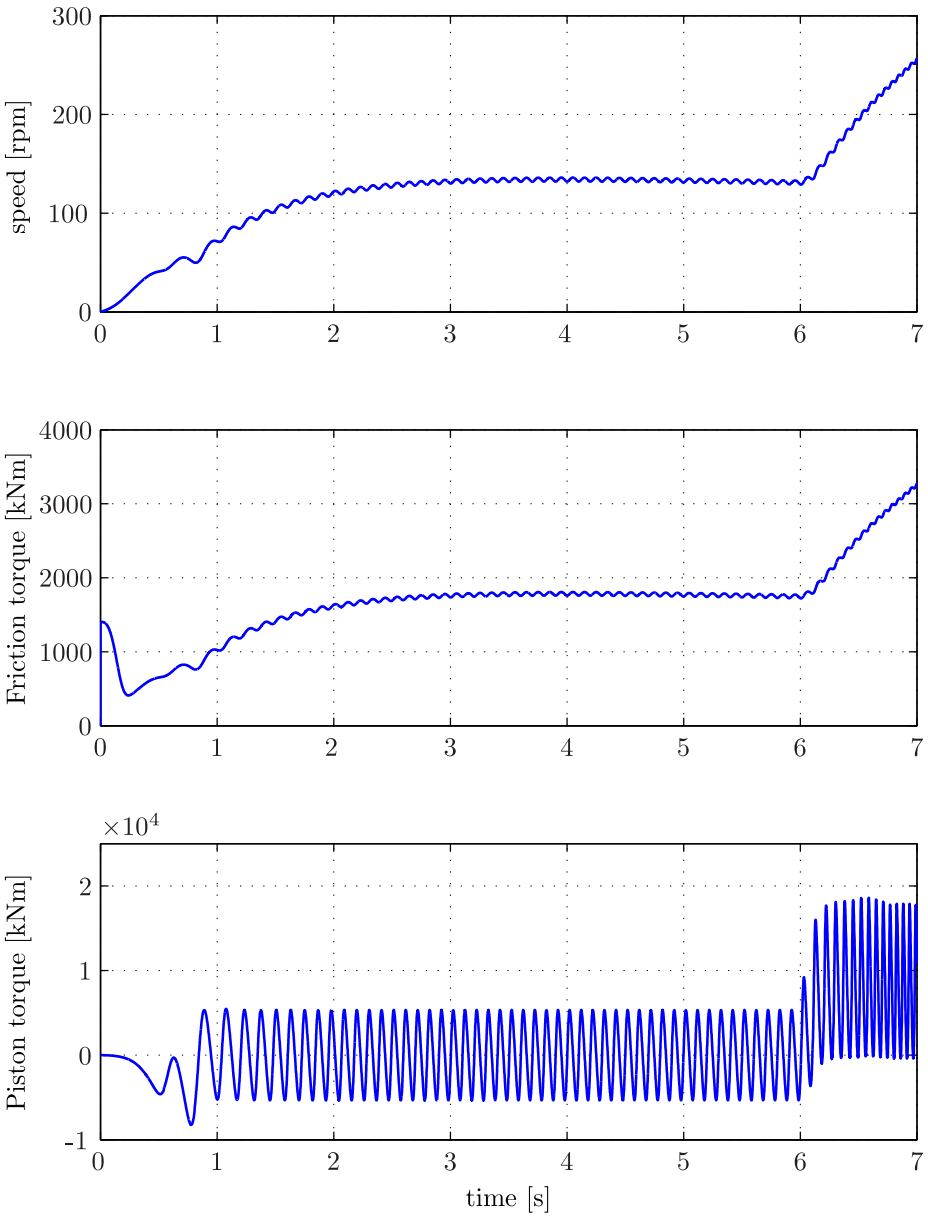

Figure 6.1: Speed, friction torque and piston torque during a typical starting sequence.

due to increased viscous friction and falling starting bottle pressure. The engine then accelerates again when the fuel gas ignites after about 6.0 [s].

From the second and third plot, it can be observed that the by far largest resistance appear during the first second of the starting sequence. Mainly due to large negative piston torque, but also break-away friction. During the purging

period, from about 1.0 - 6.0 [s], the starting system only needs to overcome the friction torque, since the piston torque has a zero mean contribution. This can be used in the controller design. The largest control action should be used during the first seconds. Moreover, since both friction and air consume increases with speed, the speed during purging should be kept low to reduce air consume.

6.4.1 Friction torque

The friction torque is large at the break-away point due to stiction, then decreases before it increases again due to the velocity proportional viscous friction. The expression for the friction torque is given by Eq. 3.42 and repeated here

$$\tau_f(\omega) = \tau_c + (\tau_s - \tau_c)exp\left[-\left(\frac{\omega}{\omega_s}\right)^2\right] + f_v\omega. \tag{6.9}$$

For practical applications the values of the parameters F_s, F_c, f_v and ω_s will be such that the largest friction during starting is experienced at the break-away point, or at the disengagement speed of the starting system. To put a bound on the friction torque, we assume 20 percent uncertainty in the model. That is, the friction of the real system will never exceed,

$$|\tau_f(\omega)| \leq \rho_1(\omega) = 1.2\tau_{f,sim}(\omega) \tag{6.10}$$

where $\tau_{f,sim}(\omega)$ is equal to Eq. 6.9, implemented with the parameters used in the simulations.

6.4.2 Piston torque

The piston torque gives both positive and negative contributions to the total torque. The full model for the piston torque is found in Chapter 3, but it can in general be expressed as a function of engine velocity, crank angle, and time

$$\tau_f = \tau_f(\phi, \omega, t), \tag{6.11}$$

where the time dependency is due to the varying fuel rack position.

The time evolution of the piston torque during starting, can be divided into three parts with regards to its net contribution to the total torque. Reference is made to the bottom plot in Figure 6.1. During the first 1-2 revolutions of the engine, the piston torque will give a *negative* contribution to the total engine torque. The main parameters effecting the shape of the torque curve and the magnitude of the torque, is the initial crank angle, the cylinder geometry and the number of cylinders. Since the initial crank angle is not measured, we have

to take the uncertainty in this parameter into account when putting bounds on the piston torque.

After the first 1-2 revolutions, the torque will fluctuate, and the net torque from the pistons will be equal to zero. The frequency of the torque oscillations depends on the engine speed. The amplitude of the torque oscillations is constant and mainly dependent on the the cylinder geometry and the number of cylinders. Since the cylinder geometry and number of cylinders are well defined parameters, we assume five percent uncertainty in the model to account for the simplifications made when developing the model. This gives the bound

$$|\tau_f(\omega)| \leq 1.05\tau_{p,a} \textbf{ if } \ 2\pi < \phi \leq \phi_p \vee \omega < \omega_{fo},$$

where $\tau_{p,a}$ is the amplitude of the piston torque from the simulations. Furthermore, we assume that the torque during the first rotations is bounded by

$$|\tau_f(\omega)| \leq 1.5\tau_{p,a} \textbf{ if } \phi \leq 2\pi.$$

The piston torque before ignition, can be interpreted as a lossless, nonlinear spring initially at equilibrium. That is, it needs an initial energy input to bring it out of equilibrium. But once it is out of equilibrium it will oscillate with constant amplitude since it is lossless. The magnitude of the negative piston torques during the first revolutions, usually exceed the maximum friction torque obtained during starting and hence becomes the dimensioning value for the starting system.

When the fuel gas ignites, the torque will oscillate, but the net torque contribution is *positive*. The magnitude of the net torque is a function of the heat released from the fuel oil in the combustion process. The piston torque in this part of the starting sequence has a time dependence, due to the variabel fuel rack position. However, we can bound the torque uniformly in t, e.g. by looking at the load limit of the combustion engine. We use,

$$|\tau_f(\omega)| \leq \tau_{c,a} \textbf{ if } \phi \geq \phi_p i,$$

where $\tau_{c,a}$ is a bound on the torque resulting from the combustion process, found from the engine load limit.

To get a smooth continous function which bound the piston torque, we can apply saturating functions of the form

$$f(\phi) = \frac{1}{1 + exp\left[u(\phi + v)\right]}, \tag{6.12}$$

to the bounds, where u and v are parameters defining the shape of the exponential function. The total bounding function for the piston torque is implemented as,

$$\rho_2(\phi) = \tau_{p,a}\left[\frac{1.5}{1+exp\left[-6(\phi-0.4)\right]} + \frac{0.4}{1+exp\left[2(\phi-\frac{3\pi}{2})\right]} - 0.4\right] + \frac{\tau_{c,a}}{1+exp\left[-6(\phi+84)\right]}. \tag{6.13}$$

6.4.3 Boundedness of the system dynamics

Using the bounds on the friction and piston torque given by Eqs. 6.10 and 6.13, and assuming that the shafting inertia can be estimated by $\hat{I} \in [I_0, I_1]$, we can bound the system dynamics $f(\phi, \omega, t)$ uniformly in t

$$|f(\phi,\omega,t)| = \rho(\phi,\omega) = \frac{1}{I_0}\left[\rho_1(\omega) + \rho_2(\phi)\right]. \tag{6.14}$$

In Figure 6.2, $\rho(\phi, \omega)$ is plotted against simulations results for the absolute value of $f(\phi, \omega, t)$. These bounds are used in the control design, later in this chapter.

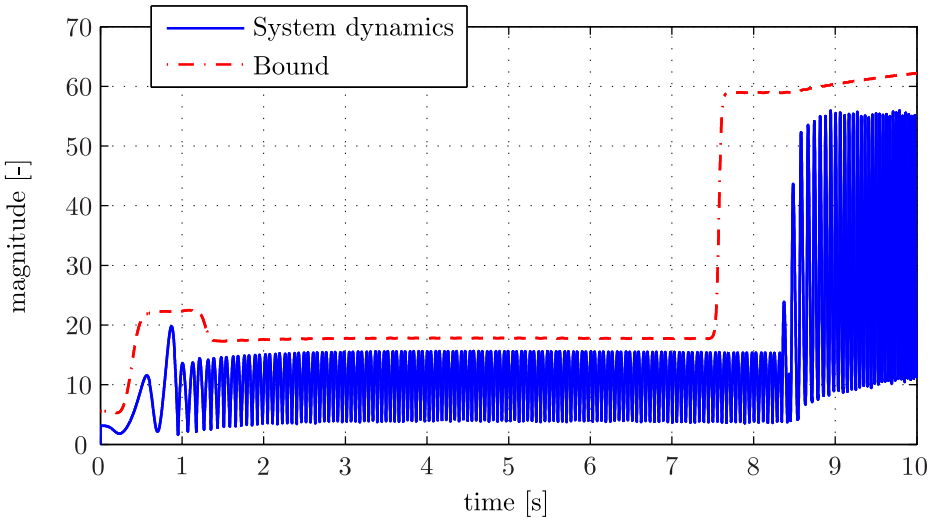

Figure 6.2: Absolute value of the system dynamics $f(\phi, \omega, t)$ plotted as a function of time, versus the bounding function given by, 6.14

6.5 Filter design

The high frequency velocity oscillations resulting from the zero-mean piston torque (ref. Section 6.4.2), should not be included in the feedback signal to the PID-controller. Since they have zero mean contribution, and the engine

usually have a large enough inertia to reduce the fluctuation to ±5 [rpm], they do not have significant impact on the starting sequence. Trying to counteract these oscillations, would result in increased air consume and wear and tear of the starting system equipment. To prevent the oscillations caused by the piston torque from entering the control loop, a filter can be used.

There are several methods for filtering the feedback signal to remove these oscillations. An ideal band-stop filter, filters all signals within a specified frequency band. However, real band stop filters, like the Cascaded notch filter, have a gradual transistion between passband and stopband. In addition, the phase-characteristics of the filter is important for control purposes, since delays in the feedback signal is undesirable. The transfer function of the cascaded notch filter is given by Sørensen [2011]

$$h(s) = \prod_{i=1}^{r} \frac{s^2 + 2\zeta_{ni}\omega_i s + \omega_1^2}{s^2 + 2\zeta_{di}\omega_i s + \omega_1^2}, \tag{6.15}$$

where ω_i is the peak frequencies of the filter and ζ_{ni} and ζ_{di} are damping ratios. We want to filter the frequency given by

$$\omega_{osc} = \frac{n\omega}{2} \tag{6.16}$$

where n is the number of cylinders for the engine and ω is the rotational speed in [rad/s]. Assuming our control system is able to keep the engine speed relatively constant while purging, we can use a casceded notch filter with three center frequencies distributed around the velocity set point. In Figure 6.3 the amplitude and phase characteristics of a cascaded notch filter with center frequencies, corresponding to rotational velocities of 80, 85 and 90 [rpm], is shown.

To get a steeper characterstic and thus better phase properties, the damping ratios of the outer center frequencies are kept lower then the damping ratios of the middle center frequency.

Simulation results for filtered and unfiltered speed is shown in Figure 6.4. The engine speed during the purging period is kept constant by using feedback control. The amplitude of the velocity oscillations is reduced to ±0.2 [rpm] for the filtered signal. The time delay due to the filtering is approximately 0.1 [s].

It was also attempted to implement low-pass filters of Butterworth and Chebyshev type, of different orders. However, these were found to give worse performance than the notch filter due to unfavourable phase characteristics and ripple in the pass-band. Another alternative could be to use a Kalman filter. This would improve the phase characteristics compared to notch and low-pass filters. But it would complicate the filter design, due to the tuning procedures connected to the design of Kalman Filter. Kalman filtering of the speed measurement will not be further examined here. Instead, the filtering performance obtained with the cascaded notch filter are assumed to be good enough.

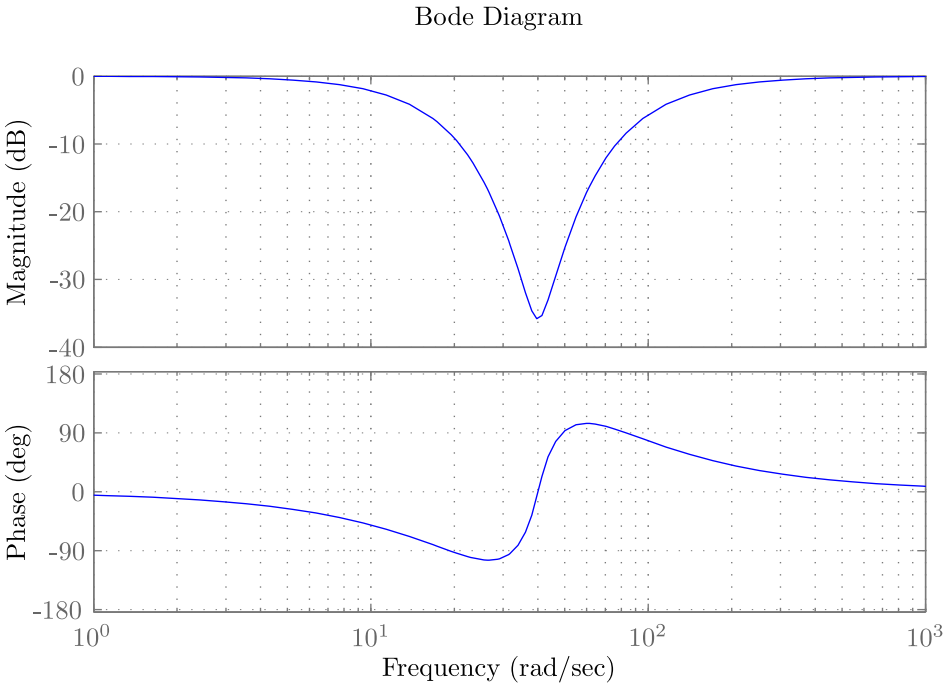

Figure 6.3: Amplitude and phase characteristics for a cascaded notch filter with three center frequencies.

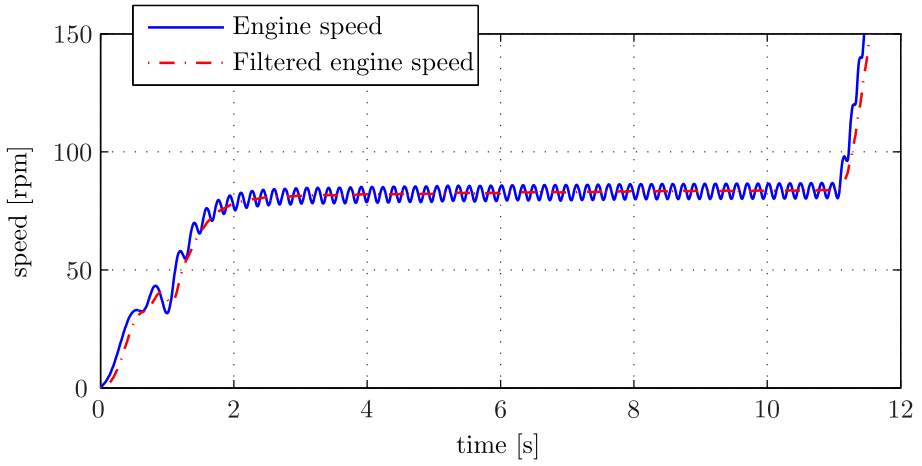

Figure 6.4: Filtered and unfiltered engines speed from simulations with a cascaded notch filter.

6.6 Problem statement

Control problems can be roughly divided into two categories; regulation (or stabilization) problems, where the reference x_{ref} is constant and tracking problems where the reference is a function of time, $x_{ref} = \text{f(t)}$ (Khalil [2002]). The control objectives stated in Section 6.1, can be achived by using set point regulation, i.e. by defining set points which fullfills the control objectives, or by tracking a tracetory for the engine speed ω and crank angle ϕ. A tracetory could be predefined, or could be generated by using a reference generator, e.g. by filtering the set points.

Good tracking performance would require that we always have sufficient control forces to counteract the negative system forces. This can not always be guaranteed for the starting system. Therefore, we will state the control problem as a regulation problem.

Since we don't not have any requirements on reducing the time of the starting sequence, we consider feedback controllers acting on the speed error $e_\omega = \omega_{ref} - \omega$ only. The crank angle can be found by integrating the speed measurement. However, since the engine always reaches the purging crank angle as long as it has positive speed, the crank angle error $e_\phi = \phi_p - \phi$ is only used in the fuel supply logic.

6.6.1 Speed reference

We want to keep the speed low during purging to reduce the air consume, but high enough to avoid extensive friction due to the Stribeck effect. A simple first approach could be to define the speed set point as the fuel-on speed. However, to keep the engine exactly at the fuel-on speed during the purging period, we would have to counteract the zero-mean torque oscillations generated by the piston torque. Since these oscillations are filtered out and not subject for control, we have to take into account that the actual speed will oscillate around the setpoint even for zero regulation error $e_\omega = 0$. Therefore, the first set point should be somewhat higher than the fuel-on speed, to ensure that the actual speed is higher than the fuel-on speed. We define

$$\omega_{ref} = \omega_{fo} + A_{\omega,max}, \tag{6.17}$$

where $A_{\omega,max}$ is an upper bound on the amplitude of the speed oscillations caused by the piston torque.

When the fuel supply is opened, we want a fast acceleration to the disengagement speed. Under normal circumstances the torque from the combustion process will be large enough to give a fast disengagement, such that we don't have to use the starting system to accelerate the engine. If the set point is kept constant also after the fuel supply is started, the control action will be gradualy reduced as the engine accelerates, and we reduce the air consume. However, in the case of reduced combustion torque, e.g due to engine misfire, the speed is still kept at the reference.

Control laws for the reference defined by Eq. 6.17 will be developed later in this chapter. This reference results in a simple system, which for low regulation error ensures that the control objectives is reached, while the air consume is reduced compared to the existing starting sequence by keeping the speed low during purging.

6.6.2 Problem statement

Using the control plant model, given by Eq. 6.4, we can state our control objects mathematically. Before the fuel supply to the combustion engine is opened, our control objects is number one and two in Section 6.1. We seek a control law which gives convergence to the reference speed and purges the exhaust system. By calculating the number of rotations necessary for purging, as described in Section 6.1.2, the two control objectives can be expressed as

Control Task 1. $\lim_{t \to t_p} \mid \omega_{ref} - \omega(t) \mid \; = 0 \; ,$

Control Task 2. $\lim_{t \to t_p} |\phi_p - \phi(t)| = |\phi_p - \int_0^{t_p} \omega(t)dt| \leq 0.$

where ϕ_p is the purging crank angle resulting from Eq. 6.2. After the fuel supply is opened, our control objective is to accelerate the engine to the disengagement speed of the starting system. This can be stated as

Control Task 3. $\lim_{t \to t_{de}} \mid \omega_{de} - \omega(t) \mid \; \leq 0.$

In this thesis, we assume that by achiving Control Tasks 1 and 2 before opening the fuel supply to the engine, we satisfy the requirements from our safety performance criteria. The second performance index will be measured primarily by watching the number of starts which can be achived for fixed bottle size, but also by considering costs related to other parts of the system. System robustness is tested by simulating the control system with varying model parameters.

6.7 Fixed set point pressure control

We consider a spring controlled pressure control valve. The flow area of the valve, is regulated by using a spring which balance the downstream pressure (ref. Section 2.3). Usually, there is no means of automaticly changing the pressure set point of the valve. For an ideal valve, the pressure is kept constant as long as the supply pressure is larger then the pressure set point.

We want a constant pressure set point which gives convergence to speed reference. A requirement for convergence is zero acceleration when the engine reaches the reference. This can be expressed as

$$\dot{\omega} = f(\phi, \omega_{ref}, t) + \frac{1}{I}\tau_e = 0 \tag{6.18}$$

We assume that the piston torque give a zero-mean contribution when $\omega \geq \omega_{ref}$ (ref. Section 6.4.2). That means that we only need to counteract the friction forces in this region. Inserting the bound on the friction torque from Eq. 6.10, and solving for the τ_e gives

$$\tau_e = \rho_1(\omega_{ref}) \tag{6.19}$$

Inserting the result from Eq. 6.22 in the control allocation algorithm defined by Eq. 6.8, we can find the necessary pressure set point $\bar{u}_1$ to keep the speed at, or over, the reference

$$\bar{u}_1 = P_d(\tau_e, \omega). \tag{6.20}$$

Calculating $\bar{u}_1$ from Eqs. 6.22 and 6.21, gives a value of 4.5 [Bar]. However, the constant pressure must also yield a starting engine torque large enough to accelerate the engine to the reference. If we let $\bar{u}_2$ be the neccesary set point to accelerate the engine to the reference, the minimum pressure u_3 set point can be found from

$$\bar{u} = max(\bar{u}_1, \bar{u}_2), \tag{6.21}$$

and the control law becomes,

$$\tau_e = \begin{cases} \tau_e(\bar{u}_3, \omega_{ref}) & \textbf{if } \omega < \omega_{de}, \\ 0 & \textbf{if } \omega \geq \omega_{de}, \end{cases} \tag{6.22}$$

Simulations and experimental results indicate that the supply pressure needs to be at least 14.2 [Bar] to accelerate the engine. Hence, the pressure will be considerably higher than needed to keep the engine at the reference, which also gives higher speed. However, the speed will be lower than for the on/off valve.

6.7.1 Simulation results

To test the system we run several consecutive starting simulations, starting with a bottle pressure of 30 [Bar]. To simulate how many starts can be achieved before reloading the bottle, the bottle pressure for each run, is implemented as the end pressure for the previous start. A starting bottle volume of 1.5 $[m^3]$ is used in the simulations and time delay of 0.2 [s] is applied to the control input.

For comparision, this configuration gives four starts for the existing starting sequence implemented with the time based fuel-on logic, and three starts for the existing starting sequence altered with the crank angle base fuel-on logic described in Section 6.1.2.

Tabel 6.7.1 show pressure before start, pressure drop and air consume for the simulations. Four starts is achived with the logic based controller. The minimum bottle pressure where the engine is able to start is 16.11 [Bar].

	Bottle pressure at start [Bar]	Pressure drop in bottle [Bar]	Air consume relative to atmospheric pressure $[m^3]$
Start 1	30.00	4.64	4.77
Start 2	25.36	4.64	4.79
Start 3	20.71	4.60	4.78
Start 4	16.11	4.01	4.19
Start 5	12.10	Failure	

Table 6.1: Bottle pressure at start, pressure drop and air consume for 6 consecutive starting simulations with the fix set point pressure control valve

The speed for the last sucessful start is plotted in Figure 6.5. We see that the engine speed is considerably higher than the reference, leading to increased friction and air consume.

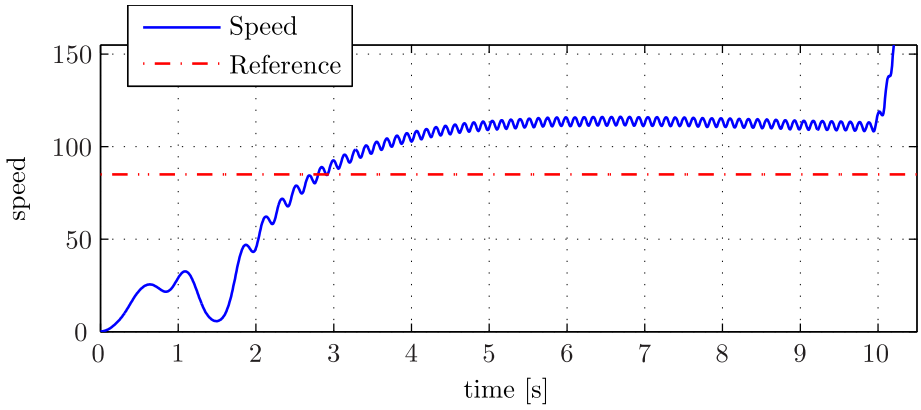

Figure 6.5: Simulation result for engine speed when implemented with a spring controlled pressure control valve. The pressure set point is 14.2 [Bar].

6.8 PID control

By using an electrically controlled pressure control valve, in combination with a proportional-integral-derivative (PID) controller, we can actively control the supply pressure to the starting engine. Hence, we can to reduce the air consume, by keeping the engine speed low. The standard time domain form of the ideal

PID controller, is

$$\tau_e = -K_p e_\omega(t) - K_d \dot{e}_\omega(t) - K_i \int_{t_0}^{t} e\omega(t)dt, \tag{6.23}$$

where e is regulation error. The proportional part put a linear penalty on the regulation error, whereas the integral term integrates past error to counteract the static disturbance caused by the Coulomb friction. Derivative action is added to increase the response and reduce overshoot. The control inputs $\bar{u}$, corresponding to the control torque from the PID-controller is found from the control allocation algorithm.

6.8.1 Linearization

For the purpose of analysing the PID-controller, the control design model from Eq. 6.3, will be simplified and linearized about the reference speed ω_{ref}. The reference speed is chosen, because it is important that the controller have good performance here. We assume that the piston torque is neglectable at the reference, since is has a zero mean contribution. The crank angle dependence of the system torque disappear, and the new system equation becomes,

$$\dot{\omega} = h(\omega, \tau_e) = -\frac{1}{I}\tau_f(\omega) + \frac{1}{I}\tau_e. \tag{6.24}$$

A linear system has the general form

$$\dot{x} = Ax + Bu. \tag{6.25}$$

To calculate the linear system coefficients A and B, we calculate the Jacobian of the system at the point $\omega = \omega_{ref}$. Inserting the expression for the friction torque from Eq.6.9 in, Eq. 6.24, and calculating the Jacobians, yields

$$A = \frac{\partial h(\omega, \tau_e)}{\partial \omega} = -\frac{1}{I}\left[f_v - (\tau_s - \tau_c)\frac{2\omega_{ref}}{\omega_s^2} exp\left[-\left(\frac{\omega_{ref}}{\omega_s}\right)^2\right]\right], \tag{6.26}$$

$$B = \frac{\partial h(\omega, \tau_e)}{\partial \tau_e} = \frac{1}{I}. \tag{6.27}$$

When inserting the parameters, we see that the exponential part of the A coefficient, gives a very small number. This is expected, since this part of the friction model depicts the Stribeck effect, which is only relevant for low speeds. Neglecting the exponential part, gives the simple system

$$\dot{\omega} = -\frac{f_v}{I}\omega + \frac{1}{I}\tau_e, \tag{6.28}$$

which has an open loop eigenvalue of $-\frac{f_v}{I}$. Since f_v and I are positive non-zero parameters, the open-loop system is stable for the ideal case with no delays. The transfer function of the system is found by taking the Laplace transform of the state space model, Eq. 6.26. This yields

$$h_u = \frac{\omega}{\tau_e} = \frac{1}{Is + f_v} \tag{6.29}$$

6.8.2 Controller design and tuning

A time delay of 0.2 [s] is considered in the controller design, to account for delays in the measurement and the valve dynamics. The time delay gives a negative phase contribution of,

$$\angle h_d = -0.2\omega. \tag{6.30}$$

To reduce the effect of measurement noise on the derivative action, we implement a PID-controller with a limited derivative term. The transfer function of the controller can be written

$$h_r = K_p + \frac{K_d s}{\alpha s + 1} + \frac{K_I}{s}, \tag{6.31}$$

where α is a coefficient which limits the bandwidth of the derivative action.

The controller is tuned based on a combination of the trial and error approach, using the full non-linear simulation model, and by looking at the bode diagram of the open loop transfer function h_0 of the linearized model, given by

$$h_0 = h_r h_u h_d, \tag{6.32}$$

where h_d is the transfer function for the time delay. Good stability and response were obtained by using the parameters,

$$\begin{aligned} \mathbf{K_p} &= -105, \\ \mathbf{K_d} &= -20, \\ \mathbf{K_I} &= -16, \\ \alpha &= 0.1 \end{aligned}$$

which gives the open loop amplitude and phase characteristics for the linearized system, shown in Figure 6.6. The time delay is implemented in the plot by using a 3^{rd} order pade approximation, given by the Matlab function pade.

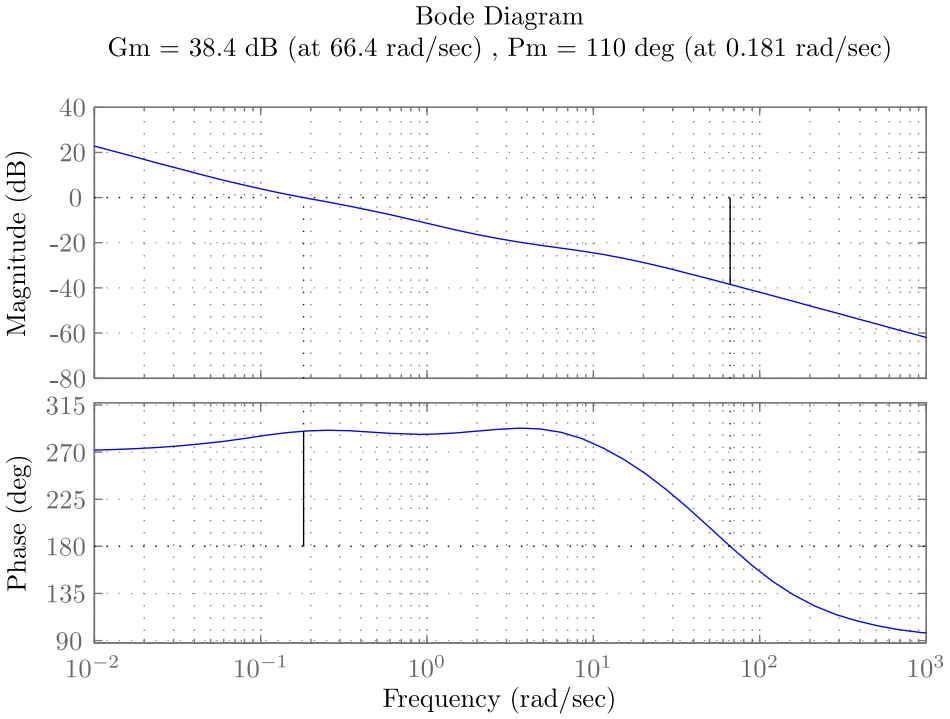

Figure 6.6: Amplitude and phase chracteristics of the linearized system model, implementeted with a pid controller and a phase delay of 2 [s]

From the figure, we see that we get a gain and phase margin of 38.4 [dB] and 110^0, respectively. This is well within the 6 [dB] and 45^0 required by Bode-Nyquist criteria, which is often used as a stability criteria for feedback controllers Balchen et al. [2003]. However, since we don't need the engine speed to reach the fuel-on speeed before the purging periode is over, fast response is not a priority. Hence, we can keep the gains relatively low to avoid chattering and increased speed oscillations due to unfiltered measurement noise and oscillations in the acceleration phase.

6.8.3 Simulation results

The PID controller is implemented in the full nonlinear model and simulated with the same simulation scenario as for the constant set point system (ref. Section 6.7.1). The results for pressure drop and air consume are shown in Table 6.2.

The PID-controller is able to give six starts for a 1.5 [m^3] bottle initially at 30 [Bar], which is twice as many starts as the existing starting system. We see that the air consume is kept relative constant for all starts.

	Bottle pressure at start [Bar]	Pressure drop in bottle [Bar]	Air consume relative to atmospheric pressure $[m^3]$
Start 1	30.00	2.84	2.90
Start 2	27.15	2.85	2.90
Start 3	24.30	2.86	2.92
Start 4	21.44	2.88	2.94
Start 5	18.56	2.92	3.00
Start 6	15.64	3.01	3.12
Start 7	12.62	Failure	

Table 6.2: Bottle pressure at start, pressure drop and air consume for 6 consecutive starting simulations with the PID controller

The speed and duty cyle P_2/P_1, for start number five are plotted in Figure 6.7. We see that the controller easily saturates the control organ. This is advantageous, since we need the largest possible torque during the first engine revolutions. However, due to the saturation, we need to limit the integral gain to avoid overshoot. Especially at low bottle pressures, overshoot can be a problem, since the control organ have to operate at the saturation limit for a longer time to accelerate the engine to the reference speed. Implementing a anti-windup scheme in the controller can reduce the risk of overshoot, such that the integral gain can be increased to give faster convergence.

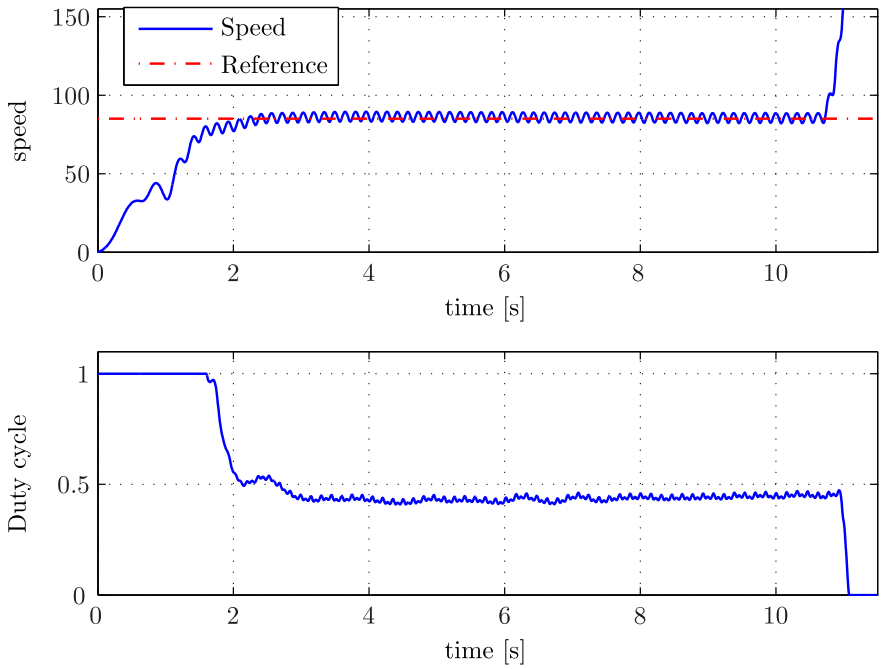

Figure 6.7: Results for speed and duty cycle for simulations with the PID controller at 21.44 [Bar] bottle pressure.

6.9 Sliding-mode control

In this section, a sliding-mode based controller will be developed and applied to the starting system model. The sliding mode control technique is a nonlinear control method, which use a combination of feedforward and feedback to control the plant. The controller forces the trajectories of the system states to reach a sliding manifold in finite time, and to stay on this manifold for all future time.

Sliding mode controllers are discountinous controllers which suffer from chattering. We will therefore develop a continous version of the controller.

6.9.1 Feedback linearization

With the assumption that the model is perfectly known, we can linearize the model by using a feedforward control law which cancel the nonlinearities. Our control plant model is given by Eq. 6.4. For set point regulation the control law, denoted feedback linearization, becomes

$$\tau_e = -I(Le + f(\phi, \omega, t)), \tag{6.33}$$

where e $= \omega - \omega_{ref}$ is the regulation error. Inserting this in the control plant model yields the simple linear closed-loop system

$$\dot{e} = -Le, \tag{6.34}$$

having a single pole at -L. Higher order linear control, such as PID, could easily be incorporated to handle potential uncertainties and to improve the response.

Unfortunately, the disadvantage of this control is that it assumes perfect knowledge of the plant in order to cancel the nonlinear terms. If, on the other hand, the model contains significant uncertainties, then a more rubust control law is needed. Using techniques from sliding-mode control can aid in robustifying the control law. We investigate this next.

6.9.2 Sliding mode control design

We follow along the lines of Skjetne and Teel [2004], and propose the feedback control law,

$$\tau_e = -\hat{I}Le - \left(\hat{I}K + \sigma(\phi, \omega, t)\right)\Psi(e) \tag{6.35}$$

where $\hat{I}$ is an estimate of the shafting inertia, the function Ψ is a robustifying term defined by

$$\Psi = sgn(e),$$

$L \geq 0$, and $K > 0$ are tunable controller gains, and the term $\sigma(\phi, \omega, t)$ is a function that will be determined through a Lyapunov analysis of the closed-loop system. By inserting the control law from Eq. 6.35 in the control plant model, we get the closed- loop system

$$\dot{e} = -\frac{\hat{I}}{I}Le - \frac{1}{I}\left(\hat{I}K + \sigma(\phi, \omega, t)\right) sgn(e) + f(\phi, \omega, t) \tag{6.36}$$

We define a Lyapunov function V(s) = $\frac{1}{2}e^2 = \frac{1}{2}|e|^2$ used to analyze stability, and note that e = $|e|sgn(e)$. Differenting V along the solution of 6.36 gives

$$\dot{V} = \frac{dV}{de}\dot{e} = -\frac{\hat{I}}{I}Le^2 - \frac{|e|}{I}\left(\hat{I}K + \sigma(\phi, \omega, t)\right) + ef(\phi, \omega, t) \tag{6.37}$$

We can apply bounds on $\dot{V}$, by using the bounds on the function $f(\phi, \omega, t)$ and the shafting inertia I, defined in Section 7.4. This yields

$$\dot{V} \leq -\frac{\hat{I}}{I}Le^2 - \frac{|e|}{I_0}\left(\hat{I}K + \sigma(\phi, \omega, t)\right) + |e|\rho(\phi, \omega, t) \tag{6.38}$$

$$\leq -\frac{\hat{I}}{I}Le^2 - \frac{\hat{I}}{I_0}K|e| - |e|\left(\frac{1}{I_0}\sigma(\phi, \omega, t) - \rho(\phi, \omega, t)\right). \tag{6.39}$$

We let the function $\sigma(\phi, \omega, t)$ be defined as

$$\sigma(\phi, \omega, t) = I_0\rho(\phi, \omega, t), \tag{6.40}$$

which, when inserted in 6.39 gives

$$\dot{V} \leq -\frac{\hat{I}}{I}Le^2 - \frac{\hat{I}}{I_0}K|e| \leq -\sqrt{2}\frac{\hat{I}}{I_0}K\sqrt{V}. \tag{6.41}$$

If we let W = $\sqrt{V} = \frac{1}{\sqrt{2}}|e|$, we get,

$$\dot{W} = \frac{1}{2\sqrt{V}}\dot{V} \leq -\frac{1}{\sqrt{2}}\frac{\hat{I}}{I_0}K \tag{6.42}$$

which, when rearranging, gives

$$\frac{d}{dt}|e| = \sqrt{2}\dot{W} \leq -\frac{\hat{I}}{I_0}K \tag{6.43}$$

When integrating 6.43, we get that for any initial condition $e_0 = |e(0)|$, that the solution satisfies,

$$|e(t)| \leq max\left[0, e_0 - \frac{\hat{I}}{I_0}Kt\right], \forall \geq \bar{t} \tag{6.44}$$

and it follows that there exists $\bar{t}\ \exists\ \left[0, \frac{I_0 e_0}{\hat{I}K}\right]$ such that $e(t) = 0, \forall t \geq \bar{t}$.

Unfortunately, the control law in Eqs. 6.35 and 6.40 results in chattering due to the discontinuous switching introduced by the signum function. Instead, the control law should be implemented with a function which gives a smooth transition from -1 to 1. This can be obtained by replacing the signum function with the function,

$$\Psi(e) = (1 + \varepsilon_1)tanh\left(\frac{e}{\varepsilon_2}\right), \tag{6.45}$$

where ε_1 and ε_2 are small positive numbers. Letting $\varepsilon := \varepsilon_2 atanh\left(\frac{1}{1+\varepsilon_1}\right)$, then this control law ensures convergence to the set $|e| : |e| \leq \varepsilon$ where ε can be made arbitrarily small. As seen, this control law guarantees regulation performance even with significant model uncertainties in the plant.

6.9.3 Simulation results and tuning

For good accuracy, the parameter ε_2 in Eq. 6.45 needs to be as small as possible. However, a too small value will induce chattering in presence of time delays or fast dynamics not modelled by the bounding function. Our system has time delays from the valve dynamics and the notch filter. Unfortunately, these time delays makes the controller hard to tune. Simulations show that there is a trade of between chattering and control performance which is hard to balance. Good regulation performance in combination with smooth control input seems infeasible.

In Figure 6.8, simulation results for speed and control input using the controller parameters

$$\mathbf{K} = 0.3,$$
$$\mathbf{L} = 0.2,$$
$$\varepsilon_{\mathbf{1}} = 0.1,$$
$$\varepsilon_{\mathbf{2}} = 0.3,$$

and a valve time delay of 0.2 [s], are shown. We see that the controller easily accelerates the engine, but extensive chattering is observed. To reduce the chattering to an acceptable level, ε_2 have to be increased to at least 10. However, this gives poor regulation performance.

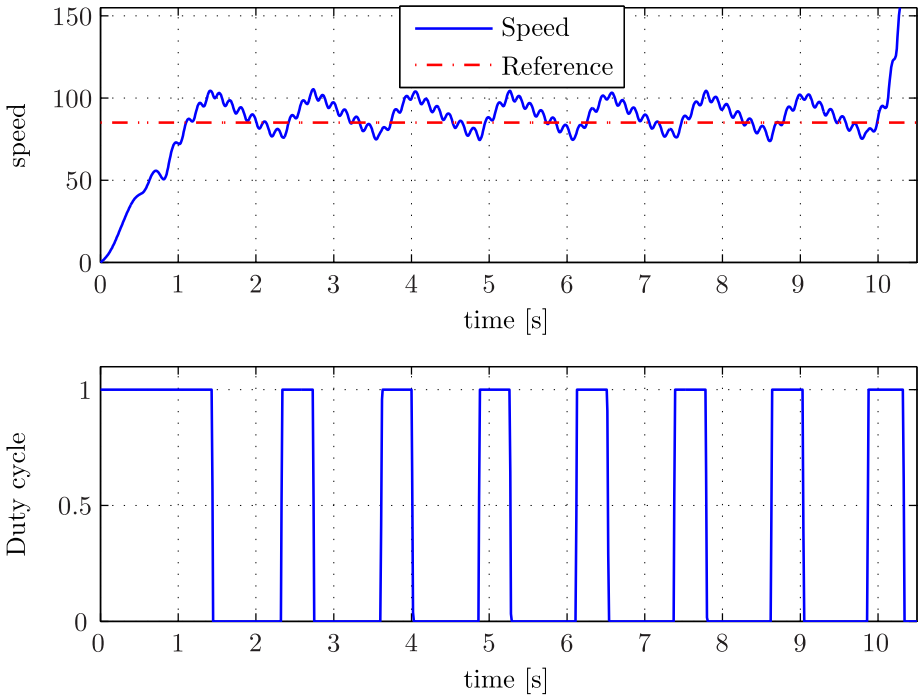

Figure 6.8: Results for speed and control input for simulations with the PID controller at 18.8 [Bar] bottle pressure.

The time delay can be reduced by removing the notch filter, however, this introduces the fast piston torque dynamics not modelled in the bounding function, in the feedback signal. To modell these dynamics in the bounding function, a measurement or observer for the initial crank angle would be necessary. Perhaps better performance could be achieved by using a Kalman Filter instead of the notch filter, but the requirements to the valve time delay would still have to be very strict.

6.10 Summary and discussion on controller performance

In this chapter the engine starting control problem has been formulated, and three concepts for control of the starting sequence have been introduced.

Control of the starting sequence by means of a pressure control valve with a constant pressure set point, was investigated in Section 6.7. A constant pressure give limited possibility of controlling the engine speed. Since the largest resisting forces of the system comes immediately after break-away, the pressure set point must be dimensioned with regards to this part of the starting sequence. Hence, the starting engine gives higher torque than necessary to keep the engine at the reference speed, which results in high speeds and larger air consume. However, the simulations indicated that the air consume is somewhat reduced compared to the existing starting system.

The air consume would probably be reduced considerably, if the pressure set point could be changed when the engine reach the speed reference. E.g. by using a simple logic based controller in combination with a valve which can have two fixed set points. However, this will not be further explored here.

In Sections 6.8 and 6.9 the concept of using an electrically controlled pressure control valve, in combination with a feedback controller to change the pressure set point, was investigated. Section 6.8 focus on a PID based feedback controller with limited derivative action to reduce the bandwidth. The simulations gave twice as many starts as the existing starting system with a starting air bottle volume of 1.5 $[m^3]$. The controller were able to stabilize the filtered engine speed at the reference and a relatively smooth control input was obtained.

Section 6.8 explore the potential for using a nonlinear, sliding-mode based controller, to control the engine speed. A continous version of the controller is developed and applied to the starting system. Simulation show that when tuning the controller, there is a trade-off between chattering and control performance. It seems infeasible to stabilize the engine at the reference speed, while obtaining a smooth control input. The chattering leads to large oscillations in the engine speed, increased wear of the valve, and increased air consume.

Since good control performance was obtained with the PID controller, methods for robustifying the sliding mode controller against the chattering problem will not be investigated in this thesis. Instead, the robustness of the PID controller will be evaluated in the next chapter.

Chapter 7

Starting sequence and controller testing

It is important that the controller gives a starting sequence which is robust, and can perform well for varying system parameters and dynamics. This is important because, in some cases, the consequence of a failed starting attempt can be severe. Especially in we get a failed starting attempt after fuel gas is allowed to the cylinders.

Even though the validation of the simulation model showed relativly good accordance with experimental result, there were also some deviations. This shows that the model is, in fact, a considerable simplification of the real system. However, the model parameters and dynamics can be altered to account for uncertainties, and the controller can be tested against worst case scenarios. The most vulnerable assumptions, and the largest uncertainties for the model, are considered to be

1. The assumptions that the starting engine and valve characteristics are perfectly known,
2. The assumption of no misfireing in the engine cylinders,
3. Uncertainties in the friction parameters, τ_c, τ_s, ω_s and μ_v,
4. Uncertainties connected to the intitial crank angle.

If the valve and starting engine characteristics used to calculate the pressure set point to the starting engine, deviates from the real system characterstics, we risk that not enough torque is allocated in the control allocation algorithm. If one or more of the engine cylinders misfire, the combustion torque is reduced, and in the wost case scenario we risk that the engine decellerate.

The friction parameters is dependent on dwell-time and lubrication. The initial crank angle which vary for each start, influences the resistance due to the piston torque.

In addition, the starting sequence should be robust with regards to,

5. Changing shaft inertia,
6. Different number of cylinders.

The shaft inertia might vary from engine to engine, e.g. due to different makes of generator or gear. The Rolls-Royce Bergen C:26:33 Engine comes in 6, 8 and 9 cylinder in-line configuration, and the starting system should be able to handle the different properties this gives. The number of cylinders obviously also effects the shaft inertia.

To verify that the controller is robust, it is useful to simulate the system against worst case scenarios. It is not feasible to test for all combinations of scenarios which might influence the controller performance, however, it is assumed that the main tendencies will interact with each other.

7.1 Simulation scenarios

Controller robustness testing will be performed by doing a set of parameter tests. Some parameters or parts of the model are altered, whereas the rest of the system and the controller is kept unchanged. The test scenarios are described below.

Test Scenario 1. *Valve and starting engine uncertainty test*

These tests are done to test how the controller performs when the valve and starting engine characteristics used in the control allocation algorithms, deviates from the real characteristics. The uncertainty is modelled by altering the interpolation tabel used to calculate the pressure set point, such that it gives 30 percent higher, and 30 percent lower pressure.

Test Scenario 2. *Engine misfire test*

These tests are performed to test how the starting sequence acts in case of engine misfire. To model the misfire, the combustion torque from five of the cylinders are omitted from the the simulation for six seconds after the the fuel supply is started.

Test Scenario 3. *Friction parameters uncertainty test*

To take into account uncertainties in the engine friction, the friction parameters are increased compared to the nominal values. To test the effect of increased friction for low speeds (the acceleration phase of the starting sequence), the static and coulomb friction τ_s and τ_c are increased, in addition to the Stribeck coefficient ω_s. To test the effect of increased friction at the higher speeds, the coulomb and viscous friction τ_c and f_v are increased.

Test Scenario 4. *Initial crank angle test*

To test the effect of changing the initial crank angle, a series of simulations are performed, while altering the angle in an even interval for each run.

Test Scenario 5. *Cylinder number and inertia test*

To test how the controller performs for plants with different properties, the number of cylinders for the combustion engine, and the inertia of the shafting is altered.

In general, for all the test scenarios, we run test at starting bottle pressures of 15.5 [Bar] and at 30.0 [Bar]. These are considered to be the extreme values, in the sense they correspond to the minimum pressure where we assume that the engine should be able to start and the maximum bottle pressure.

7.2 Simulation results

7.2.1 Valve and starting engine uncertainty test

To test how the control system performs when we have uncertainties in the valve and starting engine performance characteristics, the results from the control allocation algorithm, Eq. 6.8, are altered. The new equation for the control input becomes

$$\hat{\bar{u}} = qP_d(\tau_e, \omega), \tag{7.1}$$

where $\hat{\bar{u}}$ is an estimate of the pressure set point when we have $|(1-q)|100$ percent uncertainty in the characteristics.

The tests will be performed with an uncertainty of 30 percent, that is q = 0.7, and q = 1.3, where the lower value for q gives lower pressure set point and thus lower torque, and vice versa. The perfomance of the real valve and starting engine, are assumed to be well within this interval. To simulate the worst case scenario, the lower set point is simulated with low bottle pressure, and the higher set point, with high bottle pressure. The tests become

- **Test 1.1:** $q = 0.7$, $P_1 = 15.5$ [Bar],
- **Test 1.2:** $q = 1.3$, $P_1 = 30.0$ [Bar].

Simulation result for **Test 1.1** is shown in Figure 7.1. From the lower plot, we see that the PID controller is still able to saturate the control organ is spite of the reduced pressure set point. A slight overshoot is observed in the speed plot, due to the fact that the controller saturates for a longer time since it takes longer time to accelerate the engine to the reference.

Simulation result from **Test 1.2** are presented in Figure 7.2. Fast convergence to the reference is observed, but due to the fact that the control allocation gives to high pressure set point, the control input is more oscillatory.

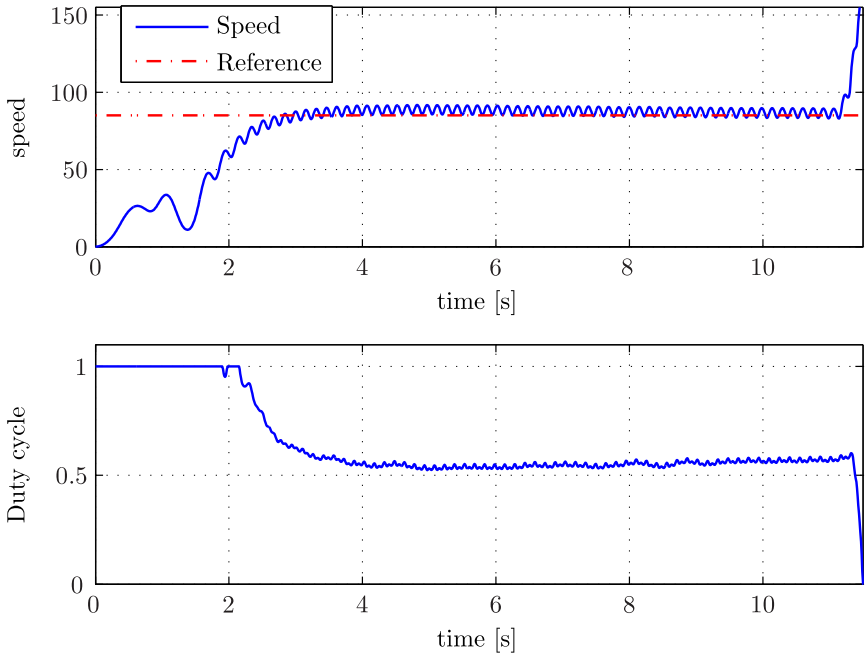

Figure 7.1: Simulation result for speed and duty cycle for **Test 1.1**

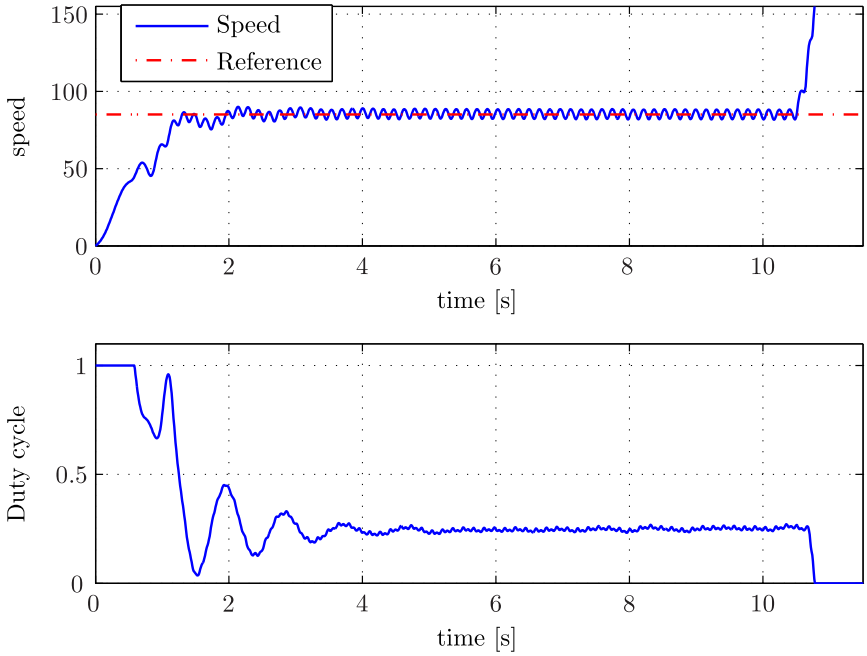

Figure 7.2: Simulation result for speed and duty cycle for **Test 1.2**

7.2.2 Engine misfire test

To simulate the effect of engine misfire on the starting sequence, we consider a worst case scenario with misfire on five out of nine cylinders. The misfire is implementet by adding a six second time delay to the fuel supply of five of the cylinders. In practice this means that the combustion torque from these cylinders will be zero for the whole starting sequence.

It seems fair to assume that the worst scenario is a misfire when the bottle pressure is low, such that the sum of the torque from the combustion and starting engine is lowest. Therefore, the engine is simulated with a bottle pressure P_1 of 15.5 [Bar].

Simulation results for speed and piston torque is plotted in Figure 7.3. We see that the misfire result in an unbalance in the piston torque after combustion. The engine is still easily accelerated to the disengament, in spite of the reduced torque from the combustion and low bottle pressure. When the starting engine is disengaged, the acceleration is reduced but still positive.

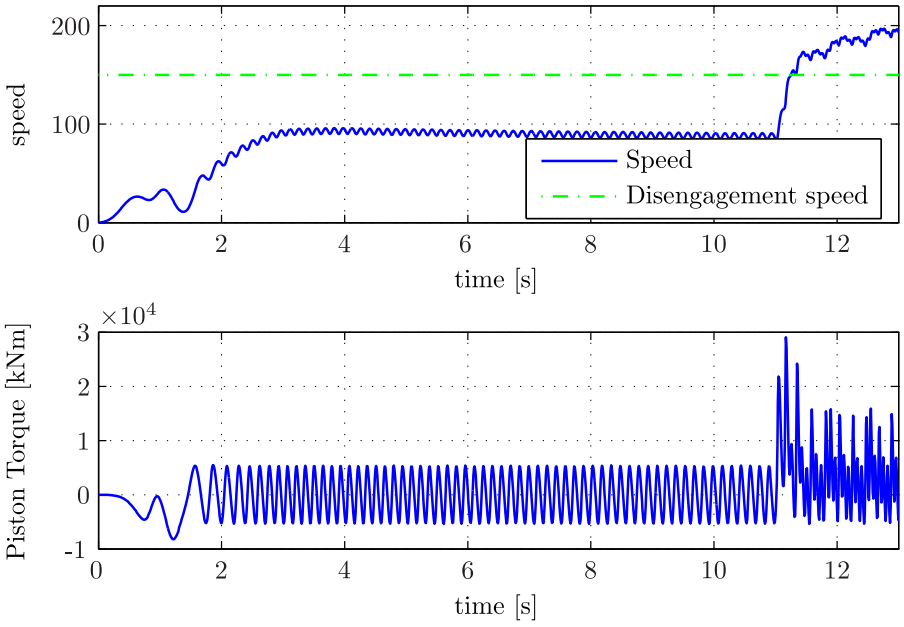

Figure 7.3: Simulation result for speed and piston torque with misifre on five cylinders

7.2.3 Friction parameters uncertainty test

Two tests are performed to test the starting sequence and controller performance in the case of varying friction parameters. Due to deformation of the junction asperities between the sliding surfaces and increased viscosity of the

lubricants, the engine will have increased friction for cold start. This is modelled by increasing the static and coulomb friction and the Stribeck parameter ω_s, which in effect will prolong the partial fluid lubrication regiment to higher velocities. The first test become

- **Test 3.1:** $\tau_s = 1.2\tau_{s,nom}$, $\tau_c = 1.2\tau_{c,nom}$, $\omega_s = 1.3\omega_{s,nom}$, and $P_1 = 15.5$ [Bar]

where the subscript *nom* implies nominal values. The simulations results with these parameters are plotted in Figure 7.4. We see that the starting system is still able to overcome the friction forces. However, we get an overshoot of approximately 10 [rpm]. The overshoot is due to wind-up of the integral term of the controller. The integral effect winds-up, because the control organ spends longer time at saturation to reach the reference. The increase in the friction, result in an increase in the air consume from 3.14 $[m^3]$ with nominal values, to 3.32 $[m^3]$, where the volumes are given with reference to atmospheric density. This increase is mainly due to increased friction load, but also because of the overshoot.

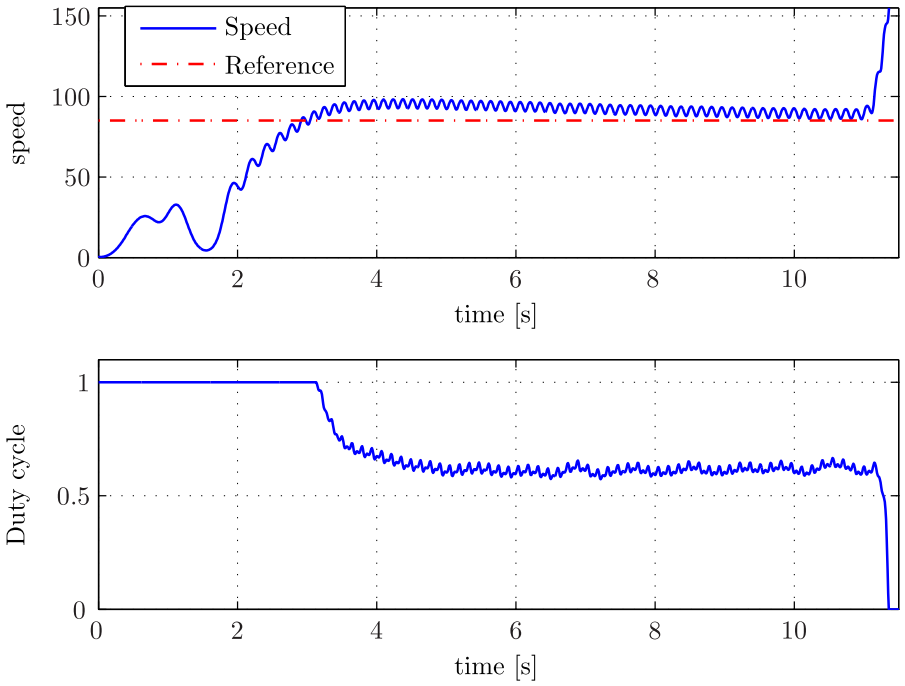

Figure 7.4: Simulation result for **Test 3.1:**. Increased friction, due to cold start

To evaluate the impact of increased friction at higher speeds, the Coulomb friction and viscous friction are increased. The test parameters are altered to

- **Test 3.2:** $f_v = 1.2 f_{v,nom}$, $\tau_c = 1.2\tau_{c,nom}$, and $P_1 = 15.5$ [Bar].

Results for this case is shown in 7.5. We see that also these parameter gives overshoot, although somewhat less than for the previous case. The increase in the air consume is 0.52 $[m^3]$ compared to nominal values.

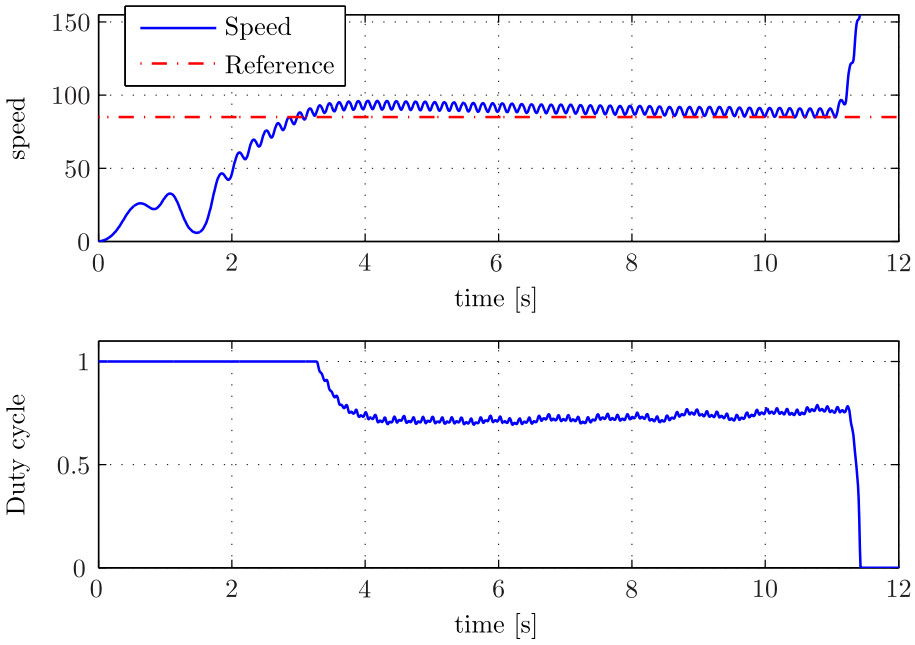

Figure 7.5: Simulation result for **Test 3.2:**. Increased viscous and coulomb friction

7.2.4 Initial crank angle test

The angular position of the crankshaft before starting the engine, is random. Changing the initial crank angle, alters the piston torque during the first couple of engine revolutions. The piston torque will vary within the interval $0 < \phi_0 \leq 4\pi/n$, where n is the number of cylinders. That is, $\phi_0 = 0$ gives the same progress of the piston torque as $\phi_0 = i4\pi/n$, where i is an arbitrary integer.

To evaluate the effect on the starting sequence of different initial crank angles, ϕ_0 is changed in steps in the interval $0 < \phi_0 \leq 4\pi/n$. The altered test parameters are given by

- **Test 4.1:** $\phi_0 = 0 : \frac{4\pi}{6n} : \left[\frac{4\pi}{n} - \frac{4\pi}{6n}\right]$ [rad], $P_1 = 15.5$ [Bar]

The results from the simulation are shown in Figure 7.6. We see that despitate the fact that the velocity gradient is grately affected by the initial crank angle

at low speeds, the engine is accelerated for all values of the angle. The effect of the starting angle at higher speed is low.

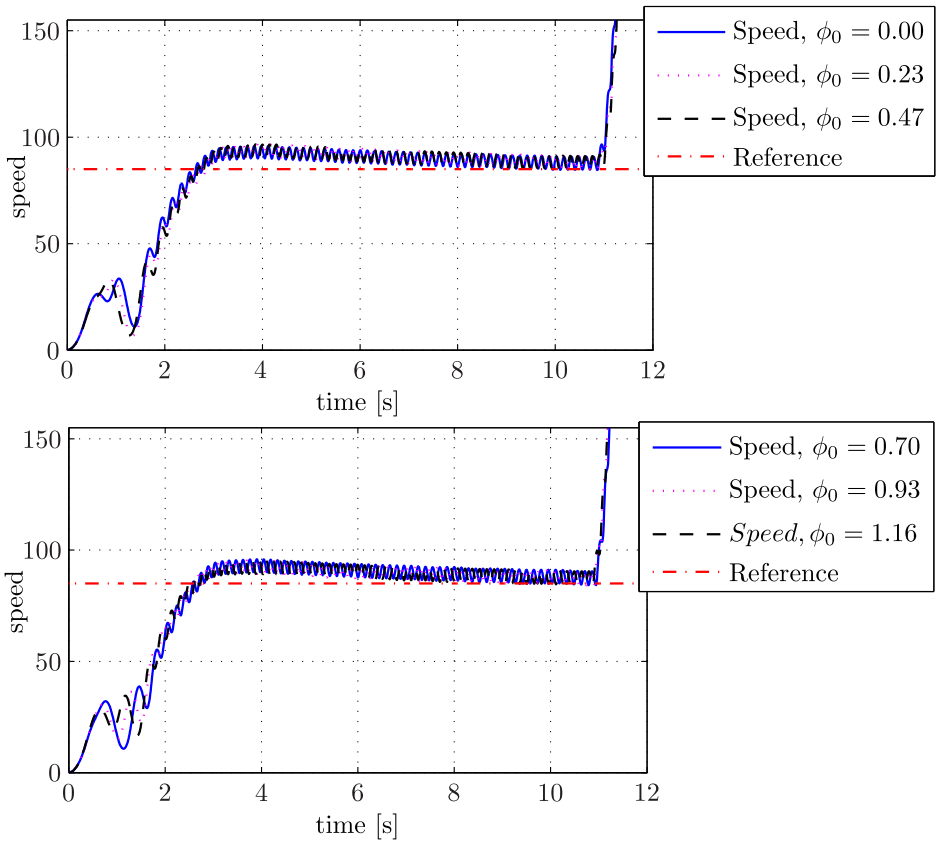

Figure 7.6: Simulation result for **Test 4.1:**. Variation in initial crank angle

7.2.5 Cylinder number and inertia test

To verify that the starting system are robust enough to handle different engine sizes in terms of shaft inertia and number of cylinders, we vary these parameters. Different cylinder number also imply different friction. Therefore also the friction will be altered by multiplying the total friction torque from the friction model with a fixed gain. We run in total ten tests, defined by

- **Test 5.1:** $n = 6$, $I = 0.6I_{nom}$ $[kgm^2]$, $\tau_f = 0.8\tau_{f,nom}$, $P_1 = 15.5$ [Bar],
- **Test 5.2:** $n = 6$, $I = 0.6I_{nom}$ $[kgm^2]$, $\tau_f = 0.8\tau_{f,nom}$, $P_1 = 30.0$ [Bar],
- **Test 5.3:** $n = 6$, $I = 1.5I_{nom}$ $[kgm^2]$, $\tau_f = 0.8\tau_{f,nom}$, $P_1 = 15.5$ [Bar],
- **Test 5.4:** $n = 6$, $I = 1.5I_{nom}$ $[kgm^2]$, $\tau_f = 0.8\tau_{f,nom}$, $P_1 = 30.0$ [Bar],
- **Test 5.5:** $n = 8$, $I = 0.8I_{nom}$ $[kgm^2]$, $\tau_f = 0.9\tau_{f,nom}$, $P_1 = 15.5$ [Bar],

- **Test 5.6:** $n = 8$, $I = 0.8I_{nom}$ $[kgm^2]$, $\tau_f = 0.9\tau_{f,nom}$, $P_1 = 30.0$ [Bar],
- **Test 5.7:** $n = 8$, $I = 2.0I_{nom}$ $[kgm^2]$, $\tau_f = 0.9\tau_{f,nom}$, $P_1 = 15.5$ [Bar],
- **Test 5.8:** $n = 8$, $I = 2.0I_{nom}$ $[kgm^2]$, $\tau_f = 0.9\tau_{f,nom}$, $P_1 = 30.0$ [Bar],
- **Test 5.9:** $n = 9$, $I = 2.5I_{nom}$ $[kgm^2]$, $\tau_f = \tau_{f,nom}$, $P_1 = 15.5$ [Bar],
- **Test 5.10:** $n = 9$, $I = 2.5I_{nom}$ $[kgm^2]$, $\tau_f = \tau_{f,nom}$, $P_1 = 30.0$ [Bar],

where I_{nom} and $\tau_{f,nom}$ are the nominal of the shaft inertia and the friction, respectively. In addition to this, the center frequencies of the notch filter is altered, to correspond with different cylinder numbers.

Tests **5.1, 5.2, 5.5, and 5.6** are meant to simulate six- and eight-cylinder propulsion engines. Medium-speed propulsion plant are usually equipped with a clutch, meaning that the propeller and propeller shaft can be clutched out during starting to reduce the total inertia. In addition, propulsion engines usually have smaller flywheels then generator sets.

Tests **5.3, 5.4, 5.7, 5.8, 5.9, and 5.10** are meant to represent six,- eight-, and nine-cylinder generator sets. These engines have more rotating mass, due to the larger generators and flywheels.

Results for all tests are found in Appendix C. Only the results of greatest interest are presented here. Figure 7.7 show simulation result for **Test 5.9**. The result show that the controller is vulnerable when the starting system needs a long time to accelerate the engine to the reference. Due to the large shaft inertia and low bottle pressure, the PID controller needs longer time to accelerate the engine, meaning that the valve saturates for a long time. This gives large overshoot due to wind-up. Form the duty cyle plot we see that the controller is really only active for the last three seconds of the starting sequence.

Figure 7.8 show simulation result for speed, duty cycle, and filter performance for **Test 5.1**. Because of the low shaft inertia, the oscillations due to the piston torque increased. This gives lower stability of the system, which can be seen in the duty cycle plot. Also, due to the lower filter center frequencies the delay from the filter is somewhat increased.

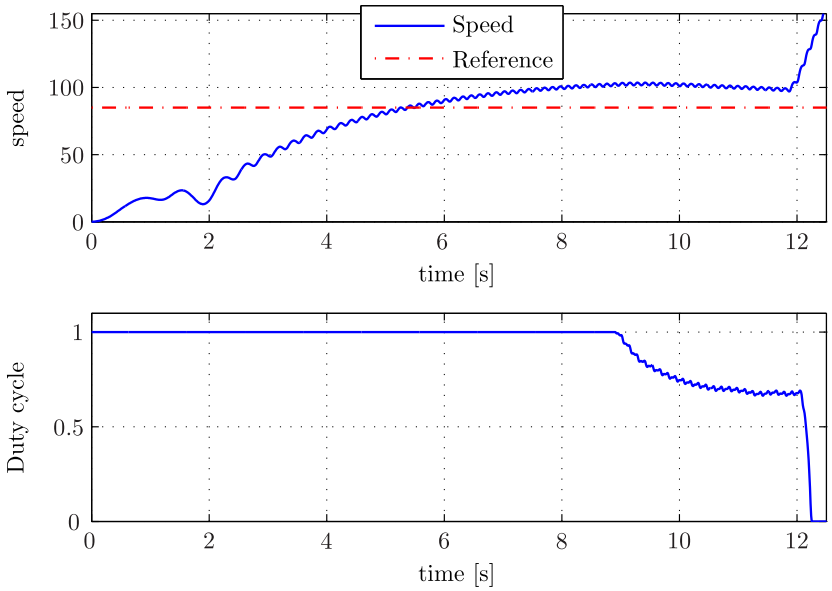

Figure 7.7: Simulation result for **Test 5.9:**.

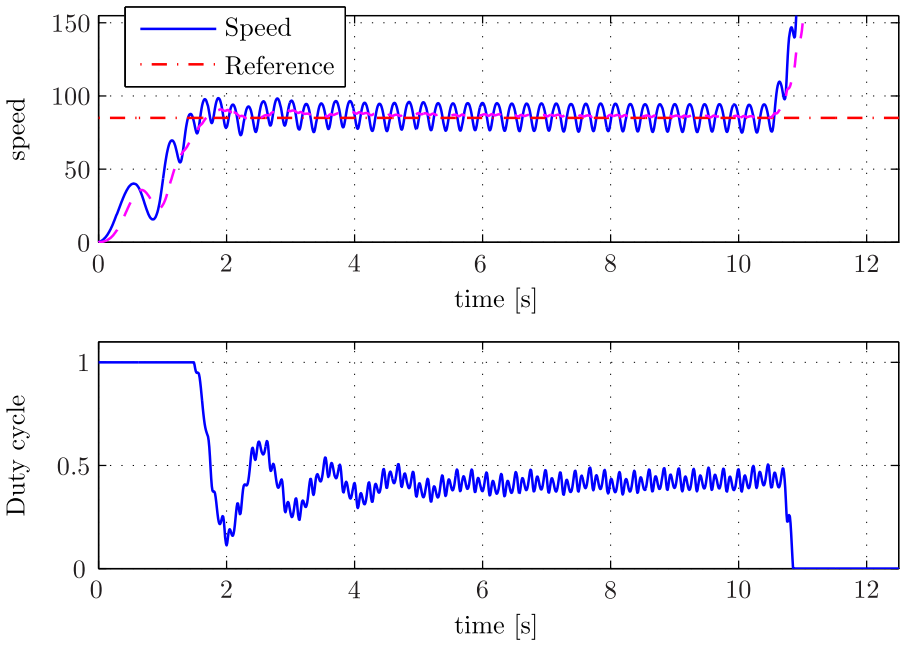

Figure 7.8: Simulation result for **Test 5.1:**.

7.3 Summary and discussion on system robustness

The result presented in the previous sections, indicate that the starting sequence with PID controller is relative robust in most operation conditions. The system is able to accelerate the engine to the disengament speed of the starting system with as low bottle pressure as 15.5 [Bar], for all test cases. The control system show strong robustness against uncertainties in the starting engine and valve characteristics, and is also able to handle variations in the friction parameters and initial crank angle.

In no cases does the system decellerate. In the case of misfire on five out of nine cylinders, the simulations show that the system is still able to accelerate the engine. Even at low bottle pressures.

A recurring issue is overshoot due to wind-up of the integral action of the controller. This is especially seen when the starting system uses a long time to accelerate the engine to the reference speed, such that the control organ operates with saturation for a long time. The overshoot result in increased air consume. Large shaft inertia, large static and boundary friction, and low bottle pressure, are cases which prolong the acceleration time and increases overshoot. It is believed that these problems can be reduced by implementing an anti windup precaution in the controller, to reduce the integral action in case of saturation.

The tests agains varying engine sizes, show reduced system performance for the extreme cases. That is, for the smallest and largest engine dimensions. In the case of a small engine, the system gets more unstable and speed oscillations and controller chattering is increased. However, the system is still able to stabilize at the reference relatively fast. The notch filter also show reduce filtering performance and increased delay for this case, due to the larger speed oscillations and lower center frequencies. In the case of a large engine, the reduced control performance is due to long acceleration time and subsequent overshoot. However, this is only a problem at low bottle pressure. At higher bottle pressure the acceleration time is reduces, which also reduces overshoot.

Chapter 8

Conclusions

8.1 Discussion

This thesis has focused on modelling and control of pneumatic starting engines for gas fueled combustion engines. The architecture of the starting system and the challenges related to starting of gas engine, was described and discussed in Chapter 1 and 2. Gas engines have an increases emission of unburned fuels during starting and stoping, which makes it necessary to take precautions to avoid igniteable concentrations of gas in the exhaust system. In addition, it is advantageous to reduce the air consume during starting to reduce system cost and space requirements.

In Chapter 3 and 4, mathematical models of the combustion engine and the starting system are developed. The objective is to develop models which cover the main physics of the system, and as such, give means for investigating, through computer simulations, how the system can be improved.

The models were validated in Chapter 5, by comparing simulating results to experimental data from starting tests of the real system. The model was found to give fairly good agreement with the experimental result, though some differences were observed. The differences are believed to stem mainly from uncertainties in the friction and starting engine parameters.

In Chapter 6, the engine starting control problem is formulated. In addition, it is suggested to change the conditions for starting the fuel supply to the cylinders, by requiring that the engine is rotated for a fixed number of rotations before turning on the fuel supply. It is believed that this will improve the safety of the starting sequence, since it will give a stricter control of the size of the purged volume. However, simulations showed that this requirement increased the air consume, due to longer purging period.

To reduce the air consume of the starting system, three concepts for controlling the combustion engine speed during starting were explored. Control of the engine speed is advantageous, since both the air consume and the friction increases with the speed.

The first concept which was investigated, was to use a spring controlled pressure control valve, to regulate the supply pressure to the starting engine. This type of valve has no means of changing the pressure set point. Therefore, a fixed pressure set point must be defined. The simualtion result showed that the valve was able to reduce the air consume somewhat. However, this method gave relatively high speeds during purging, since the set point must be relatively high to overcome the negative system torques immediately after break-away.

The combination of an electrically controlled pressure control valve which are able to adjust the set point and feedback control of the engine speed, was found to give better results. Two feedback controllers were developed and evaluated. First, a PID controller with limited derivative action, then a nonlinear, sliding mode based controller.

The best results were obtained with the PID controller. Simulations showed that the controller was able to accelerate the engine and stabilize it on the reference speed. The control law resulted in a smooth control input with little chattering. The relatively accurate speed control, gave twice as many engine starts as the existing starting system.

The sliding mode based controller proved to be difficult to tune. A trade-off between control performance and valve chattering was observed, and a combination of smooth control input and accurate speed control was not obtained. The chattering resulted in instability and increased air consume.

In Chapter 7, the robustness of the altered starting system with the PID controller was further evaluated, by performing a number of simulation tests with what is believed to be worst case scenarios. The tests focused on robustness with regards to uncertainties in the system and changing plant dimensions. The tests showed that the system has relatively good robustness. The main issue discovered, was overshooting of the engine speed in those cases that the starting system need a long time to accelerate the engine to the reference. This is because of wind-up of the integral action, due to the fact that the valve operates with saturation for a long time. It is believed that this problem can be eliminated by implementing an anti-windup precaution, to reduce the integral action when operating at, or close to saturation.

8.2 Recommendations and further work

Seeing that an engine purging based on a fixed number of rotations give a strickter control of the purged volume, it is recommended to replace the existing time-base logic for starting the fuel supply, with the rotation based logic defined in Section 6.1.2. However, this will increase the air consume. Therefore, a total evaluation on whether it is advantegous to implement methods for controlling the engine speed to reduce air consume, should be done.

If the advantage of being able to reduce the air consume is found to outweigh the extra cost related to implementing the control system, the PID control system should be further investigated. It is probably favourable to implement an anti-windup scheme in the control system to avoid overshoot. In addition, it should

be considered using a more sophisticated measurement filter. E.g. an adaptive Kalman Filter.

The system should be implementet on the engine test bed to evaluate its performance on the real system, and identify differences from the simulation results.

The control system could probably be further optimized to cope with different system properties. An in-depth analysis of methods for robustifying the sliding-mode controller against the chattering problems, could be done, since sliding mode methods are known to be very robust against changing different system properties.

Bibliography

Brian Armstrong-Helouvry. *Control of Machines with Friction.* Kluwer Academic Publishers., 1991.

Jens G. Balchen, Trond Andresen, and Bjarne A. Foss. *Reguleringsteknikk.* Institutt for teknisk kybernetikk, NTNU., 2003.

Peter Beater. *Pneumatic Drives: System design, Modelling and Control.* Springer-Verlag, Berlin Heidelberg., 2007.

Standard for certification, No. 2.11. DNV, January 1999.

Olav Egeland and Jan-Tommy Gravdal. *Modeling and simulation for automatic control.* Marine Cybernetics, 2002.

Per Magne Eidang and Konrad Magnus Haavik. Natural gas as a ferry fuel. In *Workshop on Alternate Fuels for Ferries and Other Vessels*, 2000.

Colin R. Ferguson and Allan T. Kirkpatrick. *Internal Combustion Engines.* John Wiley and Sons, Inc., 2nd edition, 2001.

John B. Heywood. *Internal Combustion Engine Fundamentals.* McGraw-Hill International Editions., 1988.

Hassan K. Khalil. *Nonlinear Systems.* Prentice Hall., 3rd edition, 2002.

Torben Kviste Jensen. *Faster CHP gas engine start with less emission.* Danish Gas Technology Centre., 2007.

Henry Liu. *Pipeline Engineering.* CRC Press LCC., 2003.

H. Olsson, K. J. Aastrm, C. Canudas de Wit, M. Gfvert, and P. Lischinsky. Friction models and friction compensation. 1998.

Michael J. Pinches and Brian J Callear. *Power Pneumatics.* Prentice Hall., 1996.

Rolls-Royce. *Project Planning Manual for Stationary Power Plants.* April 2010.

R. Skjetne and A. R. Teel. Maneuvering dynamical systems by sliding-mode control. Proceedings of the 2004 American Control Conference, 2004.

Asgeir Sørensen. *Lecture notes Marine Control Systems.* Department of Marine Technology, Norwegian University of Science and Technology., 2011.

Richard Stribeck. The key qualities of sliding and roller bearings. *Zeitschrift des Vereines Seutscher Ingenieure.*, 46(1341-1348), 1902.

A. F. Stronach and J. R. Smith. Development of a simulation model of turbocharged diesel engine prime-movers for power system studies. *International Journal of Electrical Power and Energy Systems*, 10(2):123–129, April 1988.

Frank M. White. *Fluid Mechanics.* McGraw-Hill College, 4th edition, 1998.

Doug Woodyard. *Pounder's Marine Diesel Engines and Gas Turbines.* Butterworth-Heinemann., 9th edition, 2009.

Minglian Zhou and Jian Wen. Modeling and optimum design of pneumatic gear motor. In *International Conference on Measuring Technology and Mechatronics Automation.*

Appendix A

Piston equations

A.1 Piston position

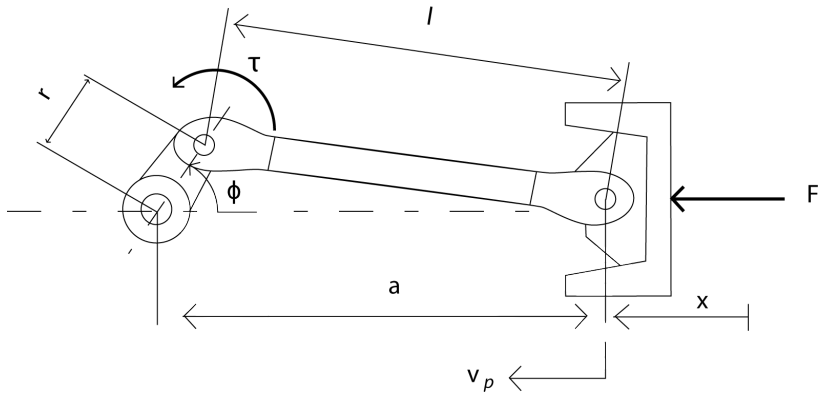

Figure A.1: Illustration of the forces acting on a 4-cylinder engine during start-up.

The derivation of a formula for the piston position as a function of the crank angle, starts with the geometric relationship defined by the law of cosine. Reference is made to Figure A.1. The law of cosine yields

$$l^2 = r^2 + a^2 - 2arcos(\phi), \tag{A.1}$$

By adding the expression, $r^2\left[\left(cos^2(\phi) + sin^2(\phi)\right) - 1\right]$, to the right side , and rearranging we obtain

$$l^2 = (a - rcos(\phi))^2 + r^2 sin^2(\phi). \tag{A.2}$$

which, when solving for a, yields

$$a = rcos(\phi) + \sqrt{l^2 - r^2 sin^2(\phi)}. \tag{A.3}$$

We want to find the piston position, x, relative to its uppermost position. The relation between x and a are given by

$$x = a - l - r. \tag{A.4}$$

In addition we introduce the crank shaft ratio λ, defined as

$$\lambda = \frac{r}{l} \tag{A.5}$$

Inserting Eqs. A.3 and A.5 in Eq. A.4, we get the equation for the piston position relative to its uppermost position as a function of crank angle

$$x(\phi) = r\left[1 - cos(\phi) + \frac{1}{\lambda}\left(1 - \sqrt{1 - \lambda^2 sin^2(\phi)}\right)\right], \tag{A.6}$$

which is equal to Eq. 3.5.

A.2 Piston velocity

The piston velocity is the time derivative of the piston position. If we start with the relation derived in Eq. A.6, we can calculate the piston velocity from

$$v_p = \frac{d}{dt}(x(\phi)) \tag{A.7}$$

Differenting this using the chain rule gives

$$v_p = \frac{dx}{dt}\omega. \tag{A.8}$$

Where the derivative $\frac{dx}{d\phi}$ can be calculated from Eq. A.6, which gives

$$\frac{dx}{d\phi} = r\left[sin(\phi) + \frac{1}{2}\frac{\lambda sin(2\phi)}{\sqrt{1 - \lambda^2 sin^2(\phi)}}\right]. \tag{A.9}$$

Multiplying with the shaft speed ω, gives the final expression for the piston velocity

$$v_p(\phi,\omega) = r\left[sin(\phi) + \frac{1}{2}\frac{\lambda sin(2\phi)}{\sqrt{1-\lambda^2 sin^2(\phi)}}\right]\omega, \tag{A.10}$$

which is equal to Eq. 3.6.

A.3 Piston acceleration

The piston acceleration can be found by using the same approach as with the piston velocity, but take the *double* derivative of the piston position. This yields,

$$a_p(\phi,\omega) = r\left[cos(\phi) + \frac{\lambda cos(2\phi)}{\sqrt{1-\lambda^2 sin^2(\phi)}} + \frac{\lambda^3 sin^2(2\phi)}{4\sqrt{1-\lambda^2 sin^2(\phi)^3}}\right]\omega^2, \tag{A.11}$$

which is equal to Eq. 3.7

A.4 Piston force from crankshaft torque

The relationship between the torque on the crankshaft and the piston force can be derived by through conservation of power. The power developed through the linear motion of the piston is given by the left hand side of Eq. A.12. This must be equal to the rotational power in the crank given by the right hand side of Eq. A.12.

$$F_p v_p = \tau_p \omega \tag{A.12}$$

Inserting the expression for the piston velocity from Eq. A.10, and rearranging, the torque is found from,

$$\tau_p(\phi) = r\left[sin(\phi) + \frac{1}{2}\frac{\lambda sin(2\phi)}{\sqrt{1-\lambda^2 sin^2(\phi)}}\right]F_p, \tag{A.13}$$

Which is equal to Eq. 3.8. Alternatively Eq. A.10 could be derived through decomposition of the piston force.

Appendix B

Simulation parameters

The nominal parameters used in the simulations are given in the tables below,

Parameter	**Nomenclature**	**Value**	**Unit**
Friction parameters:			
Viscous friction coefficient	f_v	116	[-]
Static friction	τ_s	1400	[Nm]
Coulomb friction	τ_c	155	[Nm]
Stribeck coefficient	ω_s	1	[-]

Table B.1: Friction parameters

Parameter	**Nomenclature**	**Value**	**Unit**
Shaft parameters:			
Shaft inertia	I	390	$[kgm^2]$

Table B.2: Simulation parameters

Parameter	**Nomenclature**	**Value**	**Unit**
Combustion engine parameters:			
Number of engine cylinders	n	9	[-]
Number of cylinder banks	n_B	1	[-]
Engine Combustion Efficiency	η_e	0.85	[-]
Engine Bore	B	0.26	[m]
Engine Stroke	S	0.33	m-]
Compression ratio	cr	13	[-]
Piston mass	m_p	70	[kg]
Angle for closing of air valve	ϕ_a	499.3	[degrees]
Angle for opening of exhaust valve	ϕ_e	151	[degrees]
Initial crank angle	ϕ_0	0	[degrees]

Table B.3: Combustion engine parameters

Parameter	**Nomenclature**	**Value**	**Unit**
Combustion parameters:			
Crank angle for start of combustion	ϕ_s	350	[degrees]
Duration of combustion	Δ_ϕ	33	[degrees]
Wiebe coefficient 1	a	5	[-]
Wiebe coefficient 2	m	3	[-]

Table B.4: Combustion parameters

Parameter	**Nomenclature**	**Value**	**Unit**
Fuel injection parameters:			
Angle for opening of fuel valve	ϕ_{fo}	350	[degrees]
Angle for closing of fuel valve	ϕ_{fc}	33	[degrees]
Injection coefficient	k	0.0034	[-]
Time delay fuel rack	$t_{d,f}$	1.6	[s]
Heating value natural gas	HV]	$47.5 * 10^6$	[J/kg]
Fuel-on speed	ω_{fo}	8.38	rad]
Purging time	t_p	3	[s]

Table B.5: Fuel injection parameters

Parameter	**Nomenclature**	**Value**	**Unit**
Starting system parameters:			
Disengagement speed	ω_d	15.7	[rad/s]
Gear ratio	i	260/11	[-]
Pipe diameter	D	0.036	[m]
Equivalent pipe lenght	L_e	35	[m]
Absolute pipe roughness, steel	ϵ	$45 * 10^-6$	[m]
Tank volume	V_t	0.5	$[m^3]$
Initial tank temperature	$T_{0,t}$	318	[K]
Time delay starting valve	$t_{d,v}$	0.2	[s]

Table B.6: Starting system parameters

Parameter	**Nomenclature**	**Value**	**Unit**
Properties of air:			
Atmosheric density of air	P_0	1.2	$[kg/m^3]$
Heat capacity ratio	κ	1.4	[-]
Specific gas constant	R	287.058	[J/(kgK)]
Dynamic viscosity of air	μ_a	0.00001983	[kg/(ms)]

Table B.7: Properties of air used in the simulations

Appendix C

Controller and starting sequence testing results

Simulation result for testing of the starting sequence and controller is presented below. The test scenarios are,

- **Test 5.1:** $n = 6$, $I = 0.6I_{nom}$ $[kgm^2]$, $\tau_f = 0.8\tau_{f,nom}$, $P_1 = 15.5$ [Bar],
- **Test 5.2:** $n = 6$, $I = 0.6I_{nom}$ $[kgm^2]$, $\tau_f = 0.8\tau_{f,nom}$, $P_1 = 30.0$ [Bar],
- **Test 5.3:** $n = 6$, $I = 1.5I_{nom}$ $[kgm^2]$, $\tau_f = 0.8\tau_{f,nom}$, $P_1 = 15.5$ [Bar],
- **Test 5.4:** $n = 6$, $I = 1.5I_{nom}$ $[kgm^2]$, $\tau_f = 0.8\tau_{f,nom}$, $P_1 = 30.0$ [Bar],
- **Test 5.5:** $n = 8$, $I = 0.8I_{nom}$ $[kgm^2]$, $\tau_f = 0.9\tau_{f,nom}$, $P_1 = 15.5$ [Bar],
- **Test 5.6:** $n = 8$, $I = 0.8I_{nom}$ $[kgm^2]$, $\tau_f = 0.9\tau_{f,nom}$, $P_1 = 30.0$ [Bar],
- **Test 5.7:** $n = 8$, $I = 2.0I_{nom}$ $[kgm^2]$, $\tau_f = 0.9\tau_{f,nom}$, $P_1 = 15.5$ [Bar],
- **Test 5.8:** $n = 8$, $I = 2.0I_{nom}$ $[kgm^2]$, $\tau_f = 0.9\tau_{f,nom}$, $P_1 = 30.0$ [Bar],
- **Test 5.9:** $n = 9$, $I = 2.5I_{nom}$ $[kgm^2]$, $\tau_f = \tau_{f,nom}$, $P_1 = 15.5$ [Bar],
- **Test 5.10:** $n = 9$, $I = 2.5I_{nom}$ $[kgm^2]$, $\tau_f = \tau_{f,nom}$, $P_1 = 30.0$ [Bar],

where n i the number of cylinders, I is the shafting inertia, τ_f is frictoin torque and P_1 is starting bottle pressure. Subscript *nom* denotes nominal parameter values.

C.1 Test 5.1 and 5.2: six-cylinder propulsion plant

- **Test 5.1:** $n = 6$, $I = 0.6I_{nom}$ $[kgm^2]$, $\tau_f = 0.8\tau_{f,nom}$, $P_1 = 15.5$ [Bar],

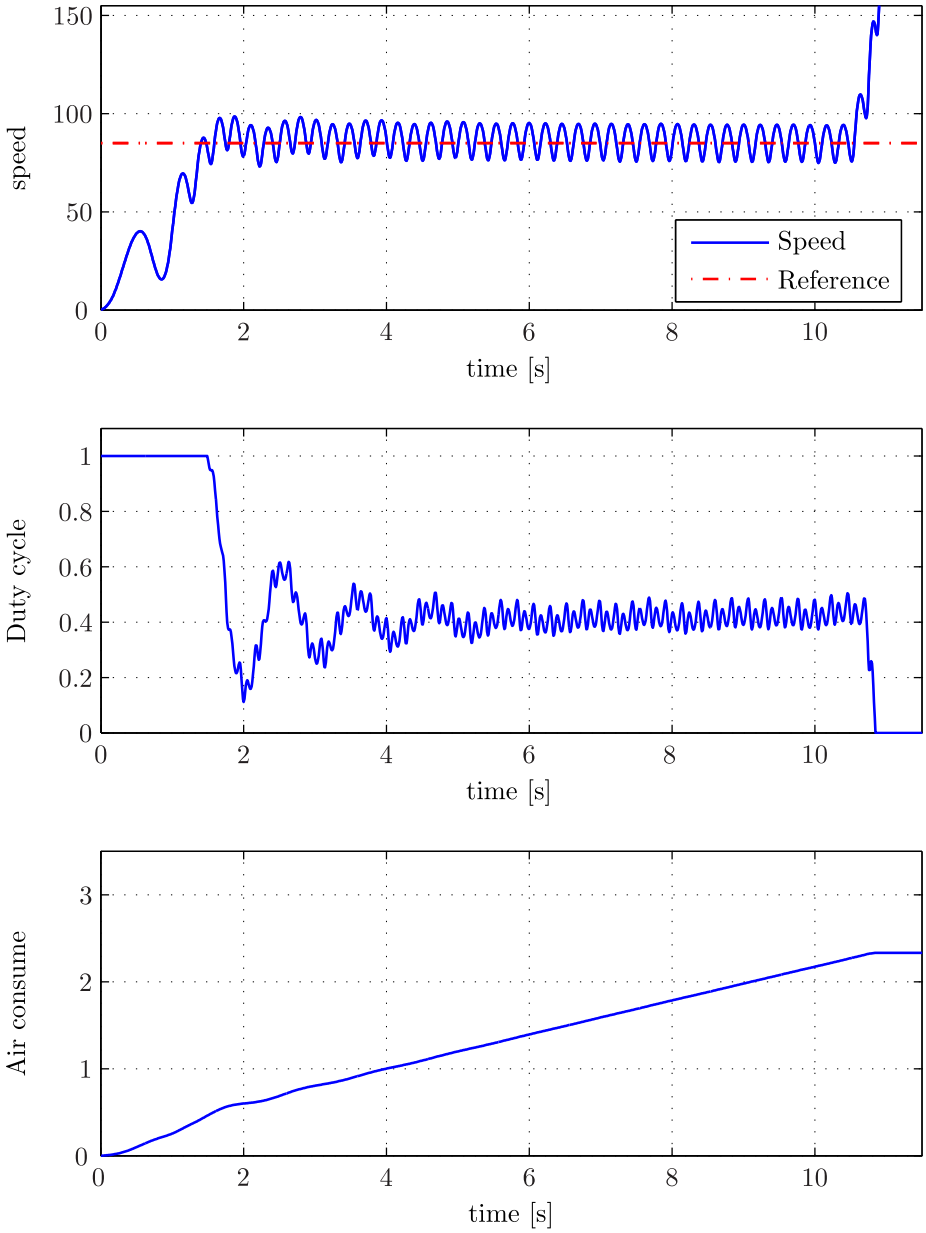

Figure C.1: Simulation result for **Test 5.1:**.

- **Test 5.2:** $n = 6$, $I = 0.6I_{nom}$ $[kgm^2]$, $\tau_f = 0.8\tau_{f,nom}$, $P_1 = 30.0$ [Bar],

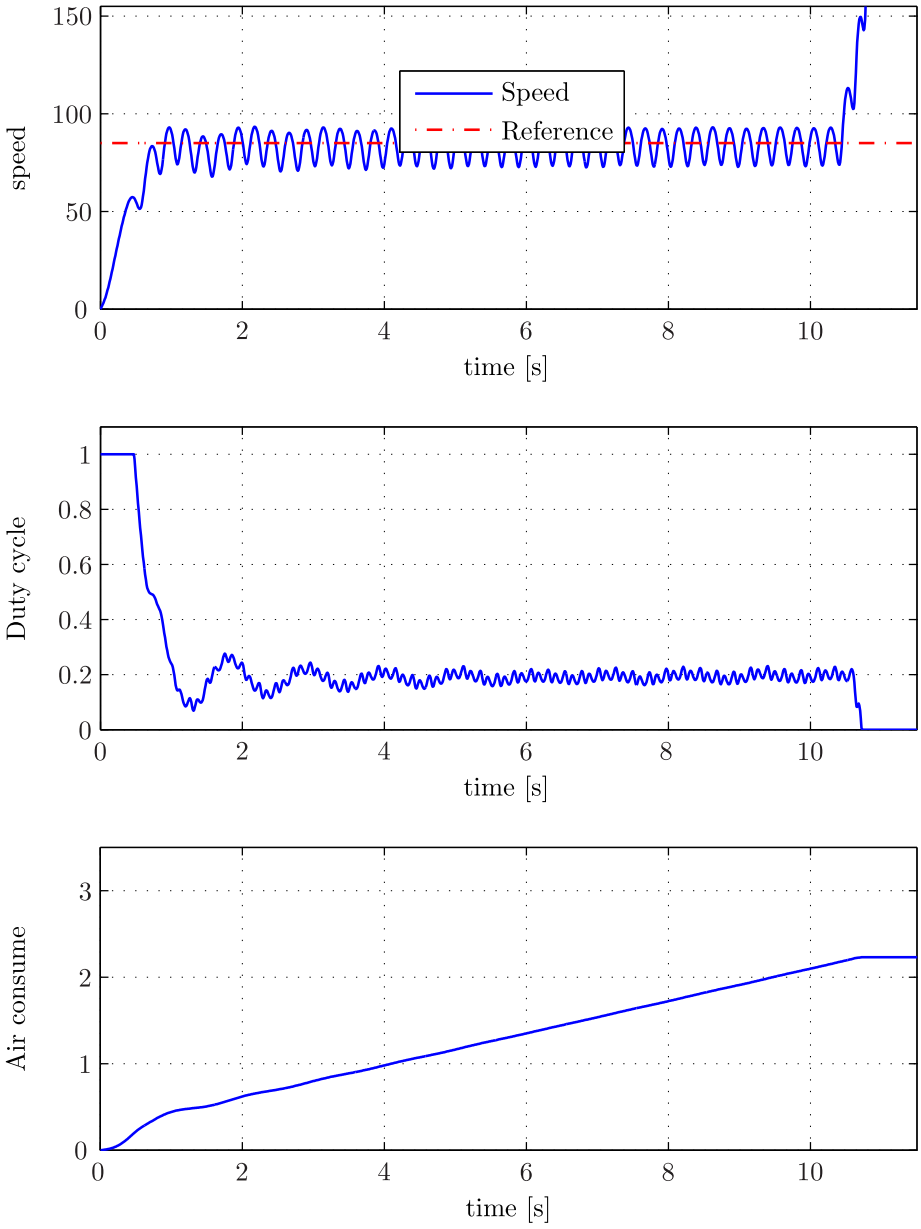

Figure C.2: Simulation result for **Test 5.2:**.

C.2 Test 5.3 and 5.4: six-cylinder generator set

- **Test 5.3:** $n = 6$, $I = 1.5I_{nom}$ $[kgm^2]$, $\tau_f = 0.8\tau_{f,nom}$, $P_1 = 15.5$ [Bar],

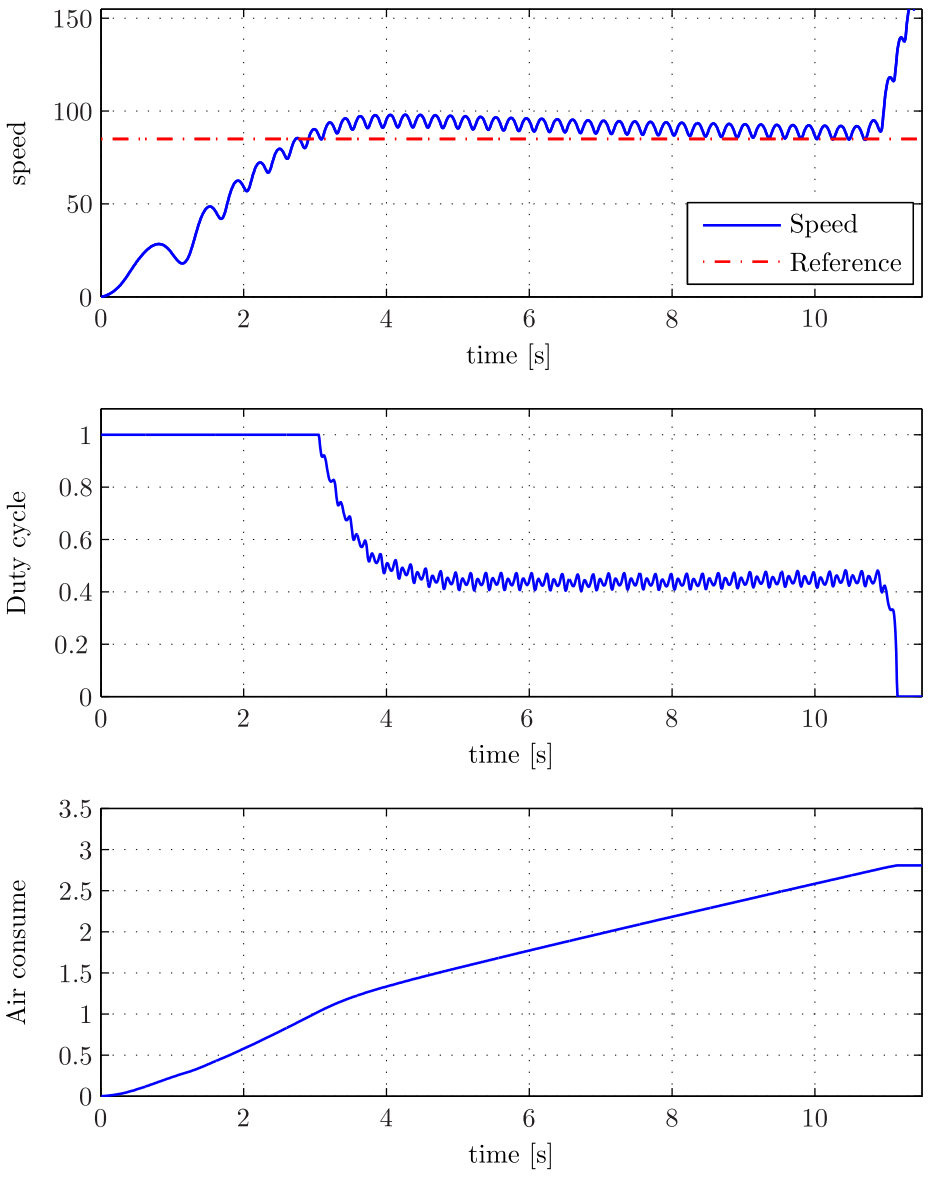

Figure C.3: Simulation result for **Test 5.3:**.

- **Test 5.4:** $n = 6$, $I = 1.5I_{nom}$ $[kgm^2]$, $\tau_f = 0.8\tau_{f,nom}$, $P_1 = 30.0$ [Bar],

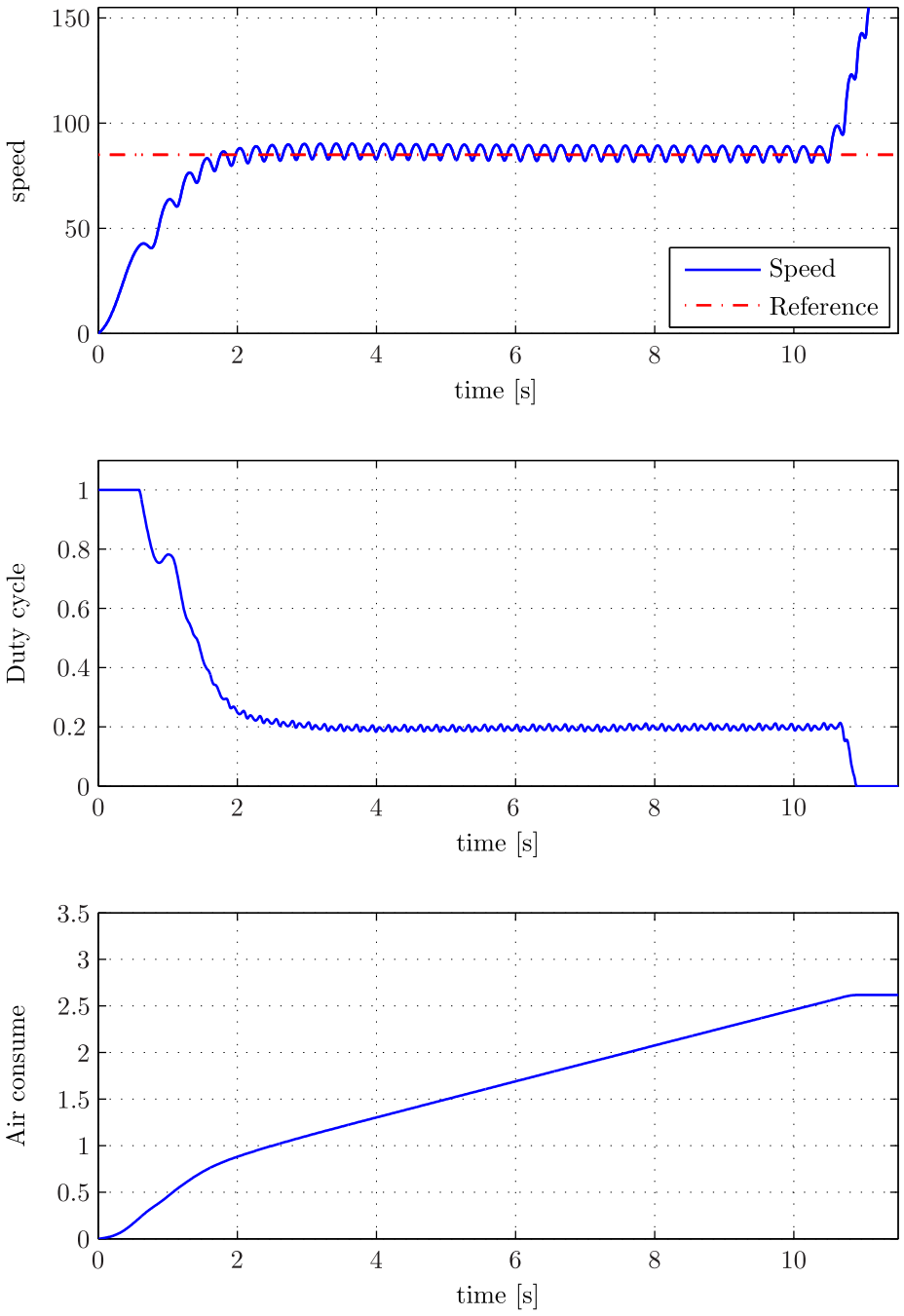

Figure C.4: Simulation result for **Test 5.4:**.

C.3 Test 5.5 and 5.6: eight-cylinder propulsion plant

- **Test 5.5:** $n = 8$, $I = 0.8I_{nom}$ $[kgm^2]$, $\tau_f = 0.9\tau_{f,nom}$, $P_1 = 15.5$ [Bar],

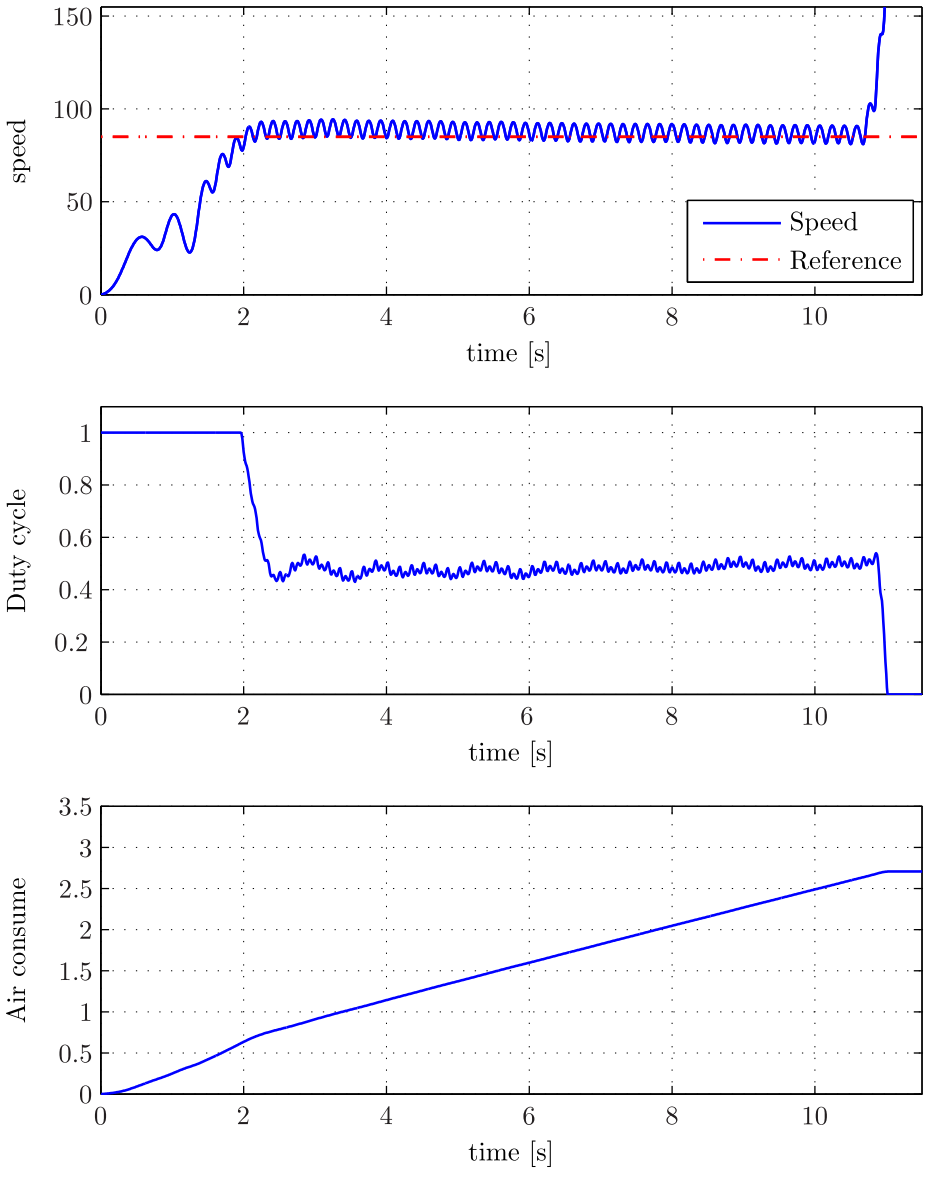

Figure C.5: Simulation result for **Test 5.5:**.

- **Test 5.6:** $n = 8$, $I = 0.8I_{nom}$ $[kgm^2]$, $\tau_f = 0.9\tau_{f,nom}$, $P_1 = 30.0$ [Bar],

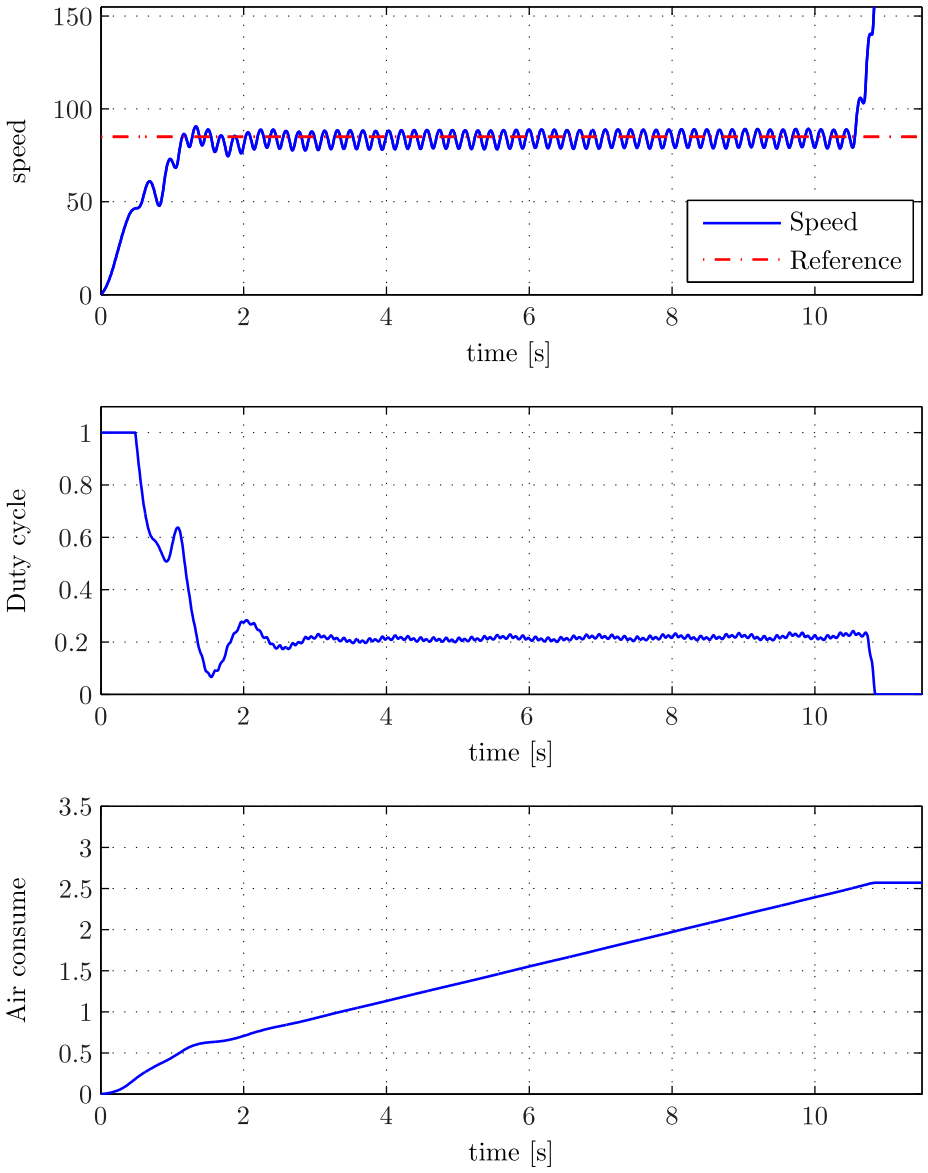

Figure C.6: Simulation result for **Test 5.6:**.

C.4 Test 5.7 and 5.8: eight-cylinder generator set

- **Test 5.7:** $n = 8$, $I = 2I_{nom}$ $[kgm^2]$, $\tau_f = 0.9\tau_{f,nom}$, $P_1 = 15.5$ [Bar],

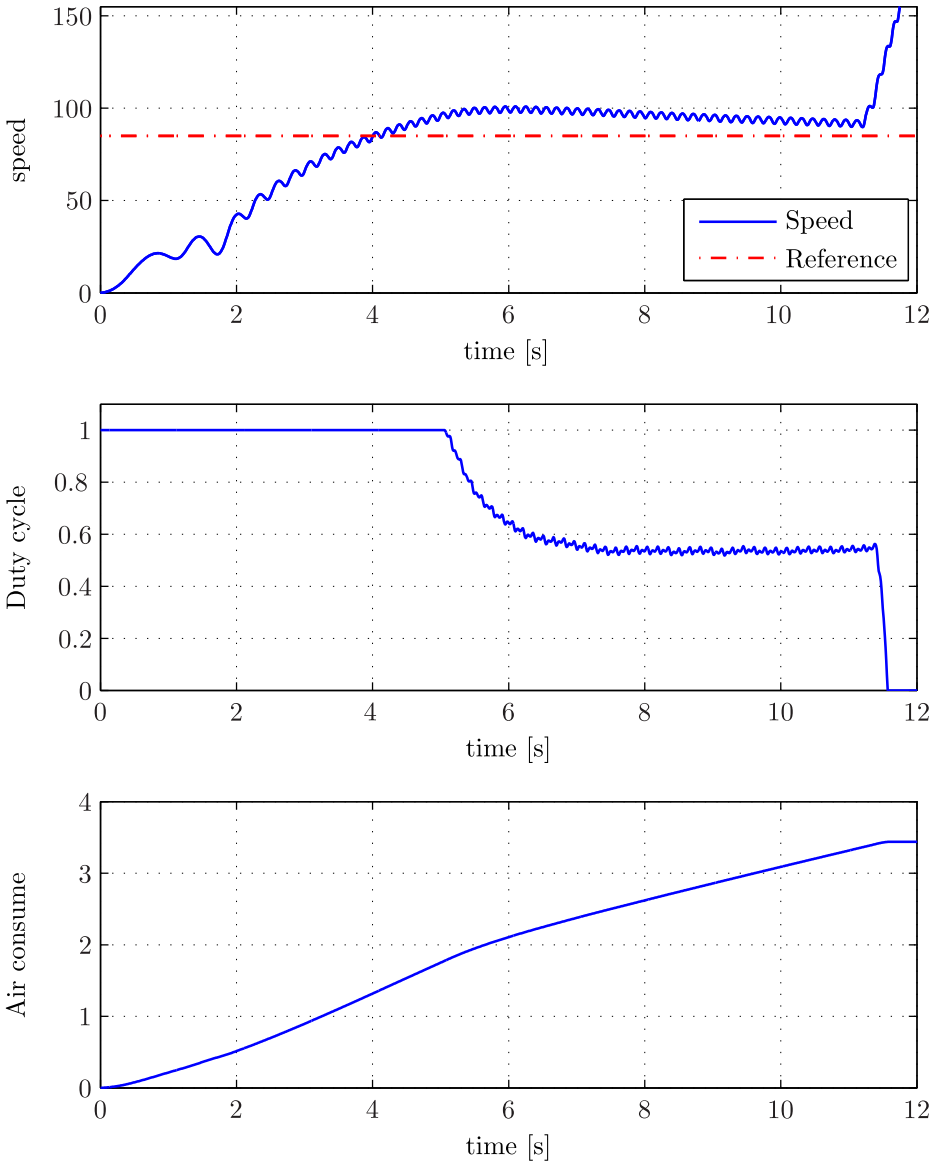

Figure C.7: Simulation result for **Test 5.7:**.

- **Test 5.8:** $n = 8$, $I = 2I_{nom}$ $[kgm^2]$, $\tau_f = 0.9\tau_{f,nom}$, $P_1 = 30.0$ [Bar],

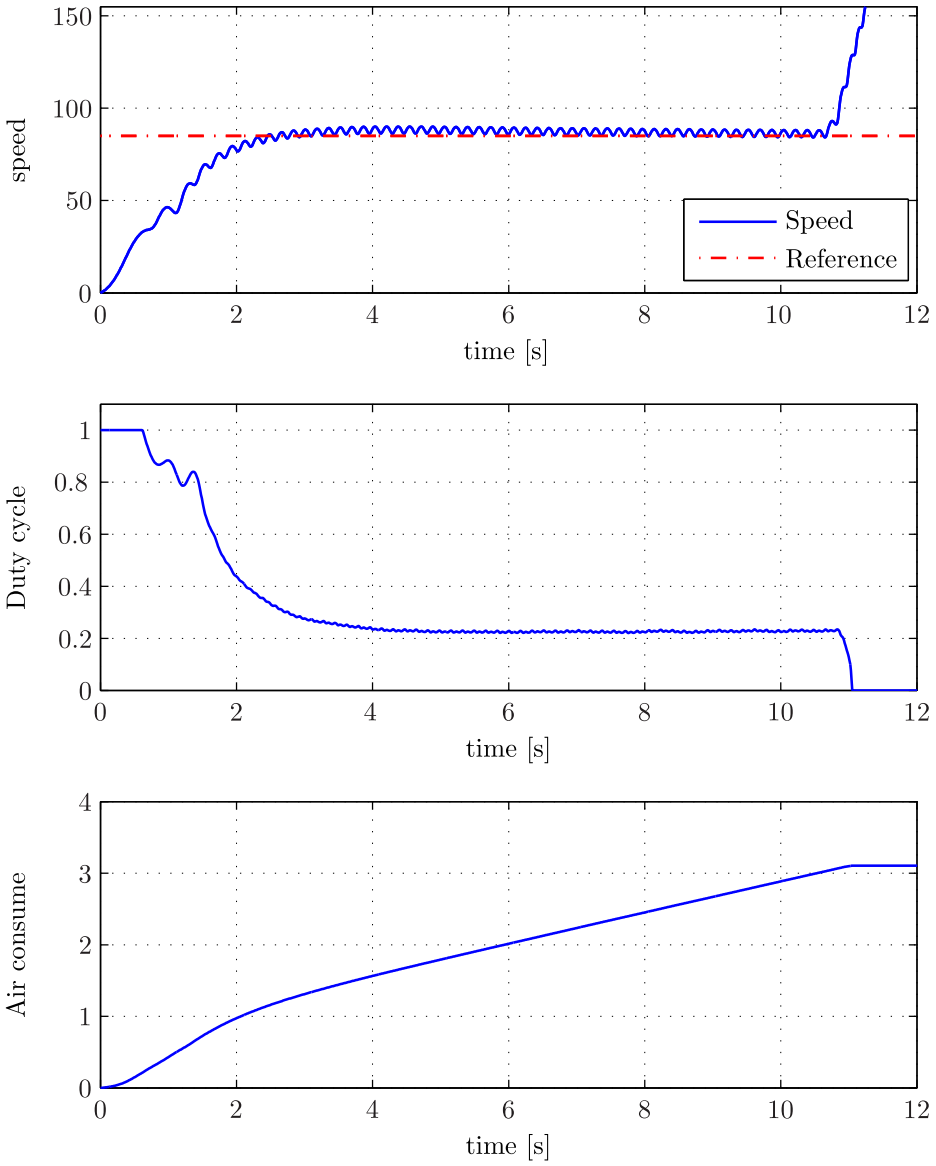

Figure C.8: Simulation result for **Test 5.8:**.

C.5 Test 5.9 and 5.10: nine-cylinder generator set

- **Test 5.9:** $n = 9$, $I = 2.5I_{nom}$ $[kgm^2]$, $\tau_f = \tau_{f,nom}$, $P_1 = 15.5$ [Bar],

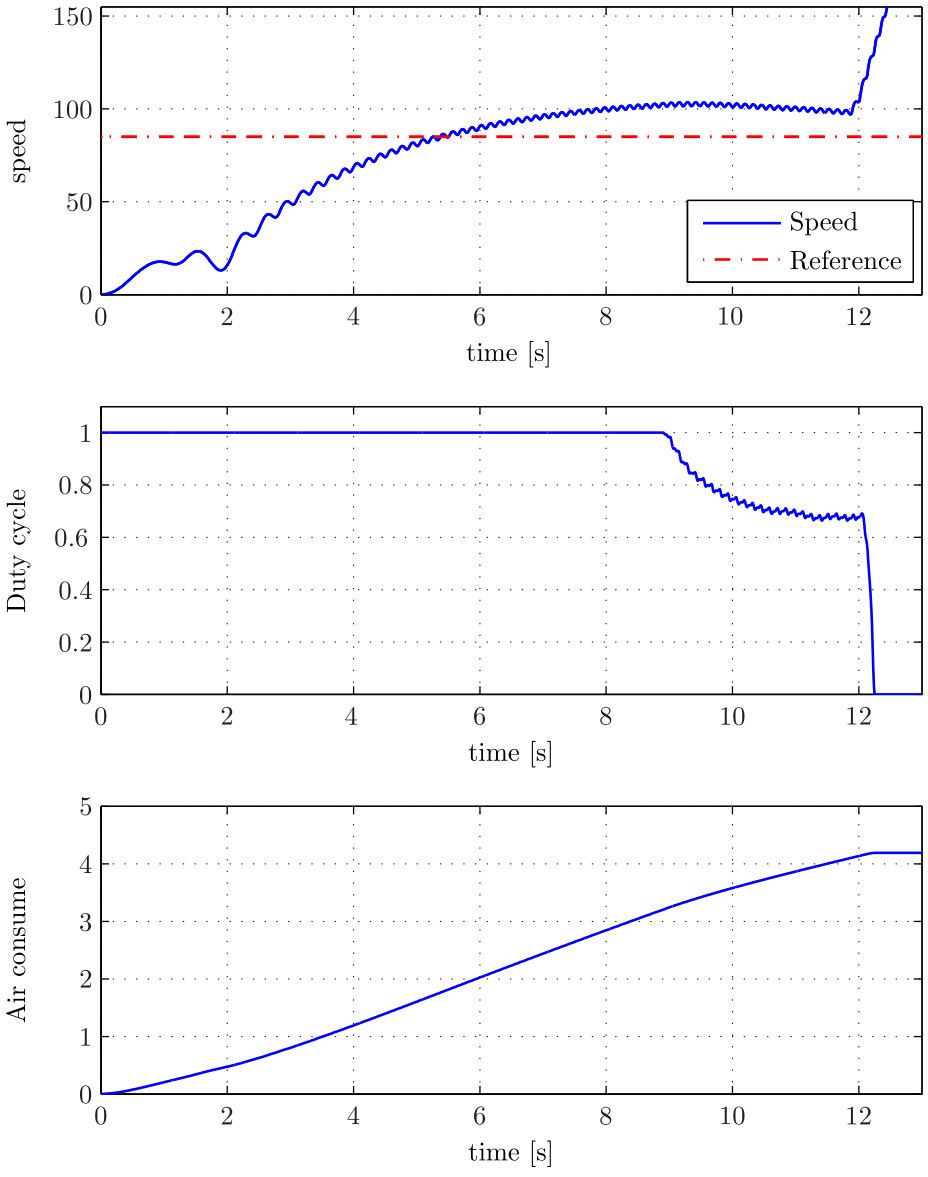

Figure C.9: Simulation result for **Test 5.9:**.

- **Test 5.10:** $n = 9$, $I = 2.5I_{nom}$ $[kgm^2]$, $\tau_f = \tau_{f,nom}$, $P_1 = 30.0$ [Bar],

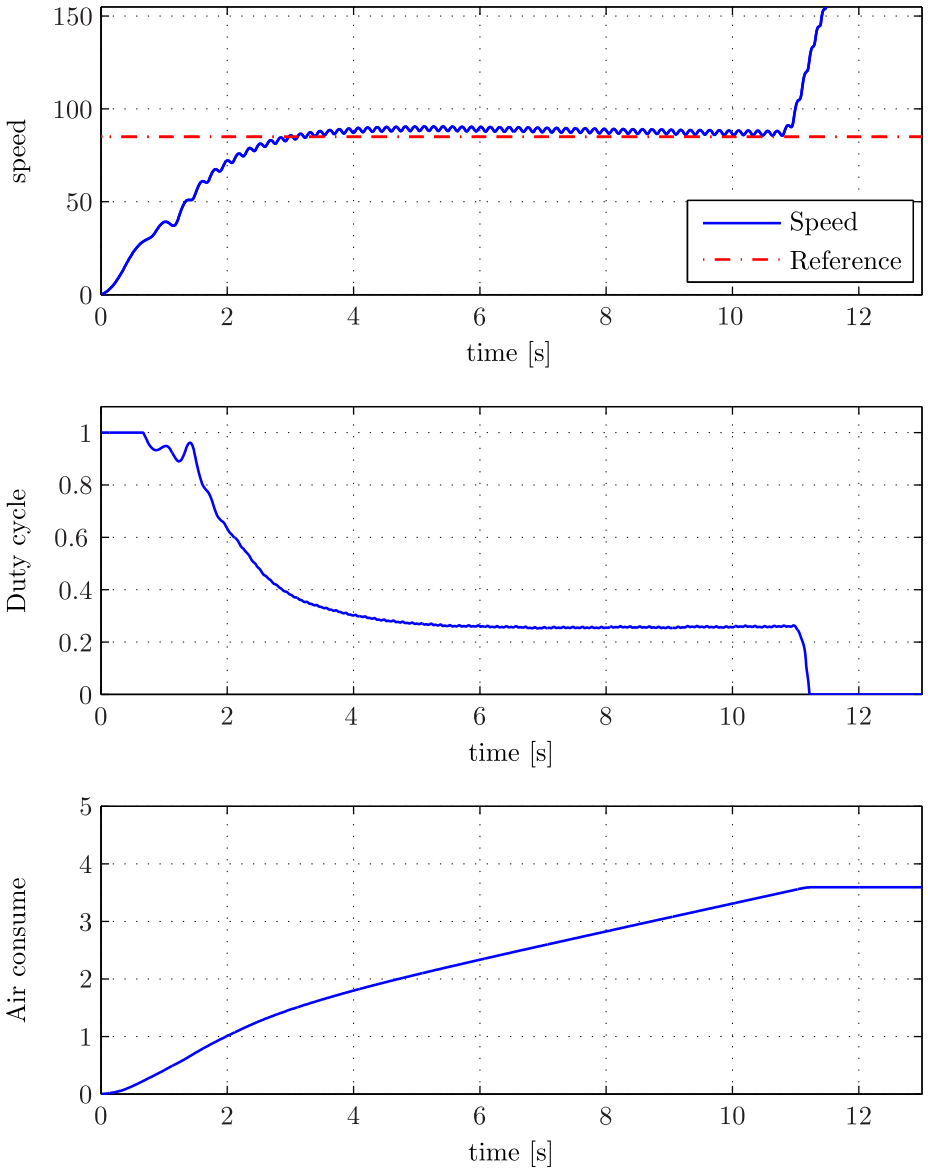

Figure C.10: Simulation result for **Test 5.10:**.

Appendix D

Simulink diagrams

D.1 Shaft dynamics

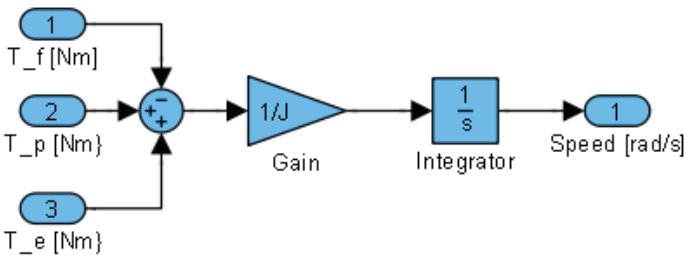

Figure D.1: Shaft dynamics model

D.2 Friction torque

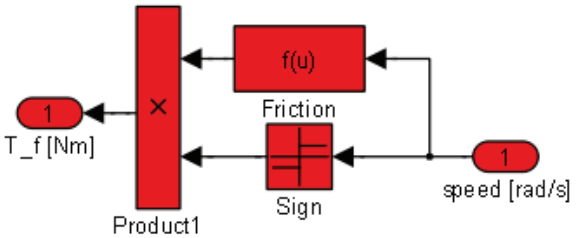

Figure D.2: Friction model

D.3 Main diagram

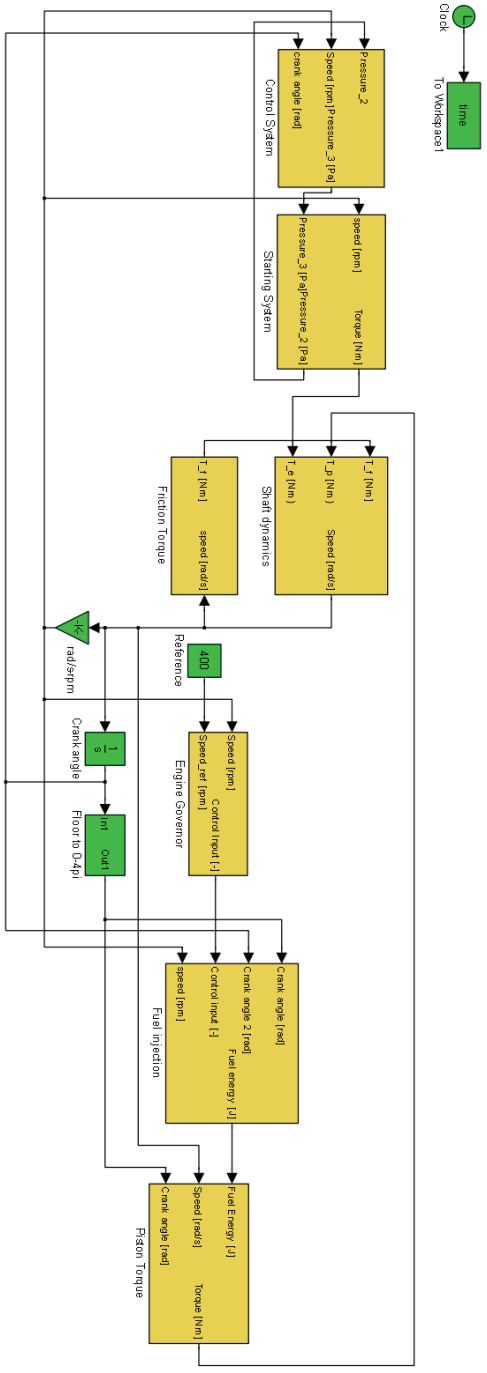

Figure D.3: Main diagram.

D.4 Piston torque

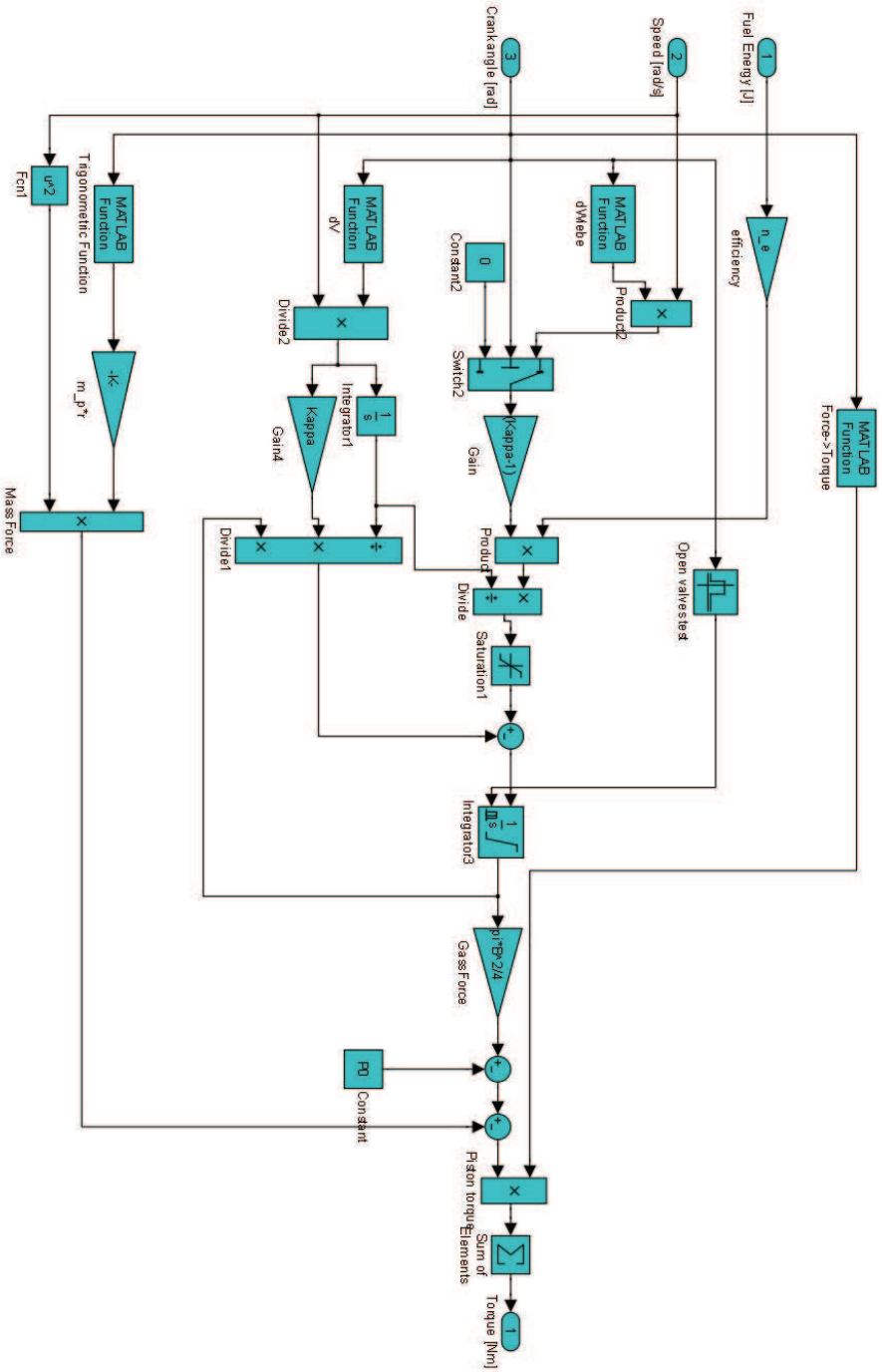

Figure D.4: Piston torque model.

D.5 Fuel injection and governor

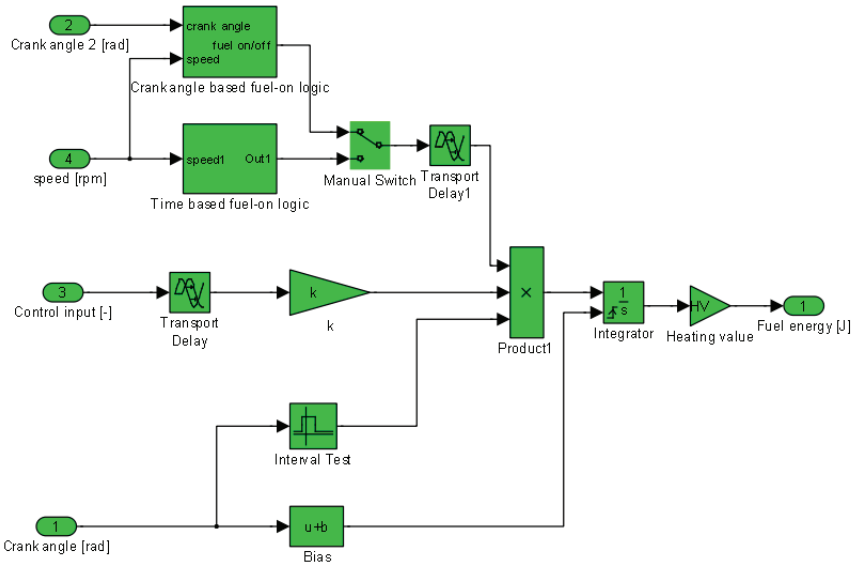

Figure D.5: Fuel injection model

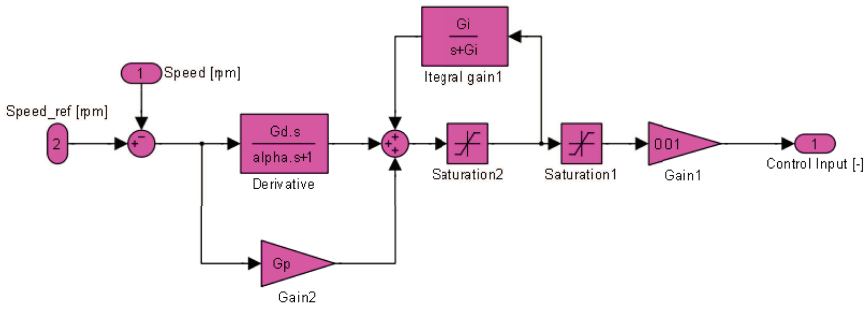

Figure D.6: Engine governor model.

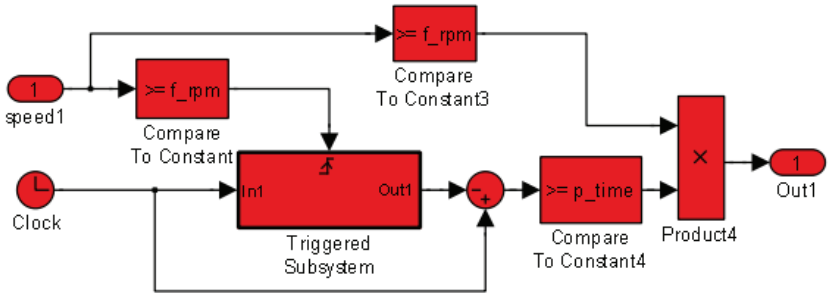

Figure D.7: Time based fuel logic.

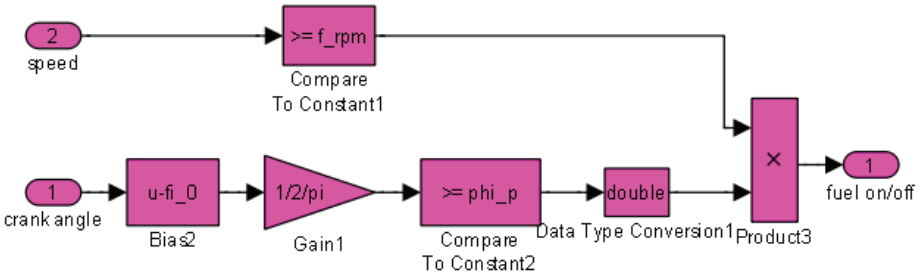

Figure D.8: Crank angel based fuel logic.

D.6 Starting control system

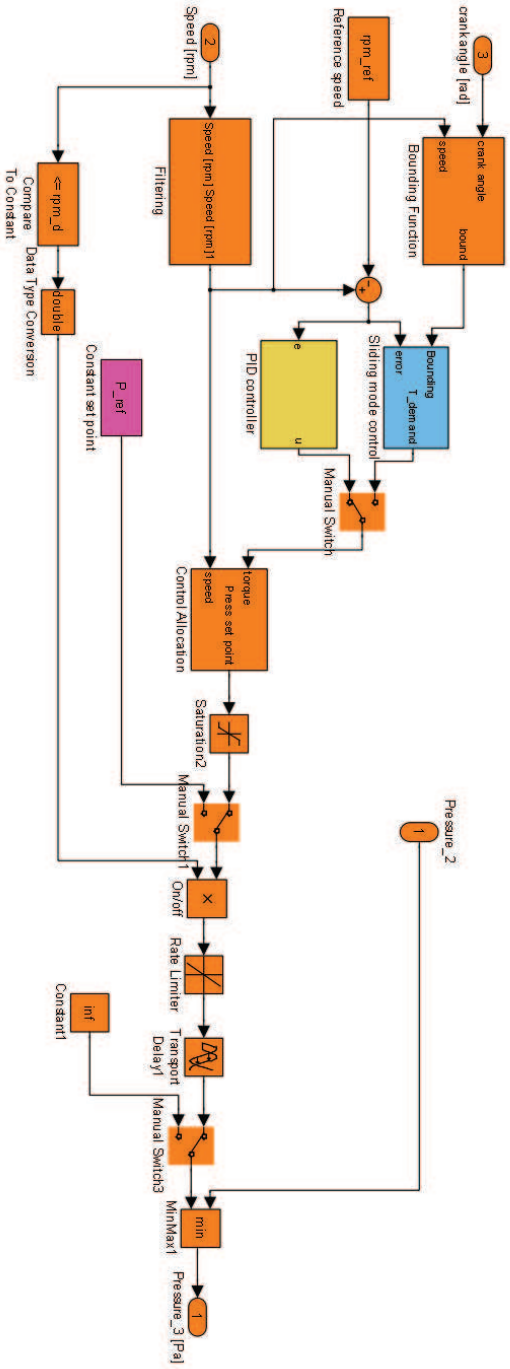

Figure D.9: Starting control system.

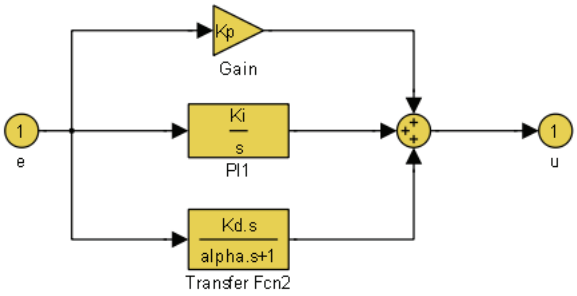

Figure D.10: PID controller.

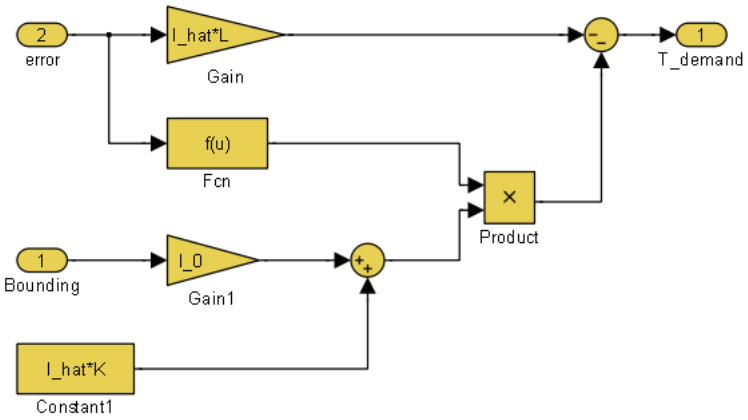

Figure D.11: Sliding mode controller

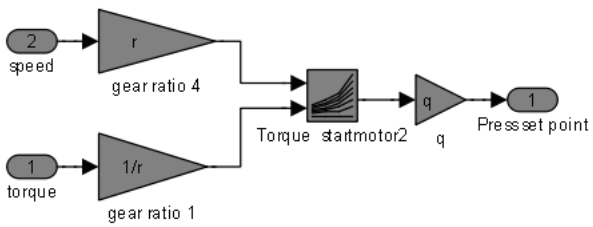

Figure D.12: Control allocation.

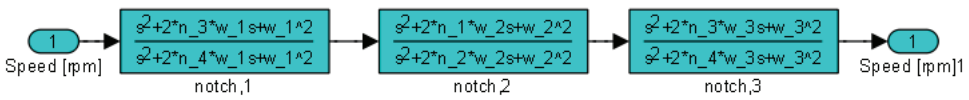

Figure D.13: Notch filter.

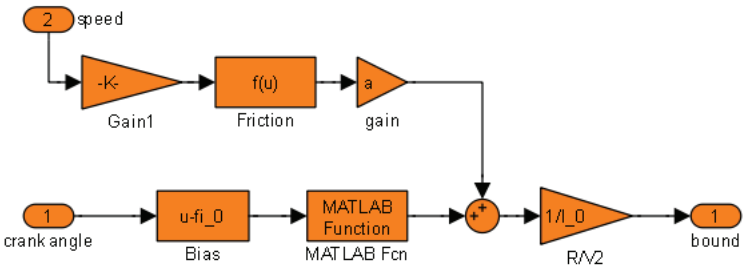

Figure D.14: Bounding function.

D.7 Starting system

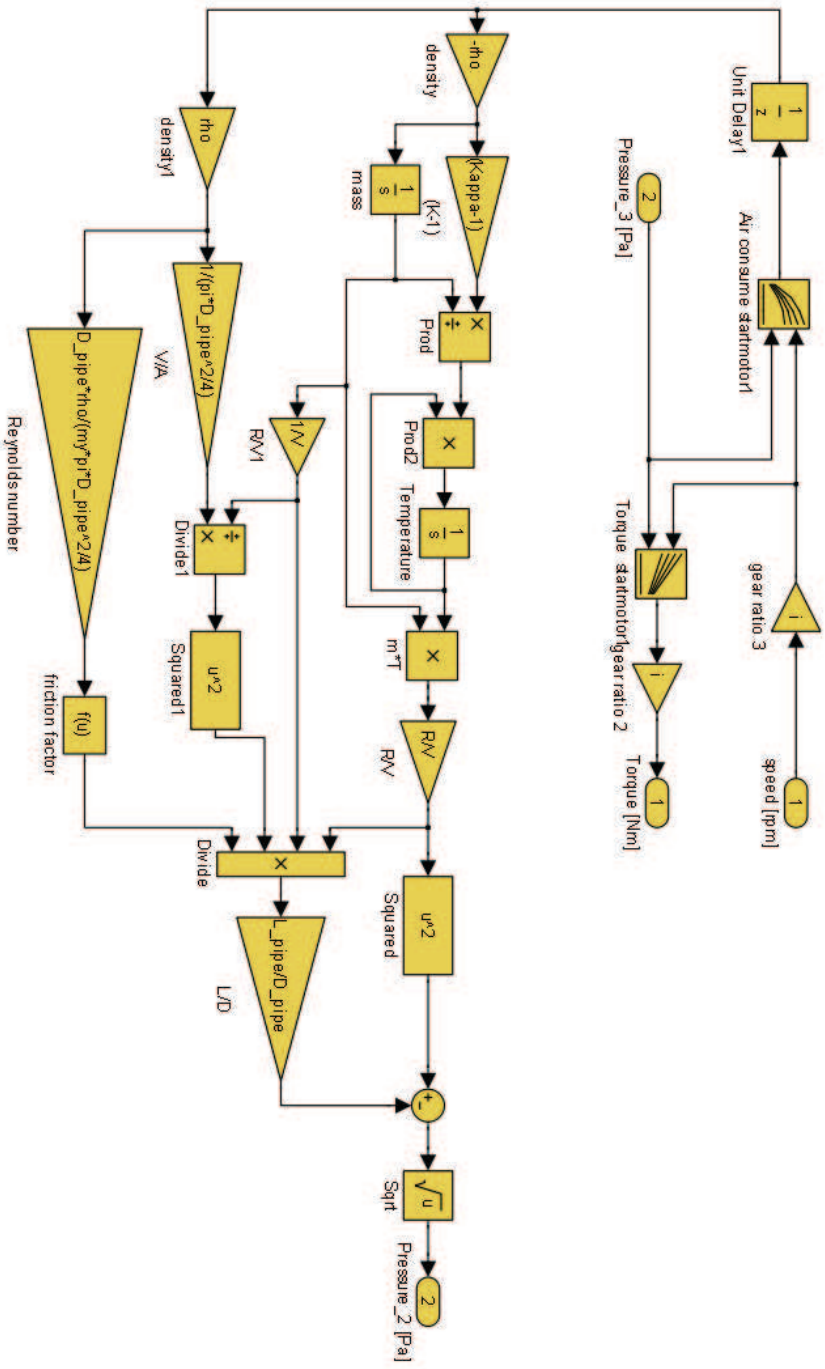

Figure D.15: Starting system model.